NASA TECHNICAL NOTE

NASA TN D-7821

NASA TN D-7821

CASE FILE
COPY

PREDICTION OF AIRFRAME NOISE

Jay C. Hardin, David J. Fratello, Richard E. Hayden,
Yoran Kadman, and Steven Africk

Langley Research Center
Hampton, Va. 23665

NATIONAL AERONAUTICS AND SPACE ADMINISTRATION • WASHINGTON, D. C. • FEBRUARY 1975

1. Report No.	2. Government Accession No.	3. Recipient's Catalog No.
NASA TN D-7821		

4. Title and Subtitle	5. Report Date
PREDICTION OF AIRFRAME NOISE	February 1975
	6. Performing Organization Code
7. Author(s)	8. Performing Organization Report No.
Jay C. Hardin, David J. Fratello, Richard E. Hayden, Yoran Kadman, and Steven Africk	L-9912
	10. Work Unit No.
9. Performing Organization Name and Address	500-06-23-01
NASA Langley Research Center Hampton, Va. 23665	11. Contract or Grant No.
	13. Type of Report and Period Covered
12. Sponsoring Agency Name and Address	Technical Note
National Aeronautics and Space Administration Washington, D.C. 20546	14. Sponsoring Agency Code

15. Supplementary Notes

Richard E. Hayden, Yoran Kadman, and Steven Africk are associated with Bolt Beranek and Newman, Inc., Boston, Massachusetts.

16. Abstract

The current understanding and methods of prediction of airframe noise, defined as the noise generated by an aircraft in flight in the absence of power, is assessed. Approaches to predictions relying upon flyover data and component theoretical analyses are developed. In addition, areas where further research is required are identified.

17. Key Words (Suggested by Author(s))	18. Distribution Statement
Airframe noise Nonpropulsive noise Noise prediction	Unclassified – Unlimited STAR Category 02

19. Security Classif. (of this report)	20. Security Classif. (of this page)	21. No. of Pages	22. Price*
Unclassified	Unclassified	114	$5.25

*For sale by the National Technical Information Service, Springfield, Virginia 22151

CONTENTS

SUMMARY 1

INTRODUCTION 1

SYMBOLS 2

MOTIVATION 9

BACKGROUND 9
- Complete Aircraft Studies 9
- Component Studies 14
  - Airfoil 14
  - Wheel wells 19
  - Landing gear 24

PREDICTIVE TECHNIQUES 28
- Total Aircraft Analysis 28
- Semiempirical Drag Analysis 34
- Component Analysis 36
  - Source identification 36
  - Source location on aircraft 38
  - Component prediction methods 38
  - Modeling considerations 44
  - Illustrative calculations 46
  - Predicted trends for various aircraft configurations and positions 48

CONCLUSIONS AND RECOMMENDATIONS 49

REFERENCES 51

TABLES 57

FIGURES 62

PREDICTION OF AIRFRAME NOISE

Jay C. Hardin, David J. Fratello, Richard E. Hayden,[1]
Yoran Kadman,[1] and Steven Africk[1]
Langley Research Center

SUMMARY

The current understanding and methods of prediction of airframe noise, defined as the noise generated by an aircraft in flight in the absence of power, is assessed. Approaches to predictions relying upon flyover data and component theoretical analyses are developed. In addition, areas where further research is required are identified.

INTRODUCTION

Airframe noise is defined for the purpose of this paper as the noise generated by an aircraft in flight from sources other than engines, auxiliary power units, and other energy-consuming accessories. The generation of airframe noise is due to airflow over the fuselage, wings, engine pods, flap systems, landing-gear struts, wheel wells, etc. These sources are illustrated in figure 1. This paper will attempt to assess the current understanding of such noise and will present a recommended procedure for its prediction. In addition, areas where further research is needed are delineated.

There are two different methods by which the task of predicting airframe noise may be approached. The first method is to consider the aircraft as a whole and to employ empirical relations developed from experimental data for prediction. Considerable effort has been and is being expended in this area and viable techniques have been produced. The second method is to consider each of the components of the aircraft as a separate entity, that is, wings, flaps, struts, wells, etc., to obtain an understanding of their individual noise-generation characteristics and then to combine these components to predict the noise of the complete aircraft. Although some work has been accomplished along these lines, much remains to be done before an approach relying totally upon a theoretical understanding of component noise generation can be employed with confidence. Both of these methods are discussed in this paper.

---

[1]Bolt Beranek and Newman, Inc., Boston, Massachusetts.

SYMBOLS

Measurements and calculations are presented in the International System of Units (SI) with equivalent values given in U.S. Customary Units in parentheses. Values were obtained in U.S. Customary Units.

A	area
A_j	constants indexed by j where $j = 1, 2, \ldots$
AR	aspect ratio
B_i	constants indexed by i where $i = 1, 2, \ldots$
C_D	drag coefficient
$C_{D,F}$	wetted-area drag coefficient
$C_{D,j}$	drag coefficient of component j
$C_{D,ref}$	reference drag coefficient
C_L	lift coefficient
C_p	pressure coefficient
D	cavity depth
$D(\theta,\psi)$	directivity factor
EPNdB	effective perceived noise level
$\dot{F}$	magnitude of fluctuating force
F_i	components of total force on aircraft
I	acoustic intensity
K	acoustic wave number, ω/a_o
$K_o = \omega/U_o$	
K_r	real part of wave number in flow direction

L	cavity length
$\dot{L}$	magnitude of fluctuating lift vector
$\vec{\dot{L}}$	fluctuating lift vector
M	Mach number or magnitude of Mach vector
$\vec{M}$	Mach vector
M_i	components of Mach vector
M_r	instantaneous Mach number in observer direction from point y_1,y_2,y_3
$M_{r'}$	instantaneous Mach number in observer direction from point y'_1,y'_2,y'_3
N_{Re}	Reynolds number
N_{Str}	Strouhal number
OAPWL	overall sound power level
OASPL	overall sound pressure level
$\frac{1}{3}$ OBSPL	one-third-octave band sound pressure level
P_a	acoustic power
$P_{a,j}$	acoustic power produced by jth component
$P_{m,j}$	mechanical power consumed by jth component
PNdB	perceived noise level
PWL	power level
Q	function of cavity dimensions, Mach number, and frequency
R	function of cavity dimensions, Mach number, and frequency

S	aircraft wing area
$S(\zeta)$	universal spectrum
S_j	relevant area for component j
$S_o(\zeta)$	multiplicative function in universal spectrum
S_{ref}	reference area
SPL	sound pressure level
T	force of one source region
U	flow speed
U_c	mean convection speed in wake
U_o	convection speed of disturbance
$U_R = U_o/U$	
V	aircraft speed or magnitude of vector $\vec{V}$
$\vec{V}$	aircraft velocity vector
V_{ref}	reference aircraft speed
W	weight of aircraft
W_c	wetted span of airfoil
X, Y, Z	Cartesian coordinates in space
a_c	speed of sound in cavity
a_o	ambient speed of sound
b	aircraft span

c	airfoil chord
d	cylinder diameter
dB (A)	A-weighted decibel
d_{eq}	equivalent diameter of airfoil, $C_D c$
d_f	equivalent fuselage length, $C_{D,F} \ell_f$
f	frequency, Hz
$\vec{f}$	fluctuating force vector
f_d	fluctuating drag
f_i	components of vector $\vec{f}$
f_ℓ	fluctuating lift
f_{max}	frequency of spectral peak
f_N	natural frequency of cavity resonance
f_{Str}	Strouhal frequency
f_v	vortex shedding frequency
g	acceleration of gravity
h	altitude of aircraft
h_{ref}	reference altitude
i	integer index
$\vec{k}$	wave number vector
k_i	components of vector $\vec{k}$

ℓ	length of cylinder
ℓ_c	correlation length along cylinder
ℓ_f	length of fuselage
ℓ_x	streamwise correlation length
ℓ_y	normal correlation length
ℓ_z	spanwise correlation length
m	number of sources
n	integer
p	acoustic pressure
p(r,f)	Fourier transform of acoustic pressure
p_c	cavity pressure
p_j	acoustic pressure produced by jth component
p_m	peak forcing pressure at open end of cavity
p_{ref}	reference pressure
$p_s(\vec{x},t)$	surface pressure
$q = \frac{1}{2}\rho_o V^2$	
r	observer distance or magnitude of vector $\vec{r}$
$\vec{r}$	observer vector
r'	magnitude of vector $\vec{r}'$
$\vec{r}'$	observer vector from point y_1', y_2', y_3'
r,θ,ψ	spherical coordinate system

r_e	effective source radius
r_v	wing-tip vortex core radius
t	time
t'	retarded time
t_w	wing thickness
u	particle speed
u_r	turbulent fluctuation in radial direction
$v(f)$	Fourier transform of normal turbulent velocity
x_1,x_2,x_3	point in Cartesian coordinate space
y_1,y_2,y_3	position of center of gravity of aircraft
y'_1,y'_2,y'_3	point on aircraft surface
Λ	characteristic length
$\Pi(\omega)$	sound power per unit bandwidth
$\Phi_a(\vec{k},\omega)$	acoustic content of turbulent boundary layer
$\Phi_F(\omega)$	force spectral density
$\Phi_p(\omega)$	spectral density of acoustic pressure
$\Phi_{p,s}(\vec{k},\omega)$	wave-number frequency spectrum of turbulent pressure
α	angle between flight path and projection in X,Y plane
α_s	constant in universal spectrum
β	angle between fluctuating force vector and observer vector

γ	angle between normal to aircraft's wings and observer vector
γ_r	ratio of specific heats
δ	boundary-layer thickness at trailing edge of airfoil
δ_w	wake thickness
ϵ_i	arbitrary powers
ζ	normalized frequency, f/f_{Str}
$\eta_{a,j}$	acoustic efficiency factor for component j
θ	angle between incident stream and observer direction
θ_s	angle between source axis and Z-axis
λ_j	proportionality constant
λ_j'	normalized proportionality constant
λ_v	mean vortex spacing over cavity
ν	coefficient of kinematic viscosity
ρ'	instantaneous far-field density
ρ_a	acoustic density, $\rho' - \rho_o$
ρ_o	ambient density
ϕ	lag of vortex sheet displacement
$\phi_{p,s}(\vec{x},t)$	space-time correlation of turbulent pressure
ω	circular frequency

A bar over a symbol indicates root mean square, unless otherwise noted.

MOTIVATION

For many years, the primary thrust of aerodynamic noise research has been to reduce the sound generation by the propulsive systems of the aircraft. This effort has met with considerable success. In fact, all aircraft in the national commercial fleet which have been introduced since 1969 meet the present noise standard FAR-36. In addition, there is reasonable expectation that these propulsive sources may be further silenced in order to meet the CARD Study (ref. 1) goal of an additional 10 EPNdB reduction per decade.

On the basis of the best available data, two recent papers (refs. 2 and 3) have, however, indicated that the airframe noise floor lies only some 8 to 10 EPNdB below the current FAR-36 levels. This is particularly true for the landing approach where the thrust levels, and thus engine noise levels, are low and the aerodynamic configuration is "dirty;" for example, the flaps and landing gear are extended and the wheel wells are open. This statement is illustrated in figure 2 which presents measured approach noise levels for several current aircraft as well as estimated airframe noise levels. The indicated levels have two important implications: First, the CARD Study goals may very well be unattainable because of the airframe noise and, second, there is little incentive for the propulsive noise to be much further reduced when the airframe noise floor is reached. Thus, there is strong motivation for methods of prediction of airframe noise as well as a fundamental understanding which could lead to its reduction.

BACKGROUND

The background for this report will be divided into the two natural subdivisions. The first will deal with the total aircraft considered as an entity and the second will consider each component separately.

Complete Aircraft Studies

Interestingly, the first study of this type was not concerned with an aircraft, but with an owl. In 1934 Graham (ref. 4) published a paper in which he studied the mechanisms which allow an owl to fly quietly in the hope that they might be applicable to airscrews. Although he did not present any quantitative measurements, he did identify three characteristics of the owl's wing – the leading-edge comb, the trailing-edge fringe, and the downy upper surface – which he felt might be important in modifying the airflow over the wing and in producing the silent flight.

This work was continued in 1972 by Kroeger et al. (ref. 5) who had in mind the potential application to military surveillance aircraft. Actual measurements of the total sound power produced by an owl in gliding flight were made in a reverberant chamber.

These levels were used to define a simple spherical source radiating in a free field in order to estimate the sound pressure levels produced by a gliding owl under free-field conditions. A spectrum resulting from such an estimate is shown in figure 3.

The primary result of this study was that the owl is not particularly quiet for its size, but that it achieves a beneficial redistribution of noise energy to lower frequencies than those expected from such a body as a result of the compliance of its wing. Although the leading-edge comb and trailing-edge fringe did produce significant aerodynamic effects, their removal had negligible impact on the sound generation.

Apparently, the first true airframe noise measurements were obtained by Hubbard and Maglieri (ref. 6) during a study of the aural detectability of aircraft in 1958. Their data included noise spectra produced by a two-place liaison airplane during a power-off glide with propeller and engine nonrotating. The overall noise level observed with the aircraft velocity 28.8 m/sec (56 knots) at an altitude of 22.86 m (75 ft) was 65 dB.

The first large-scale study of the airframe noise produced by actual aircraft is that reported by Smith et al. (ref. 7). They performed a series of noise measurements during flyovers of three gliders, a Schweizer 2-32, a Schweizer 2-33, and a Libelle. The data reported were the maximum overall sound pressure levels and corresponding spectra obtained from a single microphone as nearly as possible directly beneath the flight path. The early tests attempted to employ observers and onboard instrumentation to determine altitude and velocity. However, this system was shown to be inaccurate. Thus, theodolites were employed in the later tests. These theodolite data, in which the authors had confidence, are given in table I.

In 1970, Healy (ref. 8) undertook a study of the airframe noise radiation produced during unpowered gliding flyovers of five aircraft. The aircraft were a Prue-2 sailplane, Cessna 150, Aero Commander, Douglas DC-3, and a Convair 240 with gross weights ranging from 5783 to 173 472 newtons (1330 to 39 000 pounds). Since the aircraft were in a gliding mode while the data were taken, the results are applicable for aerodynamically "clean" configurations, that is, no flaps or gear extended, with the exception of the Cessna, which had a nonretractable landing gear.

The noise measurements were made by two microphones positioned 30.5 m (100 ft) to either side of the target flight path on a line perpendicular to it. These two measurements were averaged after data analysis to account for deviations in the flight path. Composite one-third octave spectra were obtained for each flyover by employing the maximum root-mean-square value observed in each third octave band during the flight. This, of course, implies that the values in the composite one-third octave spectra did not necessarily occur at the same time. However, the effect was small since the overall sound pressure level was observed to peak when the aircraft was overhead and the composite spectra agreed well with the peak levels.

The nominal altitude of the flyovers was 152.4 m (500 ft) whereas the actual altitudes measured by onboard instruments ranged from 97.5 to 241 m (320 to 790 ft) for the four powered craft and from 46 to 109 m (152 to 357 ft) for the glider. Data on overall sound levels obtained from these tests are given in table II normalized to an altitude of 152.4 m (500 ft). This normalization makes the reasonable assumption that the overall sound power level varies inversely with the square of the altitude and includes a correction for atmospheric absorption based upon the procedure recommended in reference 9.

A nondimensional airframe noise spectrum representative of all these aircraft is shown in figure 4. This spectrum was obtained by smoothing all the measured spectra to remove any peculiarities due to antenna, airframe protrusions, etc., normalizing each spectra by its overall sound pressure level and a characteristic frequency, and then averaging the individual spectra together. The deviation of the spectra from the average is also shown in figure 4. The characteristic frequency was obtained by assuming the peak of the spectra to occur at a constant Strouhal number. Healy employed the relation

$$f_{max} = N_{Str} \frac{V}{t_w}$$

where

f_{max} frequency of spectral peak, Hz

N_{Str} Strouhal number

V aircraft speed

t_w wing thickness approximately equal to 11 percent of the ratio of wing area to wing span

and found the Strouhal number to be approximately 1.30 although he notes that this value is 18 percent too high for large aircraft (the C-5A) to be discussed later and may not, indeed, be universal. However, it does provide a reasonably accurate means of assessing the frequency distribution of the clean airframe noise.

The five aircraft study was followed in 1973 by Gibson (ref. 10) with a program to evaluate the airframe noise produced by the C-5A Galaxy in order to extend the data into the weight range likely to be occupied by the next generation of transport aircraft. Measurements of the overall sound pressure level and spectra produced during low altitude (nominally 100 m) flyovers were made with the engines throttled back to flight idle. This aircraft could not be flown unpowered because of safety considerations. However, the airframe noise could still be seen through a low-frequency window below the fan noise

region since the airframe noise was greater than 10 dB above the low-frequency jet noise.

One of the major goals of this study was to evaluate the effect of a dirty configuration (wheels and flaps extended) on the airframe noise produced. The peak overall sound pressure levels measured are shown in table III, both clean and dirty, for various percent flap deployment as a function of altitude and velocity obtained from onboard instrumentation. A series of tests in addition to those shown were made. However, these tests were made at very low altitudes which Gibson felt were too far in the near field of the source since inconsistent results were obtained. Figures 5 and 6 portray the peak third octave band spectra for both the clean and dirty configurations. Although the absolute levels cannot be compared because of different altitudes and velocities, it can be seen that although the power spectrum of the clean configuration peaks at a frequency which can be shown to be related to the airfoil, the dirty configuration fills in the low-frequency valley. In other words, extension of the landing gear and flaps generates significant low-frequency noise. It was also shown by narrow-band analysis that the airframe noise for both clean and dirty configurations consisted not of a broad-band spectrum but more of a series of narrow-band tones as illustrated in figure 7.

The conclusions of this study were that the primary sources of airframe noise, at least for the C-5A, were the wings, landing gear, and wells. In some cases, trailing-vortex noise and noise produced by mechanical vibration were also observed. Boundary-layer noise was not evident. The effect of flap extension also was not significant. Gibson speculated that this was due to the fact that the C-5A has several short flap sections rather than the one long flap found on most aircraft. This design he felt could produce uncorrelated sources and thus might not be a universal result. The total effect of changing from a clean to dirty configuration proved to be about 4 dB in OASPL at an altitude of 27.7 m and a velocity of 102.5 m/sec.

In December 1972, a study was undertaken by NASA Flight Research Center to measure the airframe noise produced by an Aero Commander with gear down and various flap settings. Overall sound pressure levels measured by flush mounted microphones during several unpowered landing approaches are given in table III. The results of this study indicated that the flaps generate low-frequency noise and that the directivity characteristics of the airframe noise are somewhat dependent upon the flap settings. A beneficial effect of the flaps was also noted for this aircraft. As can be seen in figure 8, extension of the flaps actually lowered the noise power at low frequencies, although the high-frequency noise was increased. This condition was apparently due to a changed flow environment over the landing gear.

The NASA Flight Research Center has also run tests on the JetStar to evaluate the effects of landing gear and flaps. The measurements were made during landing approach

with the engines at idle power. Although no absolute levels of airframe noise could be obtained, relative effects could be evaluated. Flap noise could not be observed until the deployment reached 50 percent. Again this noise was found to occur at very low frequencies. The major noise production was found to be due to the landing gear, as shown in figure 9. Significant increases in spectral levels above 50 Hz were observed when the landing gear was lowered.

This work has recently been reported by Lasagna and Putnam (ref. 11). In addition to the results cited previously, one unpowered landing of the Jet Star was accomplished. These data are included in table III. When viewed on an EPNdB basis, the dirty airframe noise of this aircraft lies 11 EPNdB below its FAR-36 noise level. This paper also includes the first published sideline noise measurements which were obtained by a linear array of microphones perpendicular to the flight path.

In addition to the tests discussed earlier, The Boeing Company has conducted airframe noise studies of the 727 and 747 aircraft. The results (ref.3) indicate that the airframe noise levels lie about 8 EPNdB below the current FAR-36 standards, that is, 96 and 100 EPNdB on landing approach for the 727 and 747, respectively, and that flaps and landing gear can contribute as much as 10 to 12 EPNdB to the total approach noise.

Finally, Burley (ref. 12) has recently concluded a preliminary program for measurement of the airframe noise produced by an F-106B. This is a delta-wing craft designed for supersonic flight which was modified to carry two underwing nacelles. Airframe noise measurements were made during flyovers at a speed of Mach 0.4 and an altitude of 91 m (300 ft) with the engine at flight idle. It was argued that at this condition, the engine noise was at least 10 dB below the airframe noise except at low frequencies. The data are shown in table III. The interesting result of this study was that although the peak frequency was predicted by a Strouhal number of 1.1 based upon airfoil thickness, the airframe noise was much lower than would be expected for a conventionally designed aircraft at the same weight and Mach number. This phenomenon was attributed by Burley to the differences in aspect ratio, lift coefficient, and speed.

The major conclusions that can be drawn from the total aircraft studies conducted thus far seem to be that although the airfoil, landing gear, and wheel wells are the major contributors to the airframe noise, their relative contributions, as well as those of the flaps, depend significantly upon the particular characteristics of the individual aircraft. This result is a disquieting one in terms of prediction in that the noise is presumably not a simple universal function of the aircraft's weight, velocity, aspect ratio, etc. However, in terms of noise reduction the result is encouraging in that if the peculiar characteristics which produce beneficial effects can be understood, they may be widely employed to reduce the airframe noise levels.

Component Studies

The second method by which airframe noise may be assessed is by consideration of the individual aircraft components which radiate the sound. This approach takes on particular importance because of the evidence that the noise cannot be totally described by the gross parameters (weight, velocity, etc.) of an aircraft. Thus, unique characteristics of a particular aircraft must be examined.

The theory which underlies the sound generation of these individual components, as well as the total aircraft, is that developed by Curle (ref. 13). He extended Lighthill's (ref. 14) original work to include the case where solid boundaries are present in the flow field. The results indicate that in addition to reflecting and diffracting any sound which may already be present, the solid boundaries introduce a resultant dipole field over their surface. The far-field sound pressure generated by this additional mechanism is related to the fluctuating force acting on the surface and its intensity depends upon a characteristic velocity over the surface to approximately the sixth power. Thus, it is analogous to an acoustic dipole. The following discussion of individual components may be evaluated in the light of this theoretical background.

Airfoils. - Noise radiation by the airfoil itself was indicated by the total aircraft studies as the major contribution to the airframe noise. Fortunately, there has been a considerable amount of work on aerodynamic noise generation due to airfoils. Thus, although the following review will be chronological, it will not attempt to be exhaustive because of the vast amount of literature which exists. Only the major points of interest are discussed.

In 1959, Powell (ref. 15) considered the aerodynamic noise produced by subsonic flow over a rigid flat plate at zero incidence. On the basis of an image argument, he concluded that the pressure fluctuations on a plate are incapable of producing acoustic energy except in strips adjacent to the edges. This phenomenon, which he called "edge noise," was related to a physical picture of flow moving around the edge from one side to the other. If this idea is conceptually extended to an airfoil, it can be seen that the pressure difference between the upper and lower surfaces would produce a significant flow of this type and could create considerable noise.

This theory has been amplified by Powell (ref. 16), Ffowcs Williams (ref. 17), and Ffowcs Williams and Hall (ref. 18) on the basis of Curle's work (ref. 13). They have shown that the noise radiated from a turbulent flow adjacent to an infinite plane boundary reduces to quadrupole radiation with a reflection factor dependent upon the wall admittance. Near the edge of a finite surface, the infinite plane boundary condition is violated and dipole radiation results. These results support the experimental observation that direct radiation from turbulent boundary layers is a negligible source of airframe noise.

In 1964, Sharland (ref. 19) considered the ways in which fluctuating forces might be developed on a surface. He identified three possible mechanisms: the pressure field arising in the turbulent boundary layer over the surface, force fluctuations due to vorticity shed from the surface, and the action of any turbulence present in the incident stream. In order to evaluate these sources, a simple experiment was devised which consisted of an isolated flat plate in a flow. The directionality of the radiated sound was found to be nearly that of a simple dipole with axis perpendicular to the plate. On the basis of this work, Sharland concluded that the boundary-layer noise is negligible. The major source is vortex shedding at the trailing edge which produces lift fluctuations on the plate. Also, if there is significant turbulence in the incident stream, the noise levels are greatly enhanced.

The work of Clark and Ribner (ref. 20) in 1969 was concerned with obtaining a semiquantitative verification of Curle's theory. They correlated the far-field sound produced by an airfoil in a turbulent stream with the fluctuating lift on its surface and concluded that the theory is correct in that a surface can be an active generator of sound of the magnitude predicted by Curle.

In 1971, Dean (ref. 21) conducted a study which involved measurements of the surface pressures and far-field sound produced by several airfoils placed in a stream with an 8-percent turbulence level. The overall sound pressure levels were found to be independent of airfoil chord and angle of attack and to vary as the sixth power of the flow velocity. The acoustic signals on the two sides of the airfoil were coherent and 180° out of phase. The spectral distribution of the radiated sound was determined to depend both on flow speed and chord, the larger chords producing more low-frequency and less high-frequency sound. Furthermore, the spectral shape is scaled with the reduced frequency fc/U where f is the measured frequency, c is the chord length, and U is the flow speed. Dean also introduces the idea of employing the Sears' theory (ref. 22) as a transfer function to calculate the lift fluctuations from a knowledge of the incoming turbulence. This concept has been mentioned by others previously, including Sharland (ref. 19).

Mugridge (ref. 23) developed a theory of acoustic radiation from airfoils for particular frequency ranges by considering the integrated force on the airfoil to be a point dipole. An estimate of the controlling function in this theory, the power spectrum of the surface pressure fluctuations, was obtained from a series of experiments involving a two-dimensional airfoil in a wind tunnel. These spectra were found to be a function of the normalized frequency $f\delta/U$ where δ was the boundary-layer thickness at the trailing edge of the airfoil. Although it was difficult to obtain clean acoustic measurements in the facility employed, predictions of this theory were in reasonable agreement with the measured results.

Clark (ref. 24) considered airfoil noise on the assumption that sound generation could be related to wake properties of the airfoil. He collected data from several different airfoils placed within the potential core of a jet in an anechoic room and found that the peak energy in both the radiated sound and the normal component of turbulent velocity in the wake occurred at the same frequency. This result tends to confirm the hypothesis that the wake-generated lift fluctuations are significant contributors to the far-field sound. A typical spectrum of the radiated sound measured normal to the airfoil is shown in figure 10. The low-frequency sound power (4 to 8 kHz) Clark attributed to the low level of incoming turbulence (0.5 percent). The high-frequency sound power was evidently produced by the wake-induced fluctuations. As the incidence angle was changed from the nominal, it was observed that the spectrum became broader. In figures 11 and 12, the peak spectral frequencies produced by an airfoil with two different values of camber are plotted as a function of flow speed. On the basis of these results, Clark concluded that no simple Strouhal relation for the peak frequency exists. Clark also extended Curle's theory in order to predict the sound spectrum based upon knowledge of the wake properties. The equation obtained is

$$p^2(r,f) = \frac{4f^2\rho_o{}^2U^4\ell_y{}^2\ell_z{}^2}{a_o{}^2r^2g^2}\left[\frac{v(f)}{U}\right]^2\left[16\pi^2\left(\frac{f\ell_x}{U}\right)^2 + \left(\frac{U_c}{U}\right)^2\right]$$

where

$p(r,f)$	Fourier transform of acoustic pressure
ρ_o	density
U_c	mean convection velocity in wake
g	acceleration of gravity
a_o	speed of sound
$v(f)$	Fourier transform of normal turbulent velocity
ℓ_x	streamwise correlation length
ℓ_y	normal correlation length
ℓ_z	spanwise correlation length

This equation predicted levels in reasonable agreement with the measured data. However, there is a problem in obtaining values for the relevant correlation lengths.

In 1972, Paterson et al. (ref. 25) ran a series of tests on NACA 0012 and 0018 two-dimensional airfoils and an NACA 0012 finite-span airfoil in a low-turbulence acoustic tunnel. The result of this study was that at Reynolds numbers and angles of incidence for which a laminar boundary layer existed on the pressure surface of the airfoil, the vortex shedding produced a discrete tone in the far-field sound spectrum, and at certain speeds, a secondary tone was also present. This behavior is shown in figure 13. The overall trend in the frequency of these tones was predicted by the relation

$$f = \frac{0.011U^{1.5}}{(c\nu)^{0.5}}$$

where ν is the coefficient of kinematic viscosity. This equation is based upon the notion that the laminar boundary-layer thickness is the controlling parameter in a Strouhal relationship. However, there was a ladder-type behavior of the frequencies at a lower power of velocity. It was further observed that the surface pressure on the airfoil showed a strong signal at the same frequency as the far-field tone. This condition suggests that the origin of the multiple tones and ladder behavior is aerodynamic and is possibly connected with the feedback interaction of the wake-induced velocity field on the airfoil itself. Interestingly, a trip wire which destroyed the laminar boundary layer either removed the tone or submerged it in the boundary-layer induced noise. Effects of finite span and airfoil thickness were small. It should be noted that the vortex-shedding phenomenon discussed in this study is apparently not present at high Reynolds numbers (greater than 2×10^6 for angles of attack less than 16°) based upon airfoil chord.

The same year (1972), Hayden (ref. 26) undertook a review of the then current status of prediction techniques for interaction of flow with rigid surfaces. He begins the review with the observation that a surface in a flow can act as a different type of source in the separate acoustic regimes. In particular, he notes that a body will appear as a point dipole when $K\Lambda << 1$, a "half-baffled" edge dipole when $K\Lambda \gtrsim 1$, and a "fully baffled" dipole for radiation by "acoustically fast" disturbances ($K_0 \leqq K$) such as may be found in a turbulent boundary layer. Here K is the acoustic wave number equal to ω/a_0 where ω is the circular frequency of the radiated sound, Λ is the characteristic dimension of the body (such as chord length), and $K_0 = \omega/U_0$ where U_0 is the convection speed of the disturbance. However, he notes that no clean experimental data on direct radiation from a boundary layer exist from which this latter source could be evaluated. Some work in this area has been reported by Hubbard (ref. 27), who employed a rotating disk.

On the basis of his review, Hayden concluded that the trailing-edge sound power levels generated by an airfoil could be predicted by the expression

$$\text{OAPWL} = 10 \log (\delta W_c U^6) - 22.0 \qquad (\text{dB re } 10^{-12}\ \text{W})$$

where W_c is the wetted span of the airfoil and that the spectrum peaks at a Strouhal number of $f\delta/U = 0.04$. Thus, the spectral levels can be obtained from the universal spectrum given in figure 14. Further, he found that the wake-generated sound power level obeyed the relation

$$\text{OAPWL} = 10 \log (\delta_W W_c U^6) - 26.5 \qquad (\text{dB re } 10^{-12}\ \text{W})$$

where δ_W is the wake thickness and that the spectrum peaks at a Strouhal number of $f\delta_W/U = 0.25$. Thus, again the spectral levels can be obtained from a universal spectrum as shown in figure 15. When these recommended techniques are applied to data which Hayden obtained in an earlier study (ref. 28), the comparison shown in figure 16 results. The purpose of this study was to evaluate the effect of leading-edge serrations on the aerodynamic sound radiation from an airfoil. Note that the serrations completely removed the wake-generated noise.

Hayden also recommends relations for the prediction of the far-field overall sound pressure levels. These are

$$\text{OASPL}(r,\theta,\psi) = 10 \log \left(\frac{\delta W_c U^6 \sin^2 \theta \cos^2 \psi/2}{r^2}\right) - 17.5$$

for the trailing-edge noise and

$$\text{OASPL}(r,\theta,\psi) = 10 \log \left(\frac{\delta_W W_c U^6 \sin^2 \theta \cos^2 \psi/2}{r^2}\right) - 22.0$$

for the wake-generated noise in dB re 20 $\mu N/m^2$ where θ and ψ are angles in a spherical coordinate space.

In 1973, Siddon (ref. 29) employed the cross correlation between the far-field sound and the fluctuating pressures on circular plates placed in a jet flow to determine the surface distribution of dipole sources. He found distinctively different distributions depending upon angle of attack and level of incoming turbulence. Further, his results did not support the contention that the noise generation occurs primarily near the edge of the surface. Correlation areas were also found to be a small fraction of the surface area.

Hersh and Meecham (ref. 30) studied the directivity pattern of a small airfoil placed in an anechoic jet facility. The contributions of the lift- and drag-induced fluctuating forces were separated and compared with the dipole directivity predicted by Curle. An example of the comparison for a particular third octave band is shown in figure 17. The agreement was close enough to provide experimental verification of this aspect of Curle's theory.

This work was extended by Davis (ref. 31), who linearized equations for a thin wing in a turbulent flow. On the basis of these relations, he was able to show that the far-field noise can be predicted if only the distribution of wake velocity is known and that the peak of the broad-band sound generated occurs at a Strouhal number of 0.4 based upon the longitudinal scale of transverse turbulent fluctuations. Furthermore, his theory indicates that the dipole radiation pattern predicted by Curle should be modified by a term involving the velocity over the airfoil. This modification gives excellent agreement with an actual directivity pattern measured by Hersh and Hayden (ref. 28) as shown in figure 18.

Two interesting studies involving cross correlations of surface pressures on airfoils with far-field acoustic pressures have recently been published. Sunyach et al. (ref. 32) found the peak cross correlation to be very high (≈ 0.80) and noted that there was a slight drift in the time delay at which the positive maximum occurred. The nearer a pressure transducer was to the trailing edge of the airfoil, the closer the time delay became to that corresponding to the time taken for an acoustic wave to travel from the trailing edge to the far-field microphone. Paterson, Amiet, and Munch (ref. 33) performed a similar experiment and determined that the time delay actually corresponds to the time taken for a mass of fluid to convect from the pressure transducer to the trailing edge plus the time taken for sound to travel from the trailing edge to the far-field microphone. This experiment is presently the best experimental confirmation of the importance of the trailing edge as a source of dipole sound.

Finally, in 1974, Tam (ref. 34) has offered an explanation of the unusual behavior of the discrete tone generation by isolated airfoils which was observed by Paterson et al. (ref. 25). On the basis of stability theory, he has shown that it is possible that the acoustic field and wake flow interact in a self-excited feedback mechanism which produces the tones. This theory predicts tones given by the relation

$$f = 11.8nU^{0.8}$$

for velocity in feet per second for every integer n. Comparison of this relation with Paterson's data is shown in figure 19.

The existence of these tones exemplifies a problem in airframe noise which acousticians have rarely had to contend with – that of Reynolds number dependence. Such tones have been noted at model scale and on gliders. However, they have never been observed on a full-scale aircraft where the flow over the wing is highly turbulent and Reynolds numbers in the range of many millions typically occur. Thus, the question of scaling model results must be thoroughly investigated.

Wheel wells.- As an aircraft alters its cruise flight configuration to that for landing, a number of component noise sources are introduced. Certainly predominant among these

is the wheel-well landing-gear combination. Because of the very sophisticated flow field of the cavity (wheel well) alone, no in-depth research has been attempted on the combination. Therefore, this section will concern itself solely with a basic review of research on the acoustic response of a cavity in an aerodynamic surface.

Historically, the first apparent mention of this phenomenon came in 1896 by, most fittingly, Lord Rayleigh (ref. 35). He noted that he could achieve a very strong resonant tone by blowing across the end of a closed tube; however, he clearly characterized the next 50 years of significant work on the subject when he confessed his ". . . ignorance as to the mode of action of the wind . . . ."

In 1952, concern over the pressure loadings in aircraft bomb bays led to many serious investigations. Most significant of these was by Norton (ref. 36) who noted that dependent on velocity, high-intensity periodic pressure fluctuations could be generated within the cavity. He also discussed the use of a spoiler system which gave significant reductions in the magnitude of the periodic oscillations. This system will be discussed further.

One of the first major works concerned with the acoustic radiation from a cavity was by Krishnamurty (ref. 37) in 1955. He investigated two-dimensional shallow rectangular cutouts and reported very intense acoustic levels in high-speed flow. At a particular Mach number, the predominant frequency was shown to be inversely proportional to cavity length in both laminar and turbulent flows. (See figs. 20 and 21.) In the turbulent case two tones dominated, the one that is higher in frequency being of the same order as the laminar tone. He noted also that the radiated field was weaker with a turbulent boundary layer ahead of the gap than with a laminar layer. His conclusion was that the basic phenomenon may be associated with vortex motion and its relation to an unstable, separated, boundary layer.

At this same time, Roshko (ref. 38) presented the first detailed analysis of the pressure and velocity fields within a cavity of varying depth. The data suggest the strong tendency for a cavity at a length-depth ratio of $0.87 < L/D < 2.0$ to form a stable vortex system. This finding is further supported by Wieghardt (ref. 39), who offered visual evidence of the same phenomenon. For L/D values other than these, nonperiodic intermittencies in both pressure and velocity were noticed. These variations appeared to be due to the flow alternating back and forth between two possible stable states. This behavior is clearly shown in figure 22(a) which presents measurements of the pressure coefficient obtained during a traverse of the cavity. Figure 22(b) depicts the stable vortex system with low pressure at the center of the walls and high pressure in the corners and figure 23 indicates that as L/D increases, the vortex system weakens.

Harrington (ref. 40) studied flow excitation of the acoustic resonance of a cavity. He noted that as the velocity was increased, several regimes of discrete oscillations were

produced. However, for any particular aperture and cavity volume, these oscillations tended to conform to the same Strouhal number,

$$N_{Str} = f_N \frac{L}{iU} \qquad (i = 1, 2)$$

with f_N equal to the natural frequency of one of the modes of resonance of the cavity.

In a later work, Harrington and Dunham (ref. 41) attempted to detail the strong interaction between shear flow fluctuations and the oscillations within a cavity. They noted that if a sinusoidal normal displacement fluctuation is induced by a flexible wall in the cavity, a normal velocity flow in the opening is obtained. The fluctuating velocity field at the mouth causes the formation of vortices which induce the turbulent mixing region to curve in and out of the cavity. Thus, they concluded that the internal pressure fluctuation caused by this instability phenomenon could be the excitation mechanism of resonance.

Plumblee et al. (ref. 42) ignored the determination of the forcing mechanism with the hypothesis that regardless of what it is, the phenomenon of sound generation in a cavity is basically that of an enclosure responding in its normal acoustic mode. They showed that by assuming a rectangular cavity of arbitrary dimensions with five walls terminating in an infinite impedance and a sixth terminating in the radiation impedance of the opening, the characteristic response function of the cavity can be derived; however, the general solution is one of considerable complexity. Based on the assumption that the response is predominantly in the depth mode for cavities of $L/D < 1$, as has been experimentally indicated, they obtained the much simplified solution for the pressure amplitude response

$$\frac{p}{p_m} = \left[(R \sin KD)^2 + (Q \sin KD - \cos KD)^2\right]^{1/2}$$

Here p_m is the peak forcing pressure at the open end of the cavity. The variables R and Q are very complicated functions of the cavity dimensions, Mach number, and frequency.

In conjunction with this theoretical work, extensive experimental evaluation was done over a small rectangular cavity. A comparison between the theoretical and experimental results for a cavity with $L/D = 0.5$ is shown in figure 24. Note that the theoretical response shown in figure 24(a) predicts amplification peaks at approximately 3 and 9 kHz for the Mach number range $0.1 \leqq M \leqq 0.9$. The experimental response for a Mach number of 0.4 shown in figure 24(b) agrees with the prediction very well. This figure also indicates a significant low-frequency, random component present in the response. Further experimental and theoretical comparisons indicated that for cavities of $L/D > 2$, the response is predominantly in the lengthwise modes.

In 1963, Maull and East (ref. 43) produced evidence of three-dimensional flow in cavities with high aspect ratio. This can be seen in the typical spanwise and chordwise pressure distributions shown in figures 25(a) and 25(b), respectively. By varying the L/D value, the distribution significantly changes as in figure 26. It is of interest to note the relative two-dimensionality exhibited by the values of $L/D = 1.0$ and $L/D \leqq 0.39$. Recall that Roshko (ref. 38) found fluctuations in the flow for $L/D > 2.0$. It is possible that such phenomena are associated with the unstable three-dimensionality of the flow patterns.

Another experimental study of the pressure distribution in cavities was performed by Rossiter (ref. 44) in 1964. Working with cavities of large L/D values, he concluded that the random response component predominates in the shallow cavities ($L/D > 4$) and the discrete responses in the deeper ones ($L/D < 4$). Rossiter felt that the periodic components might cause standing wave patterns and were due to an "acoustic resonance within the cavity excited by a phenomenon similar to that causing edge tones." In an attempt to reduce these discrete pressure fluctuations, various spoilers (fig. 27(a)) were affixed to the edge of the cavity. Their effect is to alter the oncoming flow at the edge of the cavity by inducing flow turbulence and a boundary-layer thickening as it expands over the cavity opening. The resulting reduction in the strength of the shear flow periodic pressure fluctuations is shown in figure 27(b). Recall that the results of K. Krishnamurty (ref. 37) with the turbulent boundary layer support this basic explanation as does Rossiter's work on boundary-layer thickness. He found that an increase in the oncoming thickness, relative to the cavity length, tended to decrease the magnitude of both the random and periodic components. This result has been confirmed by other investigators.

As in Norton's work (ref. 36), the precise mechanism was not suggested; however, recent work by K. Krishnamurty may shed light on this topic. Applying a stability analysis to the oncoming flow field, it was shown that a turbulent boundary layer altered the relative structure and expansion characteristics of the shear layer. This alteration would reduce the shear layer excitation of the cavity acoustic field.

Rossiter further noted that there was usually only one peak in the amplitude spectra of deep cavities, whereas for the shallower ones there were usually two or more peaks. It may be of interest to compare this finding with a similar one by K. Krishnamurty, whose results related only to shallow cavities. These dominant frequencies are plotted for two cases of cavity dimensions (fig. 28). A Strouhal relation to represent these frequencies was derived as

$$N_{Str} = \frac{(i - \lambda_v) U_R}{(1 + MU_R)} \qquad (i = 1, 2, 3, \ldots)$$

It was shown through a physical argument and by shadowgraph measurements that λ_V represents the mean vortex spacing over the cavity and U_R is the ratio of the speed at which the vortices travel over the cavity to the free-stream velocity U. For cavities of $L/D \leqq 4$, the value of λ_V is 0.25 and U_R tends to vary from 0.35 to 0.66.

East (ref. 45) noted in 1965 that generally, for a given cavity, a resonant tone is generated at only one or two values of velocity. However, if the cavity received broad-band acoustic energy from the turbulent shear layer, it would be expected that the cavity resonant frequency be excited over a large (very large) range of free-stream velocities. Since it is not, the inference therefore is that a feedback mechanism exists such that under certain conditions the shear layer oscillations are amplified by acoustic coupling between the shear layer pressure fluctuations and the cavity modes. The resonant condition is defined than as "the condition under which the frequency of the acoustic response of the cavity is the same as the dominant frequency of the shear feedback system." To verify this, a plot of the cavity resonant response frequencies as predicted by the theory of Plumblee et al. (ref. 42) is shown in figure 29. These frequencies are compared with the values given by the Strouhal relation of Rossiter (ref. 44) for the excitation oscillations present in the shear layer. East felt the good comparison between the results of the two methods tends to support his feedback hypothesis.

In 1970, Covert (ref. 46) performed a stability analysis on the pressure oscillations induced in a cavity by the shear flow. A relation representing the interaction of the outer and inner perturbation potentials provides a description of the onset of instability. It was found that for a given cavity, it is possible to calculate a critical velocity below which there is no oscillatory motion. The theory indicates that the frequency of these fluctuations corresponds closely to the natural response frequency of the cavity which is substantiated by past experimental evidence.

Heller et al. (ref. 47) performed a number of experiments on shallow cavities, $L/D \geqq 4$, at high subsonic and supersonic velocities. The flow-induced pressure fluctuations were measured within the cavity and on the leading surface. Figure 30 indicates the different effects of laminar and turbulent boundary layers on the acoustic response of the cavity. These results confirm the conclusion of Krishnamurty (ref. 37).

Thermocouple measurements taken at the cavity bottom surface allowed calculation of the sound speed within the cavity. It was found that for the larger velocities, $M > 3$, a substantial difference existed between it and the sound speed in the outer uniform flow. This difference indicates that the Strouhal relation of Rossiter (ref. 44) may be in error for it is partially based on the assumption that the two speeds are equal for all velocities. Based on this data, Heller et al. derived a modified form of the Strouhal relation:

$$N_{Str} = \frac{i - \lambda_V}{\dfrac{M}{\left[1 + \dfrac{(\gamma_r - 1)M^2}{2}\right]^{1/2}} + \dfrac{1}{U_R}} \qquad (i = 1, 2, 3, \ldots)$$

where γ_r is the ratio of specific heats. The comparison between this relation and Rossiter's relation is shown in figure 31.

In a 1973 theoretical investigation, Bilanin and Covert (ref. 48) derived a formula predicting the cavity excitation frequencies as a function of Mach number and cavity geometry. The result,

$$N_{Str} = \frac{i - (3/8 + \phi/2\pi)}{\left(U_R M \dfrac{a_o}{a_c} + 1\right)} \qquad (i = 1, 2, 3, \ldots)$$

where a_c is the speed of sound in the cavity and ϕ is the lag of the vortex sheet displacement, is in the form of the equation of Rossiter (ref. 44). Thus, his empirically derived constants are more fully explained by the analysis. The U_R term is shown to be equal to $\omega/K_r U$ with K_r being the real part of the complex wave number in the flow direction. In Rossiter's work, the U_R corresponds to the ratio of the speed at which the vortices travel over the cavity to the free-stream velocity. Therefore, the convection speed may be calculated without the use of experimental measurements, as was previously required. The quantity subtracted from the integer i is a correction factor for edge effects. As earlier suggested by Heller et al. (ref. 47), a correction term is also included to adjust for the lower speed of sound within the cavity. These analytic results are in general agreement with experimental data. In conclusion, Bilanin and Covert (ref. 48) note that the instability of the shear layer as well as the interaction between the shear layer and the cavity's edge is needed for the discrete-frequency oscillations to be sustained.

Landing gear.- A third potentially important source of airframe-generated sound is due to the landing gear. On a modern aircraft, these gear can be mechanically very complex; however, the basic configuration consists of a strut with one or more wheels attached. The effect of the wheels may be computed in a manner similar to that employed for struts since the sound generated is due to the separated flow in the wake of the wheel. Thus, this section will be primarily concerned with the effect of a strut in flow.

It might be noted that the directivity of the dipole source associated with a strut by Curle's theory (essentially normal to both the strut and the flow direction) is such that the sound generated by this source would not be important in most measurements of air-

frame noise. However, it is certainly feasible that the strut might act to induce oscillations in the associated wheel well. Thus, the aerodynamic flow field of the strut, as well as its sound generation, must be examined.

The sound produced by a wire in a flow field, known as the "Aeolian tone," is apparently one of the earliest observed acoustic phenomena. The first quantitative analysis of this tone was attempted by Strouhal in 1878 (see ref. 35, p. 412). Strouhal caused a vertical wire to rotate about a parallel axis and found the frequency of the tone produced to be independent of the length and tension of the wire. Within certain limits, the frequency could be expressed by the relation

$$f = 0.185 \frac{U}{d}$$

where d is the diameter of the wire and U is the speed of the flow over it. Further, Strouhal found that the wire need not vibrate, but, if the tone frequency happened to coincide with a fundamental resonance of the wire, the tone was greatly enhanced.

Rayleigh (ref. 35) made observations upon a string excited by a chimney draught and found that the vibrations were executed in a plane perpendicular to the direction of the wind. He also found the tone frequency to be dependent upon the Reynolds number of the flow, a fact which has been confirmed by subsequent researchers. Rayleigh felt that the Aeolian tone phenomenon was connected with instability of vortex sheets shed into the wake. However, he noted that a dynamical theory had yet to be given.

In 1911, Von Karman (see ref. 49, p. 130) presented his classic study of vorticity shed by a cylinder in a flow. He found that the vortices generated on either side of the body have opposite directions of rotation and under certain conditions form a particular geometrical pattern with vortices of the same sign alining in two parallel rows. On the basis of stability theory, he showed that the only stable configuration occurs when the ratio of the distance between these two rows to the distance between adjacent vortices had the value 0.2806. This particular configuration has come to be known as the "Karman vortex street."

In 1944, the problem of buffeting of aircraft tail surfaces caused Krzywoblocki (ref. 50) to examine the flow behind cylinders and airfoils. He found that the Strouhal frequency at which vortices are shed into the wake of a cylinder was directly related to the drag coefficient

$$N_{Str} = \frac{0.256}{C_D}$$

Since the drag coefficient is a strong function of Reynolds number, this relation allowed him to explain partially the behavior noted by Goldstein (ref. 51) shown in figure 32. He

also observed that in the range $10^2 < N_{Re} < 10^5$, the wake flow is periodic. Above this "critical Reynolds number," $N_{Re} = 10^5$, the wake becomes aperiodic.

In 1954, Roshko (ref. 52) made many flow measurements in the wake of circular cylinders. On the basis of this study, he concluded that the flow exhibited three regions: a "stable range" $40 < N_{Re} < 150$ where classical Karman vortex streets are formed which remain well defined for long distances downstream; a "transition range" $150 < N_{Re} < 300$ where the flow becomes unstable; and an "irregular range" $300 < N_{Re} < 10^5$ where the free vortices which move downstream are quickly obliterated and a turbulent wake formed. These three regions may be observed in figure 33 where Roshko compared his data with that of Kovasznay (ref. 53). In the irregular range, a predominant "tone" frequency is still observed for many diameters as shown by the spectra of figure 34.

The relation between the wake shedding frequency and the Aeolian tone frequency was examined by Gerrard (ref. 54) in 1955. He placed 20 cylinders in a planar array across a wind-tunnel section and measured the sound produced. The Strouhal frequency of the Aeolian tone agreed with the Strouhal frequency of vortex production as shown in figure 35. He also rotated a single cylinder about a parallel axis and found the sound generation to be dipole in character and to consist of harmonics as well as the Aeolian tone.

In 1956, Phillips (ref. 55) examined the dependence of the Aeolian tone on the fluctuating force which is predicted by Curle's theory. At Reynolds numbers between 40 and 160, he found that the fluctuating lift per unit length on a circular cylinder could be represented by the relation

$$f_\ell = 0.38\rho_o U^2 d \cos 2\pi f_v t$$

where f_v is the vortex shedding frequency and that the fluctuating drag can be written as

$$f_d = 0.04\rho_o U^2 d \cos 4\pi f_v t$$

Note that the drag is much smaller than the lift and occurs at twice the frequency.

The axial length scale of the force fluctuations was found to be very large for Reynolds numbers less than 100, but about 17d for $100 < N_{Re} < 160$. In this range the mean-square acoustic pressure $\overline{p}^2$ associated with the tone was found to be

$$\overline{p}^2 = 0.27 \cos^2 \theta \frac{\rho_o \ell d U^6 (N_{Str})^2}{a_o^2 r^2}$$

where θ is the angle between the direction of observation and the incident stream and ℓ is the length of the cylinder. At higher Reynolds numbers where the wake is turbulent, the same expression holds but the numerical constant reduces to about 0.037. This behavior can be seen in figure 36.

Phillips' conclusions were partially supported by Etkin et al. (ref. 56) in 1957. They found a tone having the same frequency as the wake which is produced by the fluctuating lift induced by shedding vortices of alternating sign into the wake. There is also a tone of twice the frequency associated with the drag pulse induced as each vortex is shed. The fluctuating lift produces a line dipole with axis normal to the stream while the fluctuating drag produces a line dipole with axis parallel to the stream. Further, the intensity of the drag dipole is much less than that of the lift. These conclusions are illustrated in figure 37. Thus, apparently the mean-square pressure should have a directivity given more nearly by $\sin^2 \theta$ than by the $\cos^2 \theta$ dependence assumed by Phillips (ref. 55).

In 1960, Fung (ref. 57) investigated the fluctuating lift and drag at Reynolds numbers above 10^5 where the wake is no longer periodic. He found the root-mean-square fluctuating lift and drag coefficients to be approximately 0.14 and 0.04, respectively, above $N_{Re} = 4 \times 10^5$. He also measured the power spectrum of the lift force, an example of which is shown in figure 38.

In 1961, Gerrard (ref. 58) reported measurements of the lift and drag fluctuations on a circular cylinder in the intermediate range of $4 \times 10^3 < N_{Re} < 10^5$. He found the magnitude of the root-mean-square lift coefficient to achieve a maximum of about 0.8 at $N_{Re} = 7 \times 10^4$.

The drag coefficient was much less than this. He also determined that the pressure is essentially in phase over one side of the cylinder and 180° out of phase with the other side. By applying dimensional analysis to Curle's equation, he found that the acoustic intensity at large distances from a cylinder of finite length in the plane of symmetry bisecting the cylinder at right angles could be given as

$$I \approx \frac{\rho_o}{a_o^3} \frac{\sin^2 \theta}{r^2} U^6 (N_{Str})^2 \overline{\ell}_c^{\,2} \overline{C}_L^{\,2}$$

where ℓ_c is a correlation length along the cylinder and C_L is the lift coefficient.

The same year, Roshko (ref. 59) continued the investigation of vortex shedding from cylinders for Reynolds numbers greater than 10^5. He found the interesting phenomena that although the flow was aperiodic for $10^5 < N_{Re} < 3 \times 10^6$, the flow became periodic once more. Roshko suggested that in this "transcritical" regime, the boundary layers on the cylinder separate in a turbulent state.

Much of the previous work was confirmed by Jones et al. (ref. 60), who measured mean drag and fluctuating lift on a cylinder in the Reynolds number range 3.6×10^5 to 1.87×10^7. This work is considered by many to contain the definitive experimental results on the subject.

Recently, Karamcheti and Ayoub (ref. 61) have attempted to determine the pressure fluctuations on a cylinder in a cross flow from a knowledge of the wake velocity characteristics. They have shown that with a certain minimal knowledge of this velocity field, the surface pressure, and, thus, the far-field acoustic radiation may be determined.

Finally, it might be mentioned that in 1969, Bazhenov et al. (ref. 62) considered the effect of surface roughness on the intensity and frequency of the vortex-generated sound. They found that covering a cylinder with either grooves or mesh reduced the sound generation as well as the fundamental frequency. The mesh worked somewhat better than the grooves.

PREDICTIVE TECHNIQUES

Total Aircraft Analysis

This section will present an analysis of airframe noise with the intent of developing a predictive technique, based upon readily determined parameters, which will be applicable to a wide range of aircraft. This objective is only partially obtainable. In order to develop a relation in terms of gross parameters, rather sweeping assumptions must be made; on the other hand, it has been shown that airframe noise can be dependent upon unique characteristics of the configuration of particular aircraft. However, with the caution that the result obtained should not be employed on configurations, for example, delta-wing aircraft, too much different from those in the data base from which it was derived, the analysis will proceed on the philosophy that engineering estimation must often be attempted without the aid of refined data.

The geometry relevant to the analysis is shown in figure 39. The aircraft is portrayed in a landing approach as the approach is of most concern in terms of airframe noise. However, the geometry is applicable for other flight modes as well. The X,Y plane corresponds roughly to the surface of the earth. At time t, the observer is at the position x_1,x_2,x_3 and the center of gravity of the aircraft is at the position y_1,y_2,y_3. The vector from the center of gravity of the aircraft to the observer position is $\vec{r}$ and is of magnitude r. The angle between the instantaneous flight path of the aircraft and its projection in the X,Y plane is α. The instantaneous velocity of the aircraft is $\vec{V}$, with magnitude V, and the angle between the vectors $\vec{r}$ and $\vec{V}$ is θ.

The airframe noise radiation from the aircraft is primarily due to the fluctuating forces acting on its surface. Such radiation has been studied by Lowson (ref. 63). He

has shown that the fluctuating force $\vec{f} = f_1, f_2, f_3$ at the point y_1', y_2', y_3' on the surface of the aircraft would produce an acoustic density

$$\rho' - \rho_o = \frac{x_i - y_i'}{4\pi\left(1 - M_r'\right)^2 a_o^3 r'^2}\left(\frac{\partial f_i}{\partial t} + \frac{f_i}{1 - M_r'}\frac{\partial M_r'}{\partial t}\right) \tag{1}$$

at the observer position in the far field. Here, M_r' and $\partial M_r'/\partial t$ are the instantaneous Mach number and normalized acceleration in the direction $\vec{r}' = \left(x_i - y_i'\right)$, respectively, and the Einstein summation convention has been employed. Thus, since the governing equations are linear, the total acoustic density produced by the entire aircraft can be written as

$$\rho_a(x_i,t) = \int_{\substack{\text{Surface}\\ \text{of}\\ \text{aircraft}}} (\rho' - \rho_o)ds \tag{2}$$

where the integrand must be evaluated at the retarded time $t' = t - \frac{r'}{a_o}$.

If a typical wavelength of the sound produced is large compared with a characteristic dimension of the source region, the effects of the retarded time differences in equation (2) may be neglected and the sound calculated as if from a point dipole. When the span is taken as the characteristic dimension and the Strouhal relation of Healy (ref. 8) is employed, this condition implies that the ratio of span to wing thickness must be less than about eight at a Mach number of 0.1. Thus, this condition could not be expected to be generally valid for an aircraft. However, in order to examine the gross dependence of airframe noise, it will be invoked. Under this assumption, equation (2) becomes

$$\rho_a(x_i,t) = \frac{x_i - y_i}{4\pi\left(1 - M_r\right)^2 a_o^3 r^2}\left(\frac{\partial F_i}{\partial t} + \frac{F_i}{1 - M_r}\frac{\partial M_r}{\partial t}\right) \tag{3}$$

where the F_i are the components of the total force acting on the aircraft,

$$M_r = \frac{x_i - y_i}{r} M_i = M \cos \theta$$

and

$$\frac{\partial M_r}{\partial t} = \frac{x_i - y_i}{r}\frac{\partial M_i}{\partial t}$$

where M_i are the components of the Mach vector $\vec{M} = \vec{V}/a_o$ and the right side of equation (3) must be evaluated at the retarded time $t - \frac{r}{a_o}$.

Note that equation (3) includes a term involving the acceleration of the aircraft. This term comes into play when the velocity of the aircraft is changing appreciably. However, in many instances, such as a level flyover ($\alpha = 0$) or a normal landing approach ($\alpha = 3^{\circ}$), the aircraft velocity is essentially constant. In such cases, this term may be neglected. By assuming such a case and noting the acoustic relation $p = a_o^2\rho_a$, the far-field acoustic pressure may be written as

$$p(x_i,t) = \frac{\dot{F} \cos \beta}{4\pi\left(1 - M_r\right)^2 a_o r} \tag{4}$$

where $\dot{F}$ is the magnitude of the fluctuating force acting on the aircraft and β is the angle between the fluctuating force vector and the observer vector $\vec{r}$. In decibels, this equation leads to

$$\text{OASPL} = 10 \log_{10} \frac{\overline{p}^2}{p_o^2} = 10 \log_{10} \left(\frac{\overline{\dot{F}}^2 \cos^2 \beta}{16\pi^2\left(1 - M_r\right)^4 p_o^2 a_o^2 r^2}\right) \tag{5}$$

where an overbar indicates a time average and p_o is a reference pressure. However, it should be noted that, because of the relative change between the aircraft and observer positions as the aircraft flies by, the acoustic pressure is a nonstationary stochastic process. Thus, the required time average must be accomplished in a short period which leads to high variability in the estimate.

Equation (5), which yields the far-field overall sound pressure level as a function of geometry and aircraft operating conditions, is only approximate in that it assumes that the entire aircraft may be treated as a point source. Further, it is not valid near $M_r = 1$, reflection of sound by the aircraft surfaces is partially neglected, and atmospheric propagation effects are not considered. However, it does emphasize the fundamental dependence of the far-field sound intensity on the mean-square fluctuating forces acting on the aircraft.

Unfortunately, the state of the art at the present time is not such that these mean-square fluctuating forces may be estimated with any degree of accuracy for an aircraft in a real atmosphere. Thus, it is necessary to introduce a degree of empiricism in order to develop a predictive technique. The empiricism involved in this study took the form of application of a regression analysis (ref. 64) to the aircraft flyover data tabulated in tables I, II, and III. These data were obtained during nominally level flyovers ($\alpha = 0$) with microphones essentially on the ground ($x_3 = 0$) and the aircraft approximately directly overhead ($\theta = \pi/2$, $r = h$) where h is the aircraft altitude. Furthermore, note that the only component of the fluctuating force which can be important in this application is that normal to the plane of the wings since the directivity pattern of the other two components is null directly beneath the aircraft. This component is labeled $\vec{L}$ in figure 39 and is

at an angle of π with respect to an observer directly below the aircraft in level flight. Thus, for this case, equation (5) becomes

$$\mathrm{OASPL}(h,\pi/2) = 10 \log_{10} \left(\frac{\overline{\dot{L}^2}}{16\pi^2 a_o^2 p_o^2 h^2} \right) \tag{6}$$

A linear regression analysis which minimized the mean-square error was utilized to estimate the mean-square fluctuating force by employing equation (6) and the assumption that

$$\overline{\dot{L}^2} \propto M^{\epsilon_1} \left(\frac{W}{\rho_o a_o^2 b^2} \right)^{\epsilon_2} \left(\frac{h}{b} \right)^{\epsilon_3} (AR)^{\epsilon_4} \tag{7}$$

where

W aircraft weight

b aircraft span

AR aspect ratio

and the ϵ_i $(i = 1, 2, \ldots)$ are arbitrary powers. The lift coefficient might also have been included in this relation. However, the value of this parameter is not readily available in all modes of flight. Thus, the lift contribution is absorbed by the weight and velocity dependence. The data employed were the clean aircraft values shown in tables I to III, with the exception of the F-106B, as well as some wide-body aircraft data of a proprietary nature. In all, 54 flights were included in the regression. The result of this analysis yielded the relation

$$\mathrm{OASPL}(h,\pi/2) = 10 \log_{10} \left[\frac{M^{3.47} \left(\frac{W}{\rho_o a_o^2 b^2} \right)^{0.62}}{\left(\frac{h}{b} \right)^{1.59} (AR)^{2.39}} \right] + 154.9 \tag{8}$$

in dB re 20 $\mu N/m^2$.

There are several interesting aspects to this equation. First, it predicts the entire range of data from 8.90 to 4.45×10^6 newtons (2 to 10^6 pounds) with a root-mean-square error of 2.63 dB. The results are portrayed in figure 40. Furthermore, most of error occurs because of the early glider and two-seater tests which were performed at low ratios of signal to noise. It these data are removed, the root-mean-square error reduces to 1.43 dB. Also, note that for equilibrium flight, weight must be equal to lift, that is,

$$W = C_L \left(\frac{1}{2} \rho_o V^2 \right) S$$

where S is the aircraft wing area. Thus, the equation predicts essentially a fifth-power dependence on velocity and a first-power dependence on wing area as well as the inverse second-power dependence on aspect ratio. Finally, the overall sound pressure level varies with altitude to the minus three halves rather than the minus two power. This variation is apparently an indication that the measurements were not made in the acoustic far field of the aircraft.

The data may be reanalyzed to force a squared dependence on altitude. When this is done, the equation

$$\mathrm{OASPL}(h,\pi/2) = 10 \log_{10} \left[\frac{M^{3.93}\left(\frac{W}{\rho_o a_o^2 b^2}\right)^{0.39}}{\left(\frac{h}{b}\right)^2 (AR)^{3.19}} \right] + 161.8$$

results. The root-mean-square error for this analysis increases to 2.84 dB. Note also that aspect ratio becomes a more important variable in agreement with the results of Healy (ref. 8).

It is of interest to analyze the data with the questionable glider and two-seater data removed. This set of 28 data points led to the relation

$$\mathrm{OASPL}(h,\pi/2) = 10 \log_{10} \left[\frac{M^{3.43}\left(\frac{W}{\rho_o a_o^2 b^2}\right)^{0.60}}{\left(\frac{h}{b}\right)^{1.83} (AR)^{3.03}} \right] + 161.8$$

with a root-mean-square error of 1.17 dB.

These equations are valid directly beneath the aircraft. In order to develop an equation which will predict the overall sound pressure level at any position with respect to a clean aircraft, it is necessary to assume the lift fluctuations to be always the primary source of far-field sound. This assumption is probably valid at least for angles γ near π, where γ is the angle between the normal to the aircraft's wings and the observer vector $\vec{r}$. When this assumption is employed, comparison of equations (5) and (8) yields the relation

$$\mathrm{OASPL}(r,\theta) = 10 \log_{10} \left[\frac{M^{3.47}\left(\frac{W}{\rho_o a_o^2 b^2}\right)^{0.62} \cos^2 \gamma}{\left(\frac{r}{b}\right)^{1.59} (AR)^{2.39} \left(1 - M_r\right)^4} \right] + 154.9 \tag{9}$$

This equation may be employed to predict the overall sound pressure level at any far-field position with respect to a clean aircraft under the constraints imposed above.

Extensive data on the far-field spectrum produced by such aircraft do not exist. Perhaps the most comprehensive analysis is that by Healy (ref. 8) which was discussed previously. This study developed the nondimensional spectrum shown in figure 4. From this spectrum, third octave levels produced by clean aircraft can be estimated from knowledge of the overall sound pressure level given in equation (9).

This broadband sound generation by a clean aircraft is apparently due to vortex shedding by the wing and should peak at a frequency related to the wing. From the study of airfoils presented earlier, it can be seen that the relevant Strouhal parameter is the thickness of the boundary layer at the trailing edge of the wing. However, this parameter cannot be readily obtained. In an attempt to develop a Strouhal relation in terms of gross parameters, Healy obtained the expression

$$f_{max} = 1.3 \frac{V}{t_w}$$

where t_w is the wing thickness which can be crudely related to the ratio of wing area to wing span. Although it has been observed that $N_{Str} = 1.3$ is not universal, it is reasonably close for most common aircraft. However, note that this relation could not be expected to be accurate for highly tapered wings for which the fundamental frequency would vary over the span.

It must be observed that this relation was developed from measurements directly below the aircraft. For other positions this relation must be modified to account for the Doppler shift, that is,

$$f_{max} = \frac{1.3V}{t_w(1 - M \cos \theta)} \tag{10}$$

where θ must be interpreted as the average angle between the observer and flight path during the interval over which the sound pressure level is averaged. Equation (10) in conjunction with equation (9) and figure 4 can be employed to provide engineering estimates of the spectral decomposition of far-field sound pressure levels generated by the nonpropulsive sources of an aircraft in the clean configuration.

The question now arises as to what may be done when the aircraft is not in a clean configuration. It is apparent from the data shown in table III that the additional sound generation produced by changing to a fully dirty configuration (that is, flaps and landing gear fully extended) can amount to an increase in overall sound pressure level of approximately 5 dB for normal approach altitudes and velocities. This additional sound generation can appreciably increase the low-frequency spectral levels. However, it is equally apparent from the total aircraft studies that this source of noise is highly sensitive to the configuration. Thus, it is not feasible to attempt a prediction on the basis of gross parameters as has been developed for the clean configuration airframe noise. For such

cases, it is necessary to take a more refined approach as discussed in the next two sections.

Semiempirical Drag Analysis

Recently, Revell (ref. 65) has advanced a prediction technique for airframe noise which involves knowledge of the drag characteristics of the aircraft. This technique is based upon the hypothesis, not without intuitive justification, that there exists a relation between the fluctuating forces which act on the aircraft and the steady drag it experiences. This technique lies somewhere between the total aircraft and component by component approaches and has the advantage that it may be applied to both the clean and dirty aircraft configurations.

Revell postulates that the acoustic power radiated by an aircraft can be written as a sum of the mechanical power consummed by the various drag components when weighted by acoustic efficiency factors; that is,

$$P_a = \sum_{i=1}^{N} \eta_{a,j} P_{m,j}$$

He further assumes that the acoustic efficiency for a dipole must be proportional to the cube of the Mach number of the flow; that is,

$$\eta_{a,j} = \lambda_j M^3$$

Thus, since the power consumed by a given drag component can be written as

$$P_{m,j} = C_{D,j} S_j \rho_o \frac{V^3}{2}$$

where $C_{D,j}$ is the drag coefficient for that particular component and S_j is a relevant area, the acoustic power may be written as

$$P_a = \frac{\rho_o V^6}{2a_o^3} \sum_{j=1}^{N} \lambda_j C_{D,j} S_j$$

that is, the acoustic power can be determined in terms of the steady drag coefficients.

Now, treating each drag component as a simple dipole, the mean-square sound pressure produced by the jth drag component will be

$$\left\langle p_j^2 \right\rangle = \rho_o a_o \frac{3P_{a,j} \cos^2 \gamma}{4\pi r^2}$$

where $P_{a,j} = \eta_{a,j}P_{m,j}$ is the acoustic power due to the jth drag component and γ is the angle between the dipole axis and the far-field observer.

Revell then assumes that there is a correlation between the factor λ_j and the steady drag coefficient $C_{D,j}$, that $\lambda_j = \lambda_j' C_{D,j}$.

Thus,

$$\left\langle p_j^2 \right\rangle = \lambda_j' C_{D,j}^2 \left(\frac{\rho_o V^2}{2}\right)^2 M^2 \frac{3S_j}{2\pi r^2} \cos^2 \gamma$$

and the overall sound pressure level due to the jth component can be written as

$$\mathrm{OASPL}_j = A_j + 10 \log_{10} \left[\left(\frac{C_{D,j}}{C_{D,ref}}\right)^2 \frac{S_j}{S_{ref}} \left(\frac{V}{V_{ref}}\right)^6 \left(\frac{h_{ref}}{r}\right)^2 \cos^2 \gamma\right]$$

where A_j is a constant and $C_{D,ref}$, S_{ref}, V_{ref}, and h_{ref} are reference drag coefficient, area, speed, and altitude, respectively.

Revell considers three sources of drag: wing profile drag, induced drag, and fuselage drag. On the basis of available data (refs. 8 and 10), he determined the values given in table IV which may be employed to predict the overall sound pressure levels due to these components of drag on any aircraft.

The third octave spectral decomposition of these sound pressure levels is given by the universal spectrum $S(\zeta) = S_o(\zeta) \exp\left[-\frac{3}{2}\left(\alpha_s|\zeta - 1|\right)\right]$ where $\zeta = f/f_{Str}$, $\alpha_s = 0.002$, and

$$S_o(\zeta) = \begin{cases} B_1\sqrt{\zeta} & (\zeta < 1) \\ B_2/\sqrt{\zeta} & (1 < \zeta < 2) \\ B_3/\zeta & (2 < \zeta < 4) \\ B_4/\zeta^2 & (\zeta > 4) \end{cases}$$

The constants B_i are $B_1 = B_2 = 1.52$; $B_3 = 0.215$; $B_4 = 0.054$. The Strouhal frequencies are different for the different components and are determined by the following:

$$f_{Str} = \frac{N_{Str}V}{d_{eq}}$$

for the wing profile drag, where $0.05 < N_{Str} < 0.075$ and $d_{eq} = C_D c$, with C_D the profile drag coefficient for the wing section and c the chord,

$$f_{Str} = \frac{0.2C_L cV}{8\pi r_v^2}$$

for the wing-induced (vortex) drag, where r_v is the wing-tip vortex core radius approximately equal to 0.006 to 0.008 times the span of the wing and C_L is the lift coefficient and

$$f_{Str} = \frac{0.1V}{d_f}$$

for the fuselage drag, where $d_f = C_{D,F}\ell_f$. The coefficient $C_{D,F}$ is the wetted area drag coefficient of the fuselage and ℓ_f is the fuselage length.

Revell has employed this technique with good results on the data found in references 8 and 10. However, he was unable to predict the F-106B levels (ref. 12) without the addition of a correction factor for aspect ratio.

Component Analysis

A component prediction of aircraft noise radiated into the community by nonpropulsive sources requires a detailed identification of source mechanisms and the relative importance of each. This study has shown that there is indeed a substantial body of knowledge related to the pertinent source mechanisms. Thus, a careful and thoughtful application of existing techniques to actual aircraft geometries and flight conditions can be employed in the prediction of airframe noise. In some areas, primarily in the case of cavities and landing gear, there are substantial doubts as to the details of actual flow conditions around the device; thus, the estimates for noise from these areas are very approximate. However, the identification of the areas of uncertainty serves to provide topics for immediate study toward a more complete understanding and definition of airframe noise and the potential for its reduction.

The steps in a systematic approach to noise prediction are as follows:

(1) Identify all sources and source mechanisms

(2) Predict source spectra of each mechanism for each configuration of interest

(3) Take into account propagation factors between each source and the observer, including distance and azimuth of each local source region with respect to observer, moving source effects, atmospheric attenuation and ground reflection

(4) Sum contributions of each source at observation point

In the remainder of this section, these steps are outlined in detail.

Source identification.- As stressed earlier, the true sources of aerodynamic noise are the fluid dynamic disturbances themselves. The interaction of these disturbances with airframe structural discontinuities causes substantial sound radiation. In many cases, a structural discontinuity is the cause of the acoustically significant flow distur-

bance so that the cause-and-effect chain is not readily separable. Typical important structural discontinuities are trailing edges of airfoils (that is, wing, stabilizers, flaps), cavities and doors related to gear deployment and stowage, gear struts, axles, and wheels.

The fundamental fluid dynamic source of airframe noise is the turbulent boundary layer (TBL) formed over the fuselage and wing surfaces of the aircraft. This TBL contains flow disturbances which move at roughly the relative velocity between the aircraft surface and the ambient airspace: these disturbances are generally characterized as hydrodynamic pressure fluctuations and do not radiate sound except upon encountering an abrupt change in the surface impedance, that is, an edge. The TBL also contains weak acoustic disturbances which radiate sound directly. Thus, the baseline noise for an aircraft could be regarded as that associated with the acoustic content of its turbulent boundary layer. The TBL does have further acoustic significance in that upon encountering an abrupt surface discontinuity, much of the hydrodynamic pressure fluctuations are converted into compressible fluctuations at the region of discontinuity. This mechanism is dipole in nature and is often called trailing-edge noise. It is obvious that trailing-edge noise will occur at many points on a typical aircraft – the wing and flap trailing edges, stabilizer and control surface trailing edges, and at the edges of cavity lips.

The second fluid dynamic source category is the class of wake flows. These may be wakes of airfoils, which tend to be comprised of rather coherent fluctuations (spatially and temporally) when the airfoils are not stalled, or wakes from separated flow such as occur behind landing-gear struts, wheels, doors, or from the leading edge of the cavity itself. The wakes, whether highly coherent or very random, produce fluctuating forces on the element "shedding" the wake in both the streamwise (drag) and normal-to-streamwise direction. These force fluctuations may be characterized as acoustic dipoles, whose far-field sound exhibits a known dependence on frequency, amplitude, and direction (which may be determined from flow speed and element geometry). Once the baseline spectrum is determined, these known scaling laws enable accurate prediction of sound over a range of speed and/or geometric scale factors.

The final fluid dynamic source is turbulent "inflow" which may be incident upon the entire aircraft, but more importantly may be produced by one element of the aircraft and then impinge upon another. Turbulent inflow to a rigid surface produces pressure fluctuations on the surface which manifest themselves as dipole-like sources. With the exception of the gear cavities, it is expected that turbulent inflow to an element would be avoided by designers since mean velocity deficits and velocity gradients accompany the inflow turbulence. However, it is useful to summarize some potential cases of turbulent-inflow-induced noise:

(1) Deployed flaps behind wing box or behind one another

(2) Gear struts in line with each other or with upstream disturbances

(3) Gear wheels or axles in line with upstream bodies

(4) Aft edge of cavity operating in wake of leading edge of cavity and/or in wake of gear struts

(5) Deployed flap operating in wake of cavity or gear

It is now clear that only a few flow noise source models are involved in analyzing airframe noise. With this fact established, it is possible to "dissect" a typical aircraft in its various flight configurations and identify the existence and location of the source mechanisms.

Source location on aircraft.- Figure 1 shows a typical CTOL aircraft in approach configuration and identifies in a cursory manner the noise sources to be considered. Direct radiation form the entire aircraft TBL is an obvious source, as is trailing-edge noise from the wing, horizontal and vertical stabilizers, each flap, and each control surface. It is important to note that each flap and control surface must be considered separately since the edge source is very directive. Thus, the far-field sound depends upon the orientation of the flap. Furthermore, the source characteristics of the edge source are a function of local flow parameters which vary from flap to flap, etc. and along the span of a tapered wing.

The landing-gear—cavity structure may radiate noise in several ways, which are shown schematically in figure 41. The fundamental[2] type of radiation from this configuration is fluctuating forces on the gear elements arising from separated flow. Interactions of the in-line landing-gear elements will increase the radiated noise. If the gear deployment requires a door to be left open, as is often the case, then additional radiation occurs from the leading edge of the exposed cavity, from volumetric flow fluctuations across the cavity mouth, and from the interaction of separated flow from the cavity leading edge with the (usually sharp) aft edge of the cavity. The final manner in which the gear system contributes noise to the far field is an indirect but important one, that is, by creating an intense wake which "washes" over the trailing edge of the wing or deployed flaps resulting in increased strength of the edge sources at those points.

Table V summarizes the noise sources for different possible aircraft configurations.

Component prediction methods.- In this section, basic noise source models are reviewed and "engineering formulations" developed to allow reasonable estimates of airframe noise on a component-by-component basis. It will be noted that all predictions of radiated noise from turbulent boundary layers, leading and trailing edges, whole-body fluctuating forces, and surface discontinuities are intimately related to the details of the local flow fields. This fundamental point thus establishes the direction and many of the requirements for future investigations into airframe noise prediction and reduction.

[2]That which would exist if the gear protruded from an otherwise clean wing.

Direct radiation from a turbulent boundary layer: In this discussion, estimates are made of noise levels generated by the acoustic content of the turbulent-boundary-layer pressure field on the surface of the aircraft. In making these estimates, simple typical models of the mechanisms, rather than detailed flow and vehicle configurations, are considered. Use is made of available analyses and experimental data.

Consider a spatially homogeneous and temporally stationary TBL pressure field on a large, smooth, rigid, flat surface. The pressure statistics are described by the wave-number—frequency spectrum $\Phi_{p,s}(\vec{k},\omega)$, where $\vec{k} = (k_1,k_2)$ is the wave-number vector, k_1 being along the flow direction x_1 and k_2 being along the transverse direction x_2, and $\Phi_{p,s}(\vec{k},\omega)$ is the Fourier transform of the space-time correlation $\phi_{p,s}(\vec{x},t)$, where $\vec{x} = (x_1,x_2)$; that is,

$$\Phi_{p,s}(\vec{k},\omega) = \frac{1}{(2\pi)^3} \iiint_{-\infty}^{\infty} \phi_{p,s}(\vec{x},t)\, e^{-i(\vec{k}\cdot\vec{x}-\omega t)}\, d\vec{x}\, dt \tag{11}$$

The correlation $\phi_{p,s}(\vec{x},t)$ is the average over any sufficiently extensive part of the $(\vec{x}',t')$ space of the pressure product $p_s(\vec{x}',t')\, p_s(\vec{x}'+\vec{x},t'+t)$. Additional details are given by Chandiramani (ref. 66).

For any frequency ω, the portion of the wave-number plane $|\vec{k}| < K$ is termed the acoustic region. Here $K = \omega/a_o$ is the acoustic wave number. The value of $\Phi(\vec{k},\omega)$ over the acoustic region is termed the acoustic content $\Phi_a(\vec{k},\omega)$ of the TBL pressure. This acoustic content is directly related to the fact that the acoustic sources in the turbulent boundary layer, along with their images in the rigid boundary, radiate to the far field. No sufficiently quantitative estimates of either the TBL far-field radiation or of the TBL acoustic content exist to date. Experimental information on $\Phi_a(\vec{k},\omega)$ is also virtually nonexistent, chiefly for the reason that it is quite impossible in the measurements to distinguish between $\Phi_a(\vec{k},\omega)$ and any extraneous sources of sound.

In face of these difficulties, consider experimental data on TBL wall pressure at low but larger than acoustic wave numbers (these data in themselves are widely discrepant and very controversial) and extrapolate these to apply to the TBL acoustic content. Use of this procedure, guided also by theoretical considerations (Chase, ref. 67) leads approximately to an upper bound,

$$\Phi_a(\vec{k},\omega) \approx 2.5 \times 10^{-9} \frac{\rho_o^2 U^8}{\omega^3 a_o^2} \tag{12}$$

Note that the assumed acoustic content is independent of the wave-number vector $\vec{k}$ as well as of the boundary-layer displacement thickness.

The spectral density of sound pressure associated with equation (12) is simply $\left(\pi\omega^2/a_o^2\right)\left[\Phi_a(\vec{k},\omega)\right]$, whereas the spectral density of the sound power radiated per unit surface area of the vehicle is $\left(\pi\omega^2/a_o^2\right)\left(1/p_{ref}a_o\right)\left[\Phi_a(\vec{k},\omega)\right]$. Finally, the spectral density $\Phi_p(\omega)$ of the acoustic pressure at a distance r directly beneath the aircraft, semispherical spreading being assumed, is given by

$$\Phi_p(\omega) = \frac{\rho_o a_o}{2\pi r^2}\frac{\pi\omega^2}{a_o^2}\frac{1}{\rho_o a_o}\Phi_a(\vec{k},\omega) = 1.25 \times 10^{-9}\frac{S\rho_o^2 U^8}{\omega a_o^4 r^2} \tag{13}$$

where S is the horizontally projected area of the aircraft.

In determining the estimate of equation (13) from equation (12), several approximations have been made:

(1) Any effects of lack of coherency between the sources in the boundary layer and the wall pressure as a radiating source have been ignored

(2) A more detailed analysis of the radiated pressure in the Fraunhofer zone of the aircraft (implied by the assumption of semispherical spreading) for the case where the aircraft dimensions are larger than the acoustic wavelength has been bypassed

(3) Effects of ground reflections were ignored

These effects, involving corrections of factors of around 2 (3 to 6 dB) are partly self-canceling, and the estimate of equation (12) is gross enough to absorb such subtleties and complications.

Expressing equation (13) as SPL, sound pressure level in one-third-octave bands, dB re 20 $\mu N/m^2$, yields for the minimum upper bound,

$$\frac{1}{3}\,\text{OBSPL} \approx 38 + 10 \log \frac{S\rho_o^2 U^8}{a_o^4 r^2} \tag{14}$$

Note that this estimated $\frac{1}{3}$ OBSPL is independent of frequency band, a result likely to be modified at high frequencies by the increasing role of fluid viscosity.

Trailing-edge noise: Prediction of the noise produced by turbulent flow past a trailing edge has been discussed extensively in recent literature (Hayden and Chanaud, ref. 68; Hayden, ref. 26; Ffowcs Williams and Hall, ref. 18; Chase, ref. 67; Chandiramani, ref. 69). There are areas of agreement in all of these models, but several important unresolved disparities in the implied results remain. The similarities are in the prediction that for surfaces very large (for example, semi-infinite) with respect to a wavelength, the presence of the surface produces a directivity pattern resembling a cardioid oriented normal to the plane of the surface [for example, $\cos^2(\psi/2)$]. Hayden (ref. 26) showed this directivity pattern which is repeated in figure 42 for convenience. The

implications of this result for airframe noise are that substantial sound is radiated forward and down from this source on an aircraft. In the prediction of source levels, the various approaches differ primarily in terms of physical perspective of the noise-generating process. The model which has shown best agreement with measurement trends[3] is Hayden's which takes the physical viewpoint that the turbulent flow at the trailing edge leaves small uncorrelated regions of uncanceled hydrodynamic pressure which exert a force on the medium, and thus produce a dipole-like sound. This simple approach lends itself to convenient modeling in terms of easily measured parameters.

The far-field intensity I from a strip of trailing-edge sources of statistically similar characteristics is

$$I(r,\theta,\psi,\omega) \propto m\omega^2\overline{T^2}\left[\frac{\sin^2\theta}{r^2}\,\frac{\cos^2\psi/2}{\rho_o a_o^3}\right] \tag{15}$$

where m is the number of sources, T is the force of one source region (represented by pressure times correlation area), and the angles θ and ψ are as defined in figure 42. The model requires as inputs the surface pressure spectrum, spanwise correlation length spectrum (that is, wave-number spectrum), and the wetted span. Once these parameters are known, the sound spectrum and mean-square intensity are found as shown in figure 43. This approach has been used to develop normalized curves of far-field sound from a knowledge of the mean flow and geometric parameters – speed of the free stream, wetted span, and local boundary-layer thickness, which is proportional to the spanwise and streamwise correlation lengths.

The surface pressure characteristics for different types of flow fields are significantly different as shown in figure 44. Thus, one should add a new curve to Hayden's (ref. 26) wall jet noise curves – for moderately loaded airfoils – as shown in figure 45. The calculation procedure is then identical to that described in reference 26.

A further note on trailing-edge noise for finite airfoils is that the radiation field is not the same as that for a flat plate nor is it that for a point dipole. In the region in the plane of the plate (for example, $\pm 30^\circ$ from the surface plane), some constructive and destructive interference occurs which modifies the sound field in that area. For typical aircraft observation angles, this region is unimportant and the semi-infinite surface directivity function can be used.

The critical problem in all the predictions at this stage is calculation or estimation of the pertinent flow field parameters. Furthermore, if the flow field characteristics vary along an airfoil span, the airfoil noise prediction must be applied to each locally similar region if precision in the total aircraft spectrum is desired.

---

[3]Indeed, the original concept of the model was based in part upon explaining gross trends which had been observed.

Vortex noise from airfoils: This procedure is described in reference 22 and need not be reiterated except for the following considerations:

(1) The pertinent velocity in both the amplitude and frequency calculation is the component normal to the edge. Thus, the sweepback angle enters significantly in the calculation.

(2) Just as with the trailing-edge source, spanwise strips should be used if the spanwise geometry varies.

The prediction curve for this source is given by figure 15.

Landing gear: The flow separation from a gear strut or wheel produces force fluctuations in both the streamwise (drag) direction and normal direction. The fluid dynamic situation is sketched in figure 46. If one is able to describe the force field in terms of the flow and geometric parameters, the sound field is easily specified.

The sound power per unit bandwidth of a point dipole source may be written

$$\frac{\Pi(\omega)}{\Delta\omega} = \frac{\Phi_F(\omega)\ \omega^2}{12\pi\rho_o a_o^3} \qquad (\Delta\omega = 2\pi) \tag{16}$$

where $\Phi_F(\omega)$ is the force spectral density. To find spatial characteristics of the sound field, one may account for finiteness of the source and arbitrary orientation of the source axis by the following expression for far-field sound pressure (see fig. 47 for coordinate system):

$$\Phi_p(r,\theta,\psi,\omega) = \frac{\Phi_F(\omega)}{16\pi^2 r^2}\left(\frac{K^2 r_e^2}{1 + K^2 r_e^2}\right) D(\theta,\psi) \tag{17}$$

where r_e is the effective radius of the source and $D(\theta,\psi)$ is the directivity factor

$$D(\theta,\psi) = \cos^2\theta_s \cos^2\theta + 2\cos\theta_s \sin\theta_s \cos\theta \sin\theta \cos\psi + \sin^2\theta_s \sin^2\theta \cos^2\psi \tag{18}$$

where θ_s is the angle between the source axis and the Z-axis. Note that this relation simply reduces to the usual $\cos^2\theta$ dependence when the source axis is alined with the Z-axis. The parenthetical term in equation (17) accounts for the finiteness effects of noncompact sources.

The shape of the directivity pattern is the figure eight shown in figure 48, where the maxima are along the force axis and the minima exist in the plane normal to the force axis. Thus, for the landing-gear case, the orientation and local force field of each segment is important in determining the far-field sound.

There is a great body of literature on vortex-shedding noise from cylinders. (See Ross, ref. 70, for review.) Curle's (ref. 13) formulation of the problem has been supplemented by empirical data for typical elements by Gordon (ref. 71) and Heller and Widnall (ref. 72). These studies determined the normalized spectrum of sound by relating the fluctuating body forces to the steady-state drag. The ratio of root-mean-square fluctuating force to steady drag was found for a variety of bluff bodies to be approximately 2.3×10^{-3}. The characteristic frequency of the resultant sound spectrum can be found from the Strouhal relation $f_{max} \approx 0.2U/d$. This relation gives a result similar to those obtained by using Heller and Widnall's force ratio. The overall sound power for each section is calculated from equation (16) and the spectrum relative to the overall level is approximated by figure 49. The far-field spectrum level is determined from the usual considerations of directivity and distance to the observer. Each segment will have a directivity pattern associated with its drag dipole and its lift dipole.

Sound radiation from cavities: Important sound radiation from cavities comes from trailing-edge noise at the forward edge of a cavity, impingement of separated flow on the aft edge of the cavity, and volumetric flow fluctuations across the cavity mouth. The trailing-edge noise estimation procedure has been summarized, although the sound field for a typical edge geometry of a cavity would be modified from the thin airfoil or plate case. The impingement of flow on the aft edge can be considered in the same manner as any edge noise problem, wherein the inflow details are necessary for calculation of the sound field.

Under certain conditions cutouts or cavities in the surface structure of aircraft can generate discrete tones of very high intensity. One must distinguish between deep and shallow cavities. The distinction lies in their length-depth ratio,[4] which is crudely larger than unity for shallow cavities and less than unity for deep cavities.

A deep cavity responds somewhat like an acoustic resonator, the compressible fluid inside the cavity serving as the primary storage medium for oscillatory energy, which is provided by the shear layer above the cavity. The vorticity is primarily governed by the image vorticity in the forward and aft vertical walls of the cavity; therefore, the vortex motion tends to be in the direction of the depth, and the cavity is driven in a depth mode. A shallow cavity, on the other hand, converts input energy from the vortex sheet into fore-and-aft oscillations, because the vorticity is primarily governed by the images along the bottom wall; the cavity thus is driven in a length mode.

Most studies so far provided only insight into the relationship of generated frequencies, cavity geometry, and flow speed. A recent empirical study (Heller et al., ref. 47)

---

[4]The width of a cavity, that is, the dimension transverse to the flow direction, is usually unimportant in determining the resonant behavior.

provided upper bound levels inside the cavity, but no study has been conducted to date to determine the levels of noise radiated into the far-field environment.

However, an estimate of the levels to be expected from a typical cavity at typical landing speeds can be obtained. Volumetric fluctuations characterize acoustic monopoles. To derive the radiated acoustic far-field level, assume the radiating cavity to be represented by a monopole source in an infinite baffle or, equivalently, by a piston oscillating with the particle velocity of air corresponding to 124 dB, that is, about 7.5 cm/sec. The power radiated into free space by a piston of area A and speed u enclosed in a baffle is

$$\Pi = \frac{\rho_o a_o K^2}{2\pi} A^2 u^2 \tag{19}$$

where Au is the source strength of a monopole as represented by the "piston."

Thus, the free-field sound pressure from a baffled monopole may be written as

$$\overline{p^2}(r) = \frac{\rho_o{}^2 \omega^2 (Au)^2}{16\pi^2 r^2} \tag{20}$$

The difficulty with this formulation is that a knowledge of the particle velocity u is required. If it is assumed that the in-cavity pressures are representative of the upper bound acoustic pressures, then the known relationship between acoustic pressure and velocity may be used in modifying this relationship to employ the existing in-cavity pressure data in predicting far-field sound u; that is,

$$\overline{p^2}(r) = \frac{\omega^2}{16\pi^2 r^2 a_o{}^2} (p_c{}^2 A^2) \tag{21}$$

where p_c is the cavity pressure.

The frequencies and amplitudes may be determined from existing experimental data such as shown in figures 50 and 51 (Heller et al., ref. 47), which unfortunately contain most data for high subsonic and supersonic Mach numbers. In the following section, the implementation of these formulations is performed for a typical aircraft geometry.

Modeling considerations.- When modeling the airframe noise generation and propagation, it is convenient to divide the problem into three major areas:

Sources → Path → Receiver

Below is a discussion of two of these areas.

Sources: Airframe noise sources, as discussed above, can be divided into two types:

(1) Small or point sources: sources with characteristic dimensions that are small compared with the aircraft dimensions or observation distances. These sources include cavity-generated noise and gear noise.

(2) Large or distributed sources: sources either with characteristic dimensions of the same order of magnitude as the aircraft dimensions or with distributions of sources over the aircraft. These sources include TBL radiation, trailing-edge noise, and vortex shedding noise.

Once the prediction technique for point sources is established, their evaluation is relatively simple. The distributed sources, on the other hand, present additional difficulties which necessitate special techniques for their evaluation. Thus, any prediction scheme for noise generated by low flying aircraft must deal with the following problems:

(1) The aircraft is not a point source. Although some noise-producing components of the aircraft can be viewed as a point source, even for low flying aircraft, airframe noise is generated mostly by surfaces and surface discontinuities. It is obvious that even at a distance of a few hundred feet, a large commercial aircraft with a wing span of nearly 61 m (200 ft) is definitely not a point source. One must view the low flying aircraft as a distributed source having large dimensions and take into account the proper propagation laws as well as differences in distance between the observation point and the different points on the source.

(2) The source characteristics vary from point to point on the aircraft. Trailing-edge noise, for example, is governed by (among other parameters) the local boundary-layer thickness and the local velocity normal to the edge. The boundary-layer thickness, in turn, is determined by the local chord, which can vary by an order of magnitude from the wing root to the wing tip. The local normal velocity will depend on the local sweep-back angle, which, varies between the wing root (with its extended trailing edge) to the wing tip. In addition to these variations, all (nonmonopole) sources have a directivity pattern which modifies the noise propagation behavior and leads to the next problem.

(3) The observation point (microphone location) is usually in the geometric near field. FAR-36, for example, specifies the aircraft altitude above the microphone location to be 112 m (370 ft). This distance is of the same order of magnitude as the typical aircraft dimensions. The angles and the distance at which one views each part of the source will influence the noise levels measured or predicted.

One way to overcome all three problems is to divide the aircraft noise-producing sources into many elements, or sections over which the aerodynamic and acoustical variables may be considered as constant. Each of these source regions, with its own intensity and directivity pattern is then computed individually at the observation point, and the total sound pressure level is determined by summing the contribution of all the local

source regions at the microphone location. The geometry involved is somewhat tedious but straightforward.

Figure 52 shows the effect of the number of sections into which one divides the noise-generating sources – in this case the wings and stabilizers – on the SPL predicted for a Boeing 747 in the so-called clean configuration, that is, no flaps and gear up. The number of sections into which each wing is divided is given as n. For $n = 1$ (that is, the whole wing considered as a uniform line source of uncorrelated source regions), one can easily identify the vortex shedding peaks from the wings and the stabilizers. As the number of sections is increased, the spectrum is smoothed out. The convergence of this process is very rapid and $n = 20$ seems to be the maximum number of sections one may have to use. Arbitrarily invoking a number much greater than 20 could result in neglect of basic physical considerations, such as the length scale of one eddy (as a percentage of the chord or span).

Paths: It is well known that the attenuation of a point source due to spreading is directly proportional to the distance from the source. For a line source, this law changes and the attenuation is proportional to the distance to a lesser power. Figure 53 shows the 500-Hz third octave band SPL of the aircraft wing and stabilizer trailing edges as a function of the flight altitude. One notes the changing slope of the SPL with distance from $1/r^2$ at large distances to $1/r$ as the altitude decreases. This calculation was done for direct flyover. The behavior for a laterally positioned observer will vary in some of the details. However, the qualitative importance of this effect is amply demonstrated.

The following section will illustrate the application of the foregoing concepts and formulations to the calculation of airframe noise from a real aircraft in a typical low-altitude approach mode of flight.

Illustrative calculations.- In this section, the relationships developed earlier are utilized to predict the radiated noise from a large CTOL transport in approach configuration. The example selected is a Boeing 747 as it is the largest of the so-called "Jumbo Jets," and is probably representative of the airframe noise from any of the three aircraft in that class.

The pertinent geometric parameters are:

Length, m (ft)	68.5	(225)
Basic root chord, m (ft).	12.2	(40.1)
Fuselage half-width at wing root plane, m (ft) . . .	3.25	(10.67)
Semispan to trailing-edge crease, m (ft).	13.0	(42.9)

Aircraft wing semispan, m (ft)	29.7	(97.6)
Horizontal-stabilizer semispan, m (ft)	11.3	(37)
Trailing-edge thickness at wing root, m (ft)	0.003	(0.01)
Trailing-edge thickness at wing tip, m (ft)	0.0008	(0.0026)
Leading-edge sweepback angle, deg	41.5	
Basic trailing-edge sweepback angle, deg	30.2	
Extended trailing-edge sweepback angle, deg	17.7	

Landing gear:
- 4 main carriages (2 body, 2 wing)
- 4 wheels each (double axis)
- Wheel diameter ≈ 1.2 m (4 ft)
- 1 nose gear, 2 wheels

The geometry for the calculation is shown in figure 54.

The relationships developed earlier may be used directly to diagnose the sample aircraft to determine the predominant noise-producing sources. By using the previously specified geometry for the Boeing 747, the contribution of the various sources is computed as follows:

(a) Direct radiation from TBL: Use equation (14) directly.

(b) Trailing-edge noise of wing, flaps, and stabilizers: Use figure 44 (airfoil spectrum) for broadband spectrum; use figure 45 for vortex spectrum.

(c) Gear noise: (1) Direct radiation: Use equation (17) and figure 49; (2) cavity oscillations: Use equation (21) and figures 50 and 51.

As previously mentioned, the accuracy of the calculation is improved by considering local flow and geometric conditions in detail, and calculating the path of each source region to the observer directly and individually.

Such a calculation has been performed for the Boeing 747 in full approach configuration (flaps extended, gear down) for a normal approach speed of 84 m/sec (275 ft/sec). The observation point is the same as the FAR-36 certification point, 112 m (370 ft) below the aircraft. Each element of the aircraft was calculated separately. The results are summarized in figure 55. It can be seen that the edge sources clearly dominate the other sources. The gear and cavity sources which were calculated were direct radiation from the gear (via fluctuating forces) and cavity oscillations. One will note that for a direct flyover, the gear direct radiation for both drag and normal dipoles has a complete null. However, some gear elements are randomly oriented and thus would contribute something

to a direct flyover. Furthermore, in the interest of rank-ordering sources for general considerations, one should make a rather generous allowance for directivity effects. In this case, -4 dB was used for the directivity with respect to the maximum. The cavity oscillations were calculated by using in-cavity pressures to infer source levels. This procedure clearly produces upper bound levels. Furthermore, at low Mach numbers, gear-type cavities may not even oscillate. The calculated levels for the first four modes show that cavity oscillations would be important only at very low frequencies. Recent studies have shown that the levels in figure 50 are too high for individual modes; thus, it is suggested that the oscillating cavity mechanism is not too important to the overall airframe noise problem. The other sources of radiation due to gear down, namely aft-edge noise from separated flow impingement, and increased wing-flap noise from cavity-gear wakes washing the trailing edge have not been calculated here.

The calculated TBL noise is also thought to be an upper bound and is 15 to 20 dB below the wing edge noise. Thus, the edge sources appear to dominate the total radiation.

The contribution from the stabilizers and the flaps follows the same procedure as for a wing and the output of all elements is summed to give the total SPL at the observer position. Figure 56(a) is the final result for the Boeing 747 under the same conditions as in the illustrative result. In figure 56(b), a typical example of the contribution of the various component sources to such a prediction is shown.

Predicted trends for various aircraft configurations and positions.- The previously presented discussion essentially describes the functioning of Bolt Beranek and Newman's Multi-Element Airfoil Noise (MEAN) Program. This program also calculates effects of aircraft motion, atmospheric effects, and ground reflection. The Boeing 747 geometry was fed into the program and the noise was calculated for several interesting cases. The following comparisons are made:

(1) Flyover noise, flaps up compared with flaps down (figs. 57(a) and 57(b))

(2) Sideline noise, flaps up compared with flaps down (figs. 58(a) and 58(b))

(3) Flyover compared with sideline (figs. 57(a) and 58(a); figs. 57(b) and 58(b))

(4) Effects of atmospheric attenuation.

Another interesting aspect is the relative radiation forward, overhead, and aft of an aircraft. Figure 59 summarizes this effect for a fixed observer with respect to the sample aircraft flying at a level altitude of 113 m (370 ft) at a speed of 91 m/sec (300 ft/sec).

CONCLUSIONS AND RECOMMENDATIONS

This report has discussed the current understanding of airframe noise generation and has described predictive techniques which can be employed in an evaluation of this type of sound production. The more fundamental techniques, the drag and component methods, are still subject to some controversy and probably will require additional evolution. Thus, the authors recommend the empirical total aircraft approach to prediction as the most reliable at this time.

On the basis of this analysis, several areas where further research is required that would enhance knowledge of the generation of airframe noise have been identified:

1. Additional unpowered flyover or model data are required to evaluate fully the different noise generation characteristics of the clean compared with dirty aircraft configurations. Insofar as possible, these data would consist of identical tests, the only change being the configuration of the aircraft itself.

2. Much research must be accomplished on the techniques for acoustic measurement in wind tunnels. Microphones which are less sensitive to wind speed and direction need to be developed. In addition, methods of wind-tunnel construction, including model mounts, which generate lower background noise levels are required.

3. It is apparent from the literature review that much knowledge remains to be acquired on the level of sound generation by cavities in flows. Although the frequencies at which the sound is generated are understood, the intensity and directivity of such sources have not been fully researched.

4. The interaction of the flow fields over various component sound sources has not been evaluated. For instance, the landing-gear—wheel-well interaction and the flaps—landing-gear interaction are potentially important. The airfoil wake may also be a significant input to the tail surfaces.

5. The important question of phasing of the various component sources has also not been evaluated. Can the total sound production be obtained by considering the components as independent sources or is there an interdependence which must be included in the analysis?

6. It would be of interest to try the three different prediction techniques (empirical, Revell drag theory, and component analysis) on an aircraft for which accurate flyover data exist in order to evaluate the three different approaches and discover any differences among them.

7. It would be of interest to try the component analysis on the F-106B data as the other two approaches have already failed to make an acceptable prediction.

8. The whole area of scaling model data, particularly with regard to Reynolds number effects, needs to be investigated; this can be done by comparing carefully executed model tests with full-scale data. Later, tests with models in high-pressure or variable-density tunnels might be attempted.

9. A moving source experiment needs to be designed whereby a model aircraft could be compared with wind-tunnel data to evaluate the effects of moving-source—fixed medium compared with fixed-source—moving medium, and propagation of sound through a tunnel shear layer.

10. Balloon or tower-mounted microphones might be employed in a flyover test program to remove the ground effect and also allow the aircraft to operate unpowered in a clean configuration without safety considerations because of proximity to the ground.

11. There is considerable controversy at this time over the directivity of airframe noise. A carefully done flyover measurement program involving an array of microphones would help to alleviate this question.

12. It is apparent that sound generation by an airfoil—flap system is not well understood. An experiment whereby source location could be examined through cross correlation of surface pressures with far-field sound is in order.

Langley Research Center,
National Aeronautics and Space Administration,
Hampton, Va., November 26, 1974.

REFERENCES

1. Anon.: Civil Aviation Research and Development Policy Study – Report. NASA SP-265, 1971. (Also available as DOT TST-10-4.)
2. Gibson, John S.: The Ultimate Noise Barrier – Far Field Radiated Aerodynamic Noise. Inter-Noise 72 Proceedings, Malcolm J. Crocker, ed., Inst. Noise Contr. Eng., c.1972, pp. 332-337.
3. Blumenthal, V. L.; Streckenbach, J. M.; and Tate, R. B.: Aircraft Environmental Problems. AIAA Paper No. 73-5, Jan. 1973.
4. Graham, R. R.: The Silent Flight of Owls. Jour. Roy. Aeronaut. Soc., vol. 38, no. 286, Oct. 1934, pp. 837-843.
5. Kroeger, Richard A.; Grushka, Heinz D.; and Helvey, Tibor C.: Low Speed Aerodynamics for Ultra-Quiet Flight. AFFDL-TR-71-75, U.S. Air Force, Mar. 1972. (Available from DDC as AD 893 426.)
6. Hubbard, Harvey H.; and Maglieri, Domenic J.: An Investigation of Some Phenomena Relating to Aural Detection of Airplanes. NACA TN 4337, 1958.
7. Smith, D. L.; Paxson, R. P.; Talmadge, R. D.; and Hotz, E. R.: Measurements of the Radiated Noise from Sailplanes. AFFDL-TM-70-3-FDDA, U.S. Air Force, July 1970. (Available from DDC as AD 709 689.)
8. Healy, Gerald J.: Measurement and Analysis of Aircraft Far-Field Aerodynamic Noise. NASA CR-2377, 1974.
9. Anon.: Standard Values of Atmospheric Absorption as a Function of Temperature and Humidity for Use in Evaluating Aircraft Flyover Noise. ARP-866, Soc. Automot. Eng., Aug. 31, 1964.
10. Gibson, John S.: Non-Engine Aerodynamic Noise Investigation of a Large Aircraft. NASA CR-2378, 1974.
11. Lasagna, P. L.; and Putnam, T. W.: Preliminary Measurements of Aircraft Aerodynamic Noise. AIAA Paper No. 74-572, June 1974.
12. Burley, Richard R.: Preliminary Measurement of the Airframe Noise From an F-106B Delta Wing Aircraft at Low Flyover Speeds. NASA TM X-71527, 1974.
13. Curle, N.: The Influence of Solid Boundaries Upon Aerodynamic Sound. Proc. Roy. Soc. (London), ser. A, vol. 231, no. 1187, Sept. 20, 1955.
14. Lighthill, M. J.: On Sound Generated Aerodynamically. I. General Theory. Proc. Roy. Soc. (London), ser. A, vol. 211, no. 1107, Mar. 20, 1952, pp. 564-587.

15. Powell, Alan: On the Aerodynamic Noise of a Rigid Flat Plate Moving at Zero Incidence. J. Acoust. Soc. Amer., vol. 31, no. 12, Dec. 1959, pp. 1649-1653.

16. Powell, Alan: Aerodynamic Noise and the Plane Boundary. J. Acoust. Soc. Amer., vol. 32, no. 8, Aug. 1960, pp. 982-990.

17. Ffowcs Williams, John E.: Sound Radiation From Turbulent Boundary Layers Formed on Compliant Surfaces. J. Fluid Mech., vol. 22, pt. 2, June 1965, pp. 347-358.

18. Ffowcs Williams, J. E.; and Hall, L. H.: Aerodynamic Sound Generation by Turbulent Flow in the Vicinity of a Scattering Half Plane. J. Fluid Mech., vol. 40, pt. 4, Mar. 1970, pp. 657-670.

19. Sharland, I. J.: Sources of Noise in Axial Flow Fans. J. Sound Vib., vol. 1, no. 3, July 1964, pp. 302-322.

20. Clark, P. J. F.; and Ribner, H. S.: Direct Correlation of Fluctuating Lift With Radiated Sound for an Airfoil in Turbulent Flow. J. Acoust. Soc. Amer., vol. 46, no. 3 (pt. 2), Sept. 1969, pp. 802-805.

21. Dean, L. W.: Broadband Noise Generation by Airfoils in Turbulent Flow. AIAA Paper No. 71-587, June 1971.

22. Sears, William R.: Some Aspects of Non-Stationary Airfoil Theory and Its Practical Application. J. Aeronaut. Sci., vol. 8, no. 3, Jan. 1941, pp. 104-108.

23. Mugridge, B. D.: Acoustic Radiation From Aerofoils With Turbulent Boundary Layers. J. Sound & Vib., vol. 16, no. 4, June 1971, pp. 593-614.

24. Clark, L. T.: The Radiation of Sound From an Airfoil Immersed in a Laminar Flow. Trans. ASME, Ser. A: J. Eng. Power, vol. 93, no. 4, Oct. 1971, pp. 366-376.

25. Paterson, R. W.; Vogt, P. G.; Fink, M. R.; and Munch, C. L.: Vortex Noise of Isolated Airfoils. AIAA Paper No. 72-656, June 1972.

26. Hayden, Richard E.: Noise from Interaction of Flow With Rigid Surfaces: A Review of Current Status of Prediction Techniques. NASA CR-2126, 1972.

27. Hubbard, Harvey H.: Some Experiments Related to the Noise From Boundary Layers. J. Acoust. Soc. Amer., vol. 29, no. 1, Mar. 1957, pp. 331-334.

28. Hersh, Alan S.; and Hayden, Richard E.: Aerodynamic Sound Radiation From Lifting Surfaces With and Without Leading-Edge Serrations. NASA CR-114370, 1971.

29. Siddon, Thomas E.: Surface Dipole Strength by Cross-Correlation Method. J. Acoust. Soc. Amer., vol. 53, no. 2, Feb. 1973, pp. 619-633.

30. Hersh, A. S.; and Meecham, W. C.: Sound Directivity Radiated From Small Airfoils. J. Acoust. Soc. Amer., vol. 53, no. 2, Feb. 1973, pp. 602-606.

31. Davis, Sanford S.: Noise Generated by a Thin Wing in a Turbulent Jet. AIAA Paper No. 73-223, Jan. 1973.

32. Sunyach, M.; Arbey, H.; Robert, D.; Bataille, J.; and Comte-Bellot, G.: Correlations Between Far Field Acoustic Pressure and Flow Characteristics for a Single Airfoil. Noise Mechanisms, AGARD-CP-131, Mar. 1974, pp. 5-1 – 5-12.

33. Paterson, Robert W.; Amiet, Roy K.; and Munch, C. Lee: Isolated Airfoil – Tip Vortex Interaction Noise. AIAA Paper No. 74-194, Jan.-Feb. 1974.

34. Tam, Christopher K. W.: Discrete Tones of Isolated Airfoils. J. Acoust. Soc. Amer., vol. 55, no. 6, June 1974, pp. 1173-1177.

35. Rayleigh, (Lord): The Theory of Sound. First Amer. ed., Vol. II, Dover Publ., 1945.

36. Norton, David A.: Investigation of B-47 Bomb Bay Buffeting. Doc. No. D-12675, Boeing Airplane Co., Nov. 1952.

37. Krishnamurty, K.: Acoustic Radiation From Two-Dimensional Rectangular Cutouts in Aerodynamic Surfaces. NACA TN 3487, 1955.

38. Roshko, Anatol: Some Measurements of Flow in a Rectangular Cutout. NACA TN 3488, 1955.

39. Wieghardt, K.: Erhöhung des Turbulenten Reibungswiderstandes durch Oberflächenstörungen. Jahrb. 1943 deutschen Luftfahrtforschung, R. Oldenbourg (Munich), Bd. 10, Nr. 9, 1943, pp. 1-17.

40. Harrington, Marshall C.: Excitation of Cavity Resonance by Air Flow. J. Acoust. Soc. Amer., vol. 29, no. 1, Jan. 1957, p. 187.

41. Harrington, M. C.; and Dunham, W. H.: Studies of the Mechanism for the Flow-Induced Cavity Resonance. J. Acoust. Soc. Amer., vol. 32, no. 7, July 1960, p. 921.

42. Plumblee, H. E.; Gibson, J. S.; and Lassiter, L. W.: A Theoretical and Experimental Investigation of the Acoustic Response of Cavities in an Aerodynamic Flow. WADD-TR-61-75, U.S. Air Force, Mar. 1962.

43. Maull, D. J.; and East, L. F.: Three-Dimensional Flow in Cavities. J. Fluid Mech., vol. 16, pt. 4, Aug. 1963, pp. 620-632.

44. Rossiter, J. E.: Wind-Tunnel Experiment on the Flow Over Rectangular Cavities at Subsonic and Transonic Speeds. R. & M. No. 3438, British A.R.C., Oct. 1964.

45. East, L. F.: Aerodynamically Induced Resonance in Rectangular Cavities. J. Sound & Vib., vol. 3, no. 3, May 1966, pp. 277-287.

46. Covert, Eugene E.: An Approximate Calculation of the Onset Velocity of Cavity Oscillations. AIAA J., vol. 8, no. 12, Dec. 1970, pp. 2189-2194.

47. Heller, H. H.; Holmes, D. G.; and Covert, E. E.: Flow-Induced Pressure Oscillations in Shallow Cavities. J. Sound & Vib., vol. 18, no. 4, Oct 1971, pp. 545-553.

48. Bilanin, Alan J.; and Covert, Eugene E.: Estimation of Possible Excitation Frequencies for Shallow Rectangular Cavities. AIAA J., vol. 11, no. 3, Mar. 1973, pp. 347-351.

49. Prandtl, L.; and Tietjens, O. G. (J. P. Den Hartog, trans.): Applied Hydro- and Aeromechanics. Dover Publ., Inc., 1957.

50. Krzywoblocki, M. Zbigniew: Investigation of the Wing-Wake Frequency With Application of the Strouhal Number. J. Aeronaut. Sci., vol. 12, no. 1, Jan. 1945, pp. 51-62.

51. Fluid Motion Sub-Committee of the Aeronautical Research Council: Modern Developments in Fluid Dynamics. High Speed Flow. Vol. II, L. Howarth, ed., Clarendon Press (Oxford), 1953.

52. Roshko, Anatol: On the Development of Turbulent Wakes From Vortex Streets. NASA Rep. 1191, 1954. (Supersedes NACA TN 2913.)

53. Kovasznay, L. S. G.: Hot-Wire Investigation of the Wake Behind Cylinders at Low Reynolds Numbers. Proc. Roy. Soc. (London), Ser. A, vol. 198, no. 1053, Aug. 1949, pp. 174-190.

54. Gerrard, J. H.: Measurements of the Sound From Circular Cylinders in an Air Stream. Proc. Phys. Soc. (London), vol. 68, pt. 7, no. 427B, July 1955, pp. 453-461.

55. Phillips, O. M.: The Intensity of Aeolian Tones. J. Fluid Mech., vol. I, pt. 6, Dec. 1956, pp. 607-624.

56. Etkin, B.; Korbacher, G. K.; and Keefe, R. T.: Acoustic Radiation From a Stationary Cylinder in a Fluid Stream (Aeolian Tones). J. Acoust. Soc. Amer., vol. 29, no. 1, Jan. 1957, pp. 30-36.

57. Fung, Y. C.: Fluctuating Lift and Drag Acting on a Cylinder in a Flow at Supercritical Reynolds Numbers. J. Aerosp. Sci., vol. 27, no. 11, Nov. 1960, pp. 801-814.

58. Gerrard, J. H.: An Experimental Investigation of the Oscillating Lift and Drag of a Circular Cylinder Shedding Turbulent Vortices. J. Fluid Mech., vol. 11, pt. 2, Sept. 1961, pp. 241-256.

59. Roshko, Anatol: Experiments on the Flow Past a Circular Cylinder at Very High Reynolds Number. J. Fluid Mech., vol. 10, pt. 3, May 1961, pp. 345-356.

60. Jones, George W., Jr.; Cincotta, Joseph J.; and Walker, Robert W.: Aerodynamic Forces on a Stationary and Oscillating Circular Cylinder at High Reynolds Number. NASA TR R-300, 1969.

61. Karamcheti, K.; and Ayoub, Alfred: Pressure Fluctuations on the Surface of a Cylinder in a Cross Flow. Proceedings of the Second Interagency Symposium on University Research in Transportation Noise, Volume I, North Carolina State Univ., June 1974, pp. 238-248.

62. Bazhenov, D. V.; Bazhenova, L. A.; and Rimskiy-Korsakov, A. V.: Experimental Study of the Effect of Roughness of a Surface of a Bar on the Intensity and Frequency of Vortex Sound. Physics of Aerodynamic Noise, A. V. Rimskiy-Korsakov, ed., NASA TT F-538, 1969, pp. 26-34.

63. Lowson, M. V.: The Sound Field for Singularities in Motion. Proc. Roy. Soc. (London), Ser. A, vol. 286, no. 1407, Aug. 1965, pp. 559-572.

64. Rao, C. Radhakrishna: Linear Statistical Inference and Its Applications. John Wiley & Sons, Inc., c.1965.

65. Revell, James D.: The Calculation of Aerodynamic Noise Generated by Large Aircraft at Landing Approach. Paper presented at 87th Meeting of Acoustical Society of America (New York, N.Y.), Apr. 26, 1974.

66. Chandiramani, K. L.: Fundamentals Regarding Spectral Representation of Random Fields – Application to Wall-Pressure Field Beneath a Turbulent Boundary Layer. Rep. No. 1728 (Contract No. N00123-68-C-0460), Bolt Beranek and Newman, Inc., Sept. 15, 1968.

67. Chase, David M.: Sound Radiated by Turbulent Flow Off a Rigid Half-Plane as Obtained From a Wavevector Spectrum of Hydrodynamic Pressure. J. Acoust. Soc. Amer., vol. 52, no. 3 (pt. 2), Sept. 1972, pp. 1011-1023.

68. Hayden, R. E.; and Chanaud, R. C.: Sound Generation by Turbulent Wall Jet Flow Over a Trailing Edge. J. Acoust. Soc. Amer., vol. 48, no. 1 (pt. 1), Jan. 1970, p. 125.

69. Chandiramani, K. L.: Diffraction of Evanescent Waves, With Applications to Aerodynamically Scattered Sound and Radiation From Unbaffled Plates. J. Acoust. Soc. Amer., vol. 55, no. 1, Jan. 1974, pp. 19-29.

70. Ross, Donald: Vortex Shedding Sound of Propellers. Report No. 1115 (Contract NObs 86680), Bolt Beranek and Newman, Inc., Mar. 16, 1964. (Available from DDC as AD 435 765.)

71. Gordon, Colin G.: Spoiler-Generated Flow Noise. II. Results. J. Acoust. Soc. Amer., vol. 45, no. 1, Jan. 1969, pp. 214-223.

72. Heller, Hanno H.; and Widnall, Sheila E.: Sound Radiation From Rigid Flow Spoilers Correlated With Fluctuating Forces. J. Acoust. Soc. Amer., vol. 47, no. 3 (pt. 2), Mar. 1970, pp. 924-936.

TABLE I.- GLIDER NOISE DATA (REF. 7)

Flight number	h, m	V, m/sec	S, m^2	AR	W, N	OASPL (dB re 20 $\mu N/m^2$), dB
Schweizer 2-32						
45	24.4	29.0	16.7	18.05	5960.6	56
46	125.9	39.3				63
47	45.7	29.0				61
48	27.1	37.5				61
49	9.8	33.5				73
50	14.3	55.8				75
51	20.1	36.6				63
54	26.8	31.4				60
55	39.6	29.9			6561.1	57
56	33.8	40.5				59
57	26.5	49.1				66
64	50.9	34.4				62
65	32.0	26.8			6761.3	60
66	13.7	36.6				74
67	14.6	40.5				74
71	24.7	44.8			6850.3	70
Schweizer 2-33						
52	54.3	23.7	20.4	11.9	4626.2	54
53	45.1	33.5				63.5
58	24.4	43.3				74
Libelle						
68	18.3	42.7	9.5	23.6	2455.4	63
69	26.2	48.2				62
70	21.9	37.2				62.5

TABLE II.- FIVE-AIRCRAFT STUDY (REF. 8)

Flight number	h, m	V, m/sec	S, m^2	AR	W, kN	OASPL (dB re 20 $\mu N/m^2$), dB
Convair 240						
1	152.4	98.5	75.9	10.3	153.5	82.9
2		90.2				82.7
3		82.0				80.6
4		75.1				79.2
5		97.1			173.9	82.7
6		85.7				82.2
7		77.8				79.3
Douglas DC-3						
8		76.3	91.7	9.14	100.1	78.5
9		65.2				74.8
10		55.4				71.4
11		75.9			112.1	79.6
12		66.9				76.1
13		55.8				72.3
Aero Commander						
14	152.4	89.7	23.7	9.43	22.7	75.4
15		78.7				72.3
16		69.5				71.4
17		58.6				70.2
18		81.6			29.1	73.1
19		70.6				72.7
20		62.4				68.9
Prue-2 (glider)						
21		51.3	21.2	18.25	5.78	57.5
22		42.1				48.4
23		32.8				48.2
24		51.4			7.12	59.5
25		42.1				50.5
26		30.4				55.9
Cessna 150						
27		46.7	14.6	6.59	6.90	66.5
28		29.9				53.8

TABLE III. - MISCELLANEOUS DATA

Aircraft	Flight number	h, m	V, m/sec	S, m^2	AR	W, kN	OASPL (dB re 20 $\mu N/m^2$), dB	Condition Gear	Condition Flap deflection, percent	Reference
Owl		9.8	6.1	0.22	4.21	0.0068	40.25	Clean		5
2-place liaison		22.9	28.8	14.6	6.59	6.672	65	Clean		6
Lockheed C-5A	A-1	91	102	576	7.74	2700	100.5	Clean		10
	A-2	91	103			2771	104.2	Down	0	
	A-3	146	90			2740	96.1		40	
	A-4	91	86			2727	100.5		40	
	A-5	55	72			2714	103.3		100	
Aero Commander	1	115.8	59.7	23.7	9.43	29.3	77.0	Down	100	11
	2	152.4	58.1			29.2	73.5			
	3	149.4	57.6			29.0	74.2			
	4	152.4	57.6			28.8	75.2	Down	0	
	5	140.2	58.9			28.8	76.7			
	6	112.8	78.7			28.7	83.2			
JetStar	7	152.0	82.4	50.4	5.27	181.7	86.0	Down	100	11
F-106B		91.0	132.0	64.83	2.2	166.6	83.0	Clean		12

TABLE IV.- VALUES FOR REVELL'S PREDICTIVE METHOD

Component description	$C_{D,j}$, dB	$C_{D,ref}$	S_{ref}, m^2	V_{ref}, m/sec	h_{ref}, m	S_j
Wing profile drag	82	0.00848	91.7	99	152	S
Wing reduced drag	60	.00848	91.7	65	152	S
Fuselage drag	78	.00848	91.7	99	152	$\pi d_f \ell_f$

TABLE V.- AIRFRAME NOISE SOURCES

Noise source	Aircraft configuration			
	Clean	Flaps down; gear up	Gear down; flaps up	Flaps and gear down
Direct radiation from TBL	✓	✓	✓	✓
TBL interaction with trailing edge	✓	✓	✓	✓
Vortex noise from foils	✓	✓	✓	✓
Radiation from skin roughness	✓	✓	✓	✓
Radiation from skin vibration	✓	✓	✓	✓
Lift and drag fluctuations arising from separated flow behind gear			✓	✓
Volumetric flow fluctuations across cavity mouth			✓	✓
TBL interaction with forward edge of cavity			✓	✓
Impingement of separated flow on aft edge of cavity			✓	✓
Lift and drag fluctuations on doors due to separated flow			✓	✓
Edge noise from doors			✓	✓
Edge noise from gear and cavity wakes washing wing and flaps		Flap wakes may impinge on downstream flaps	✓	✓

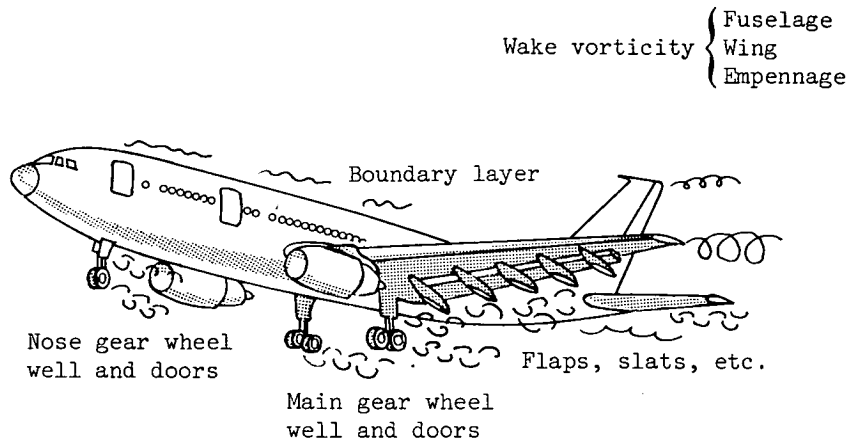

Figure 1.- Schematic diagram illustrating sources of airframe noise.

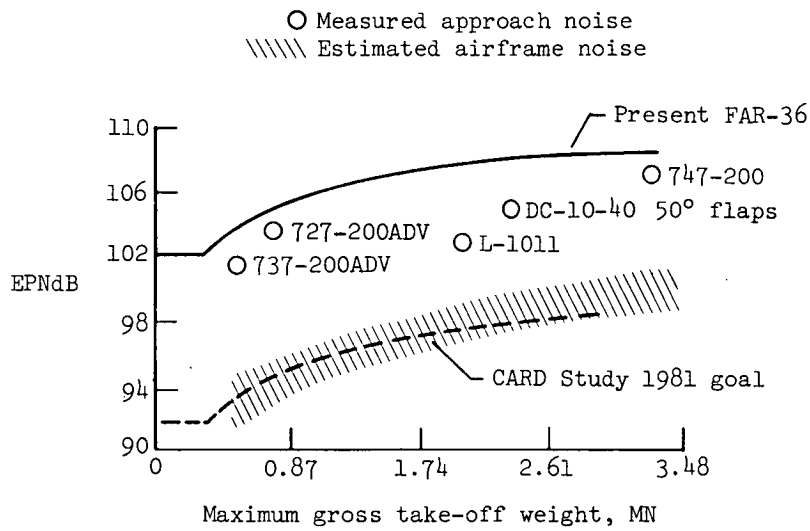

Figure 2.- Measured and predicted noise levels for several current aircraft.

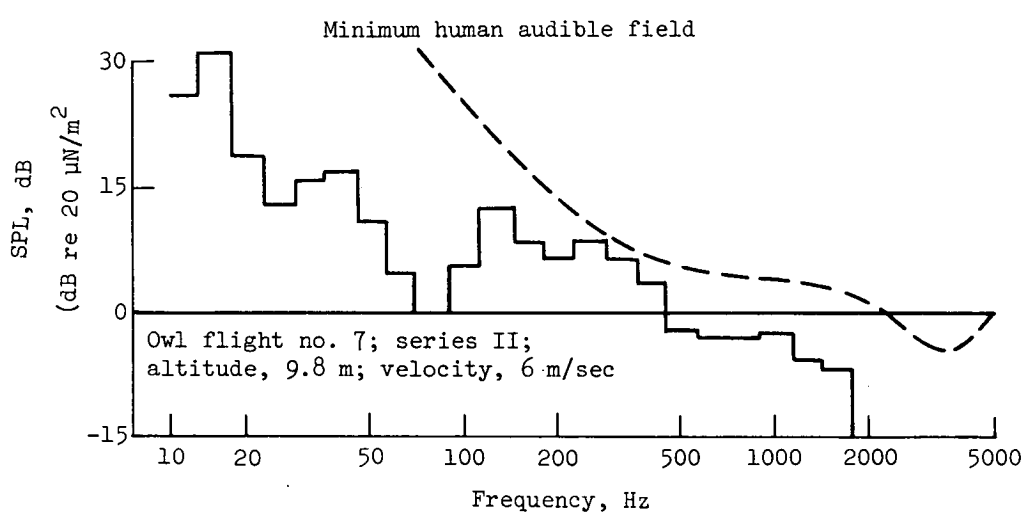

Figure 3.- Spectrum shape of aerodynamic noise produced by owl in gliding flight.

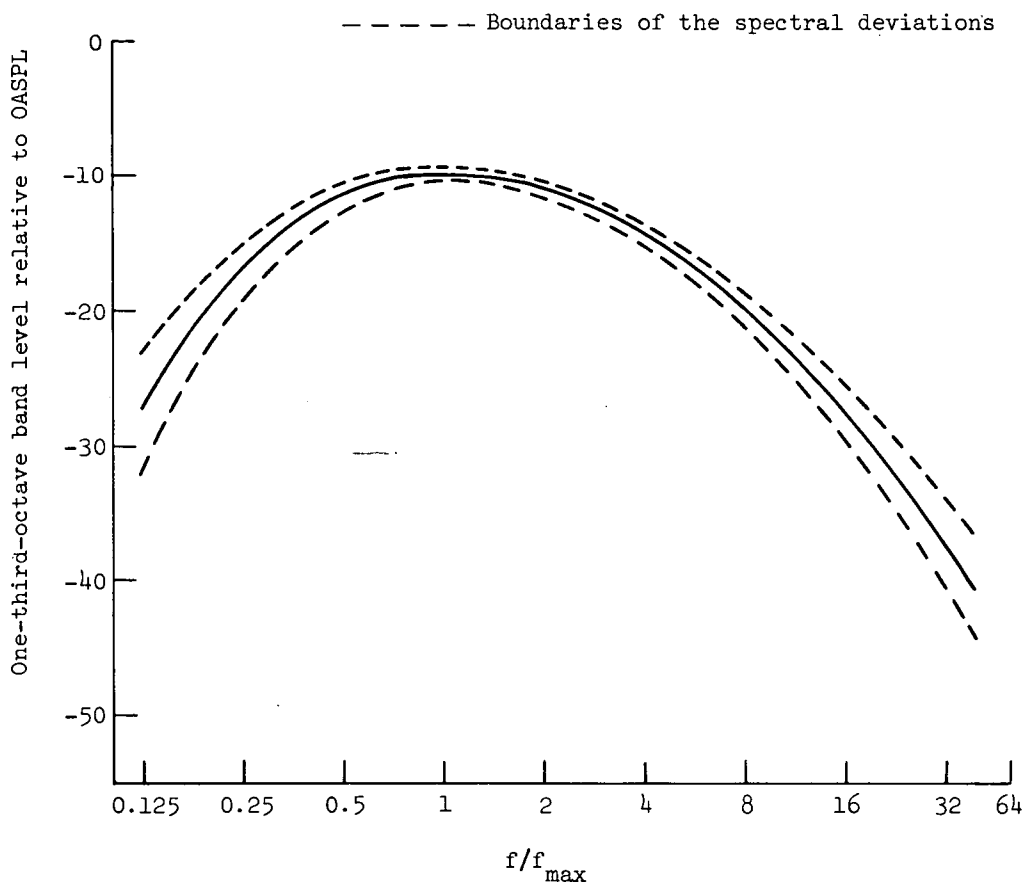

Figure 4.- Nondimensional airframe noise spectrum. Each vertical tick represents a 1/3-octave band.

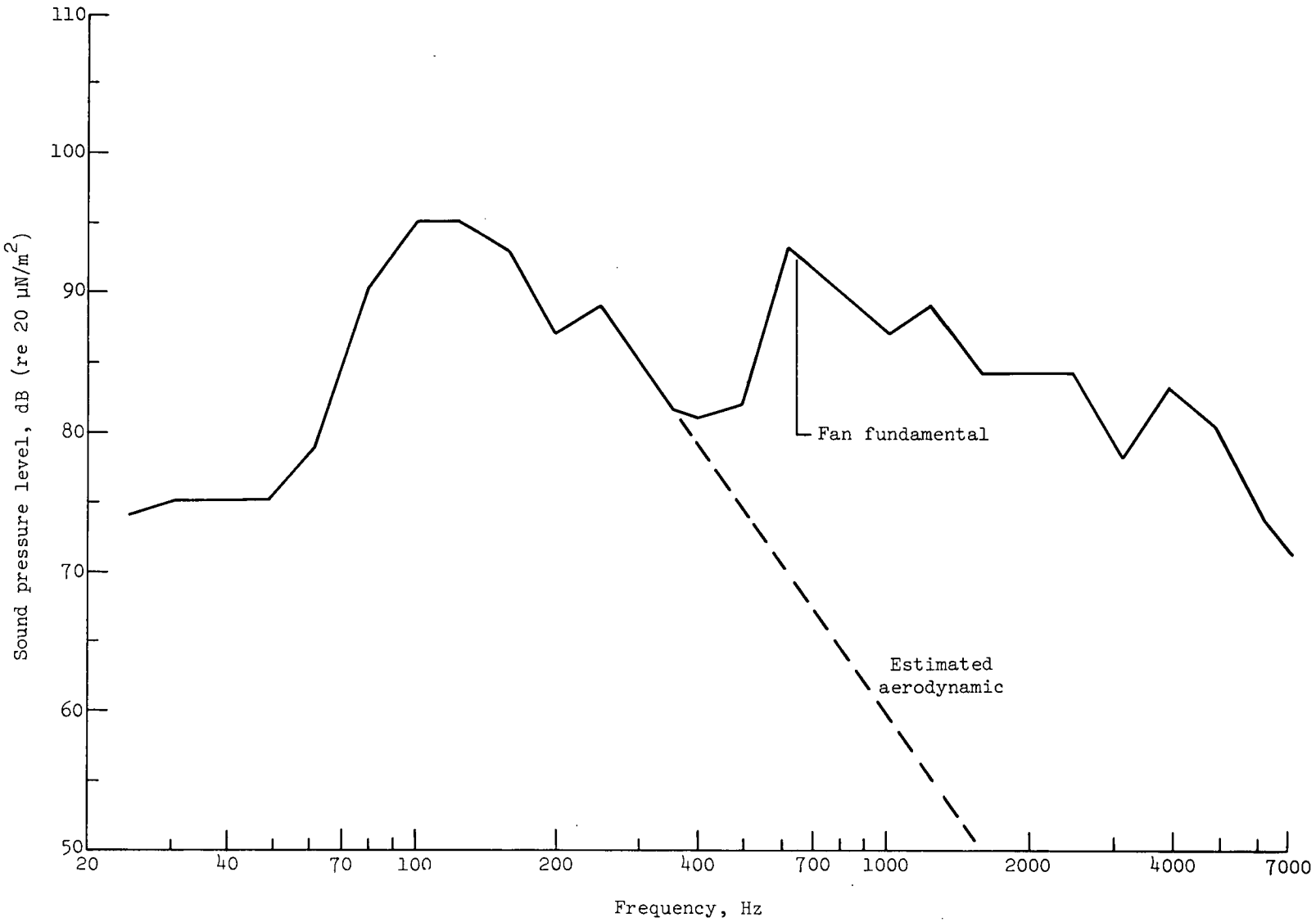

Figure 5.- Noise spectrum for "clean" configuration. 1/3-octave band; C-5A Galaxy flyover at 102 m/sec; gross weight, 275 355 kg; 91-m altitude; engines at flight idle; run A-1.

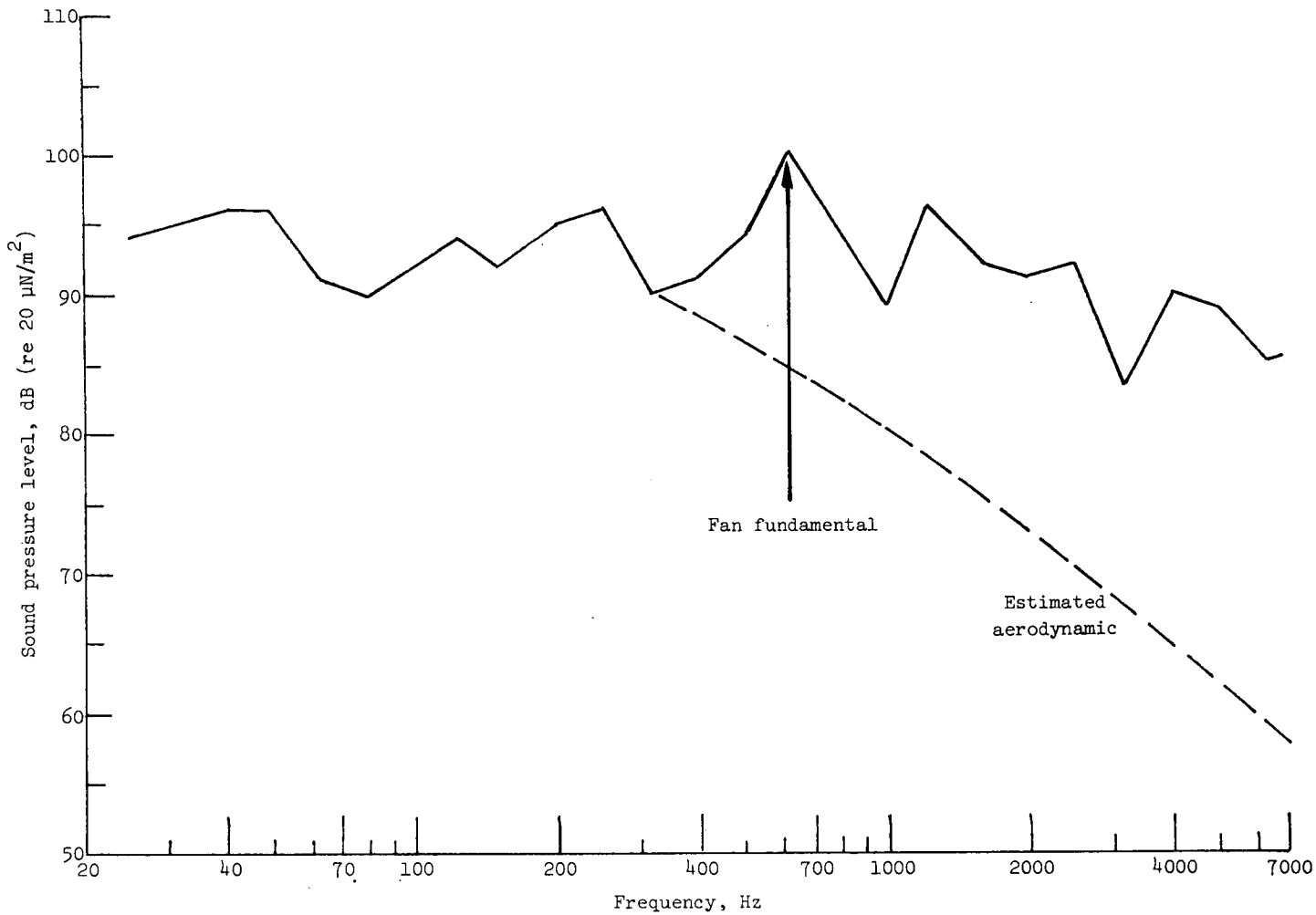

Figure 6.- Noise spectrum for "dirty" configuration. 100-percent flaps and landing gear extended; 1/3-octave band; C-5A Galaxy flyover at 72 m/sec; gross weight 276 696 kg; 55-m altitude; engines at flight idle; run A-5.

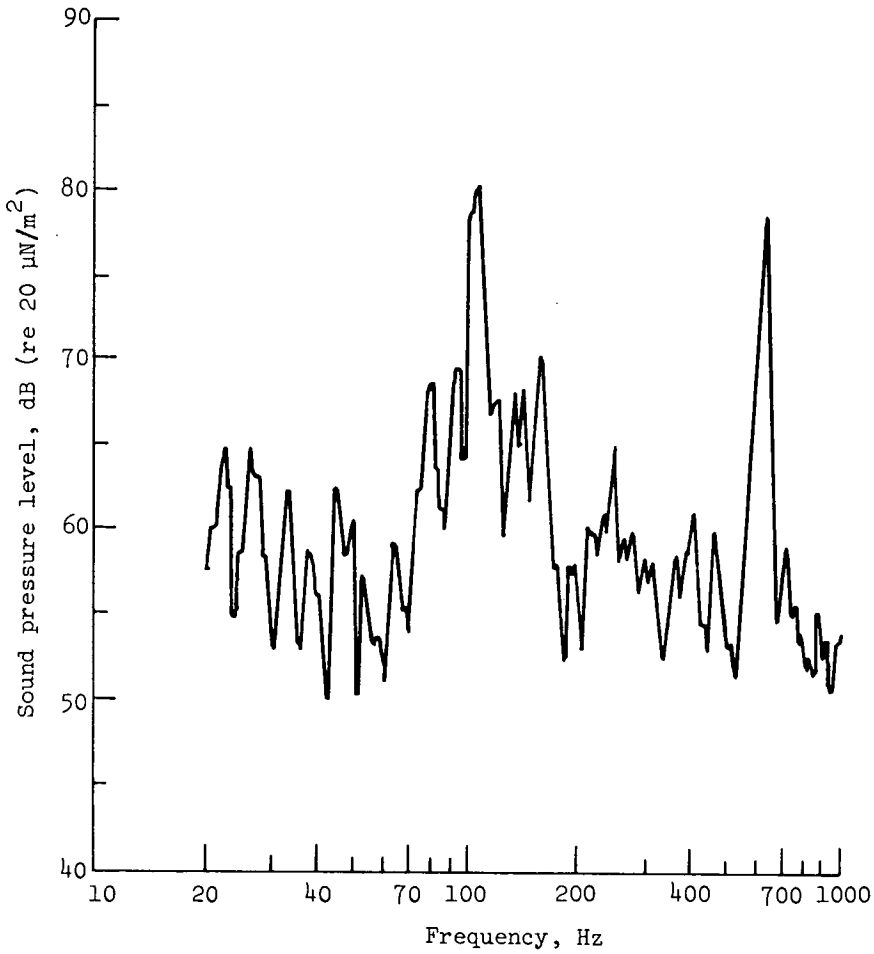

Figure 7.- Narrow band spectrum – "clean" configuration. Run A-1.

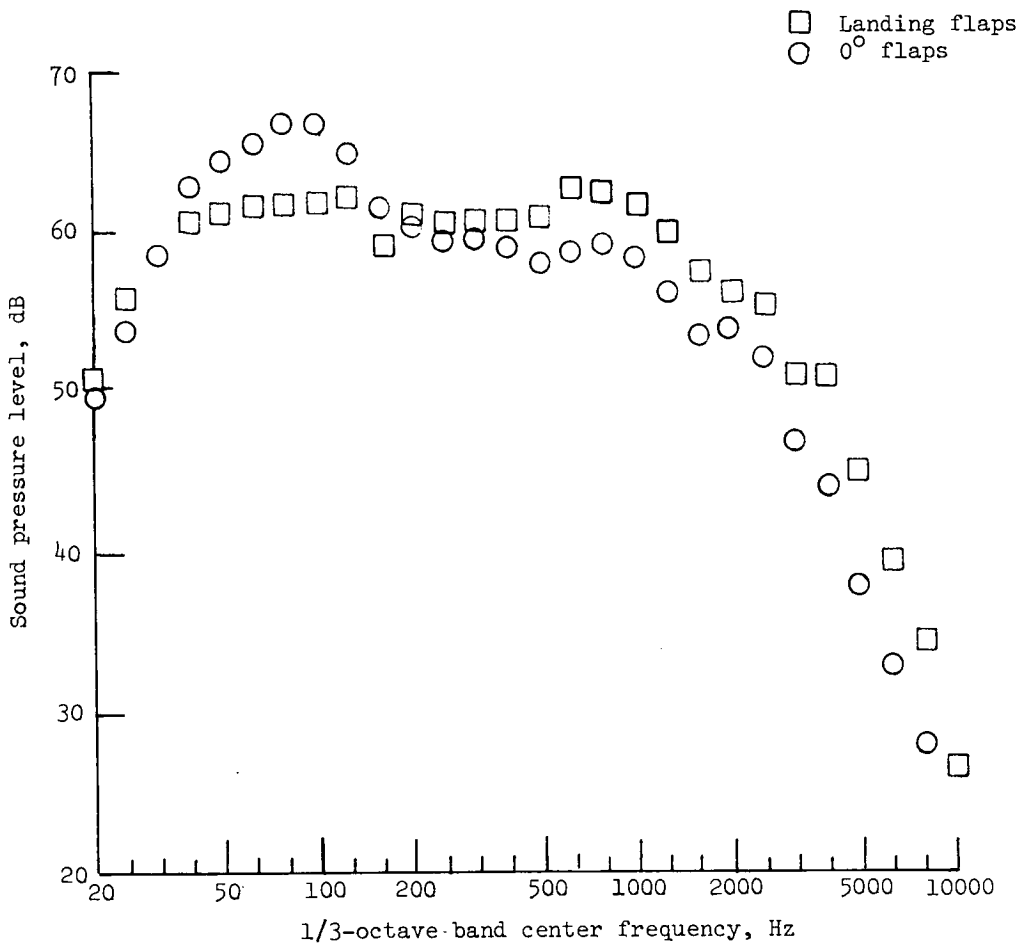

Figure 8.- Effect of landing flaps on noise spectra for Aero Commander. Airspeed, 61.7 m/sec, landing gear extended.

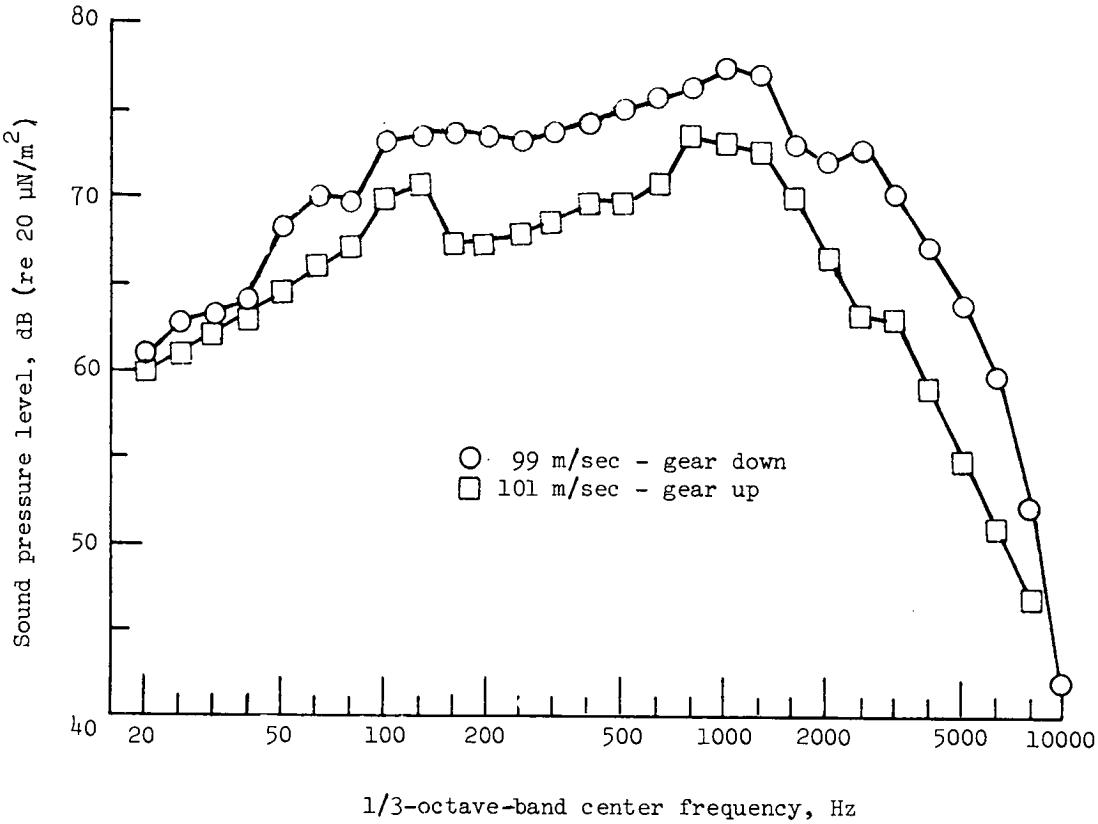

Figure 9.- Effect of landing gear on noise spectra for the JetStar with flaps retracted. Engines idle; normalized to 152 m; standard day conditions.

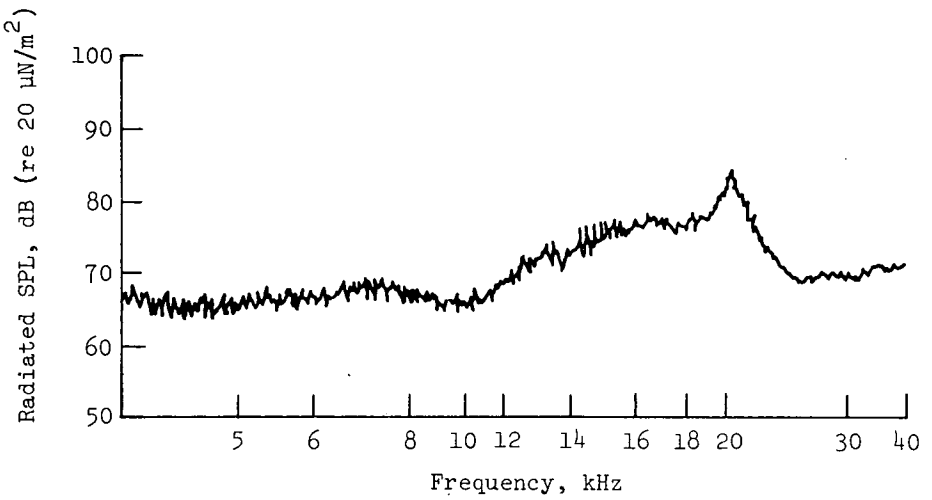

Figure 10.- Radiated sound pressure level for 65 series 0° camber airfoil. Angle of incidence, 0°; c = 5.08 cm (2 in.).

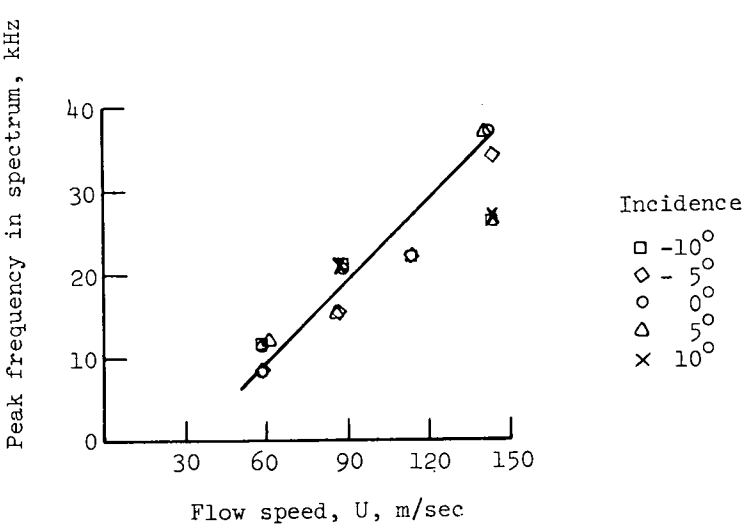

Figure 11.- Peak spectral frequency as a function of flow speed for a 65 series 0° camber airfoil. $t_w/c = 0.10$; c = 5.08 cm (2 in.).

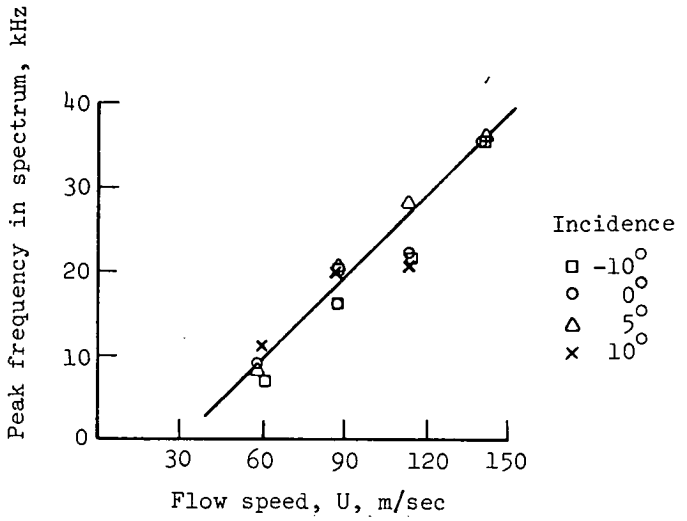

Figure 12.- Peak spectral frequency as a function of flow speed for a 65 series 12.5° camber airfoil. $t_w/c = 0.10$; $c = 5.08$ cm (2 in.).

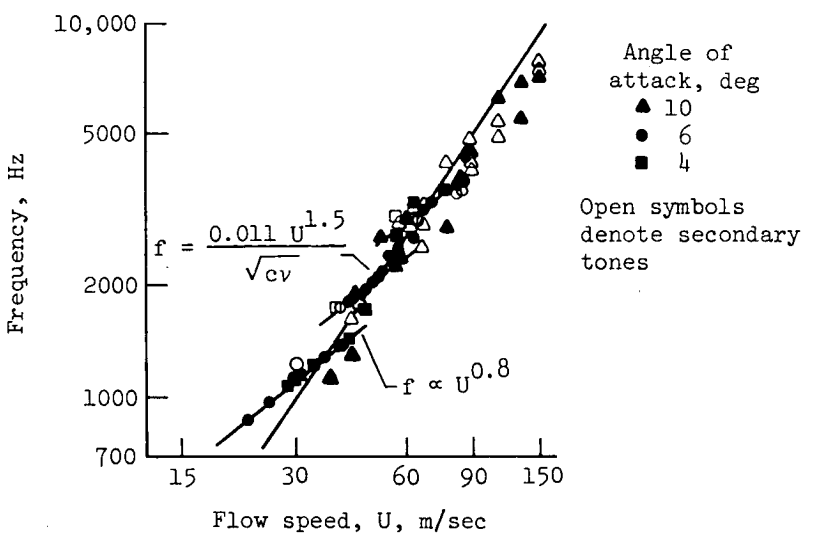

Figure 13.- Effect of velocity on far-field vortex shedding tone frequencies. NACA 0012 full-span airfoil.

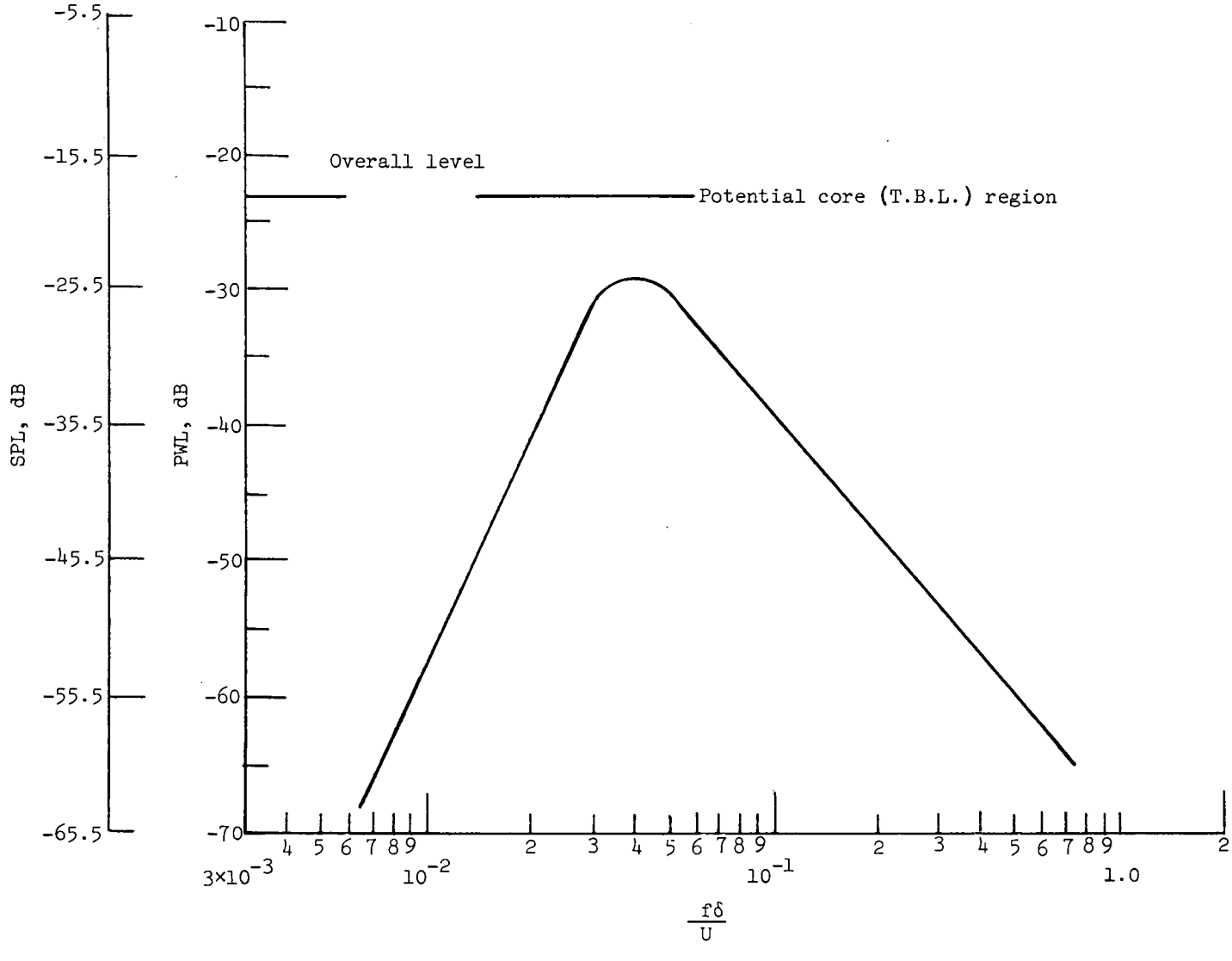

Figure 14.- Normalized 1/3-octave-band spectra of trailing-edge noise.

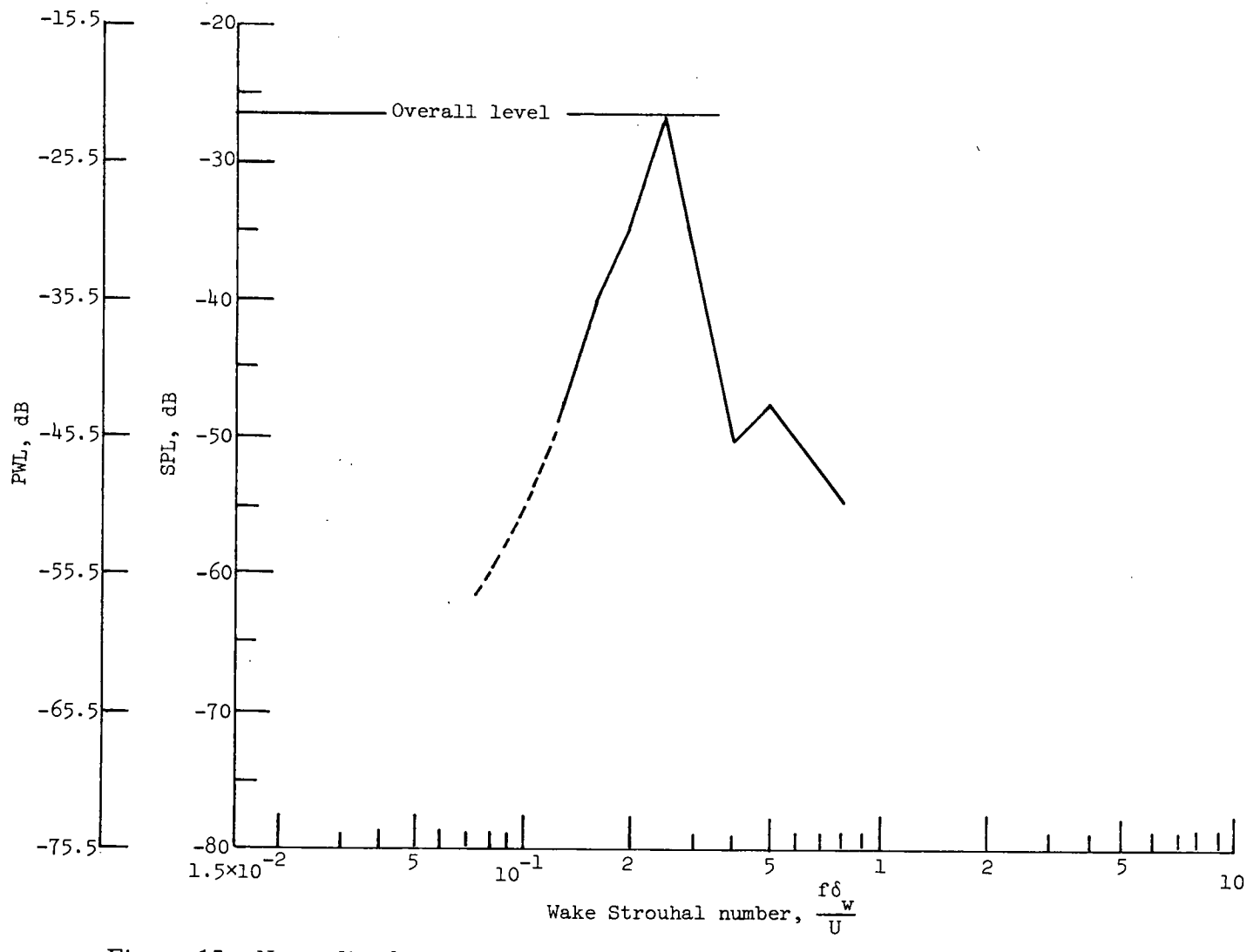

Figure 15.- Normalized spectrum of wake-generated noise; semi-infinite flat plate.

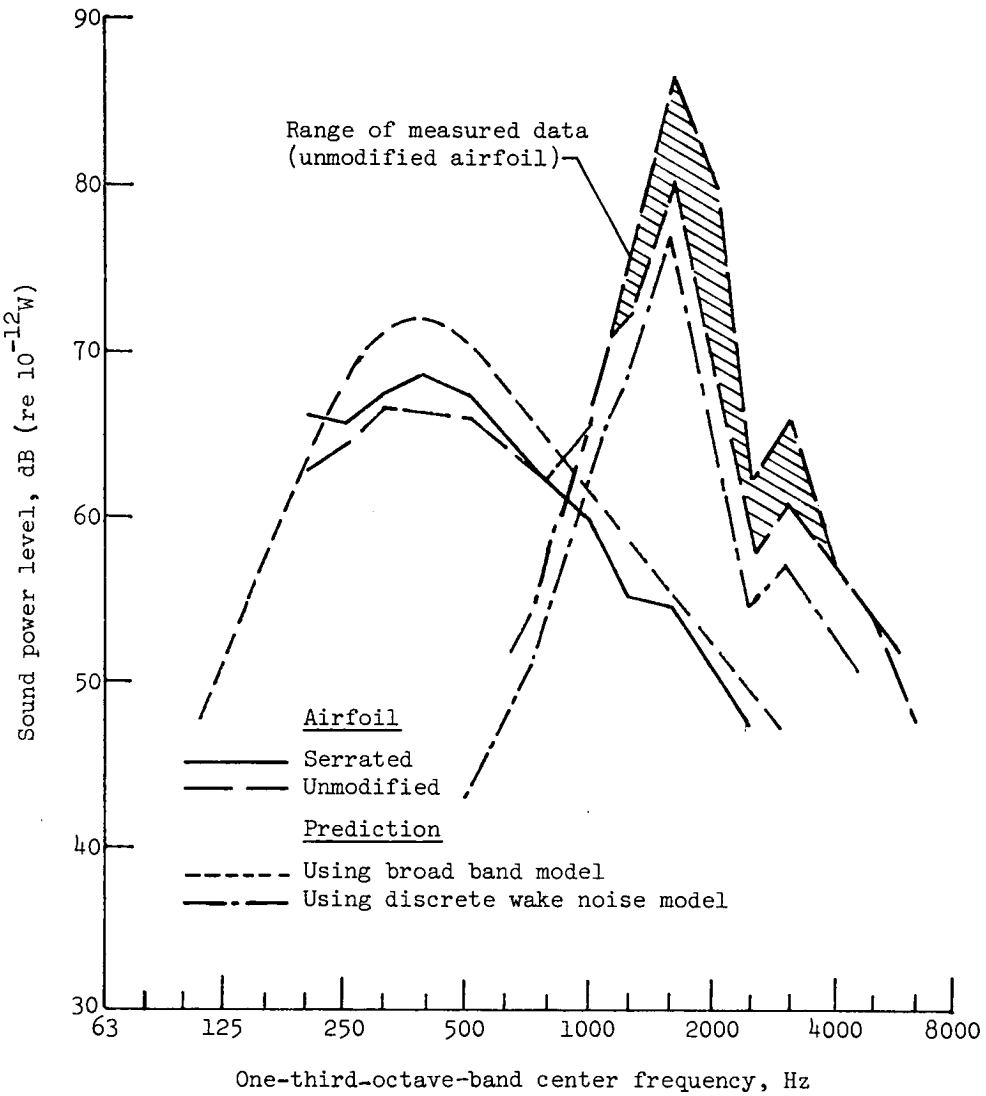

Figure 16.- Comparison of predicted airfoil noise spectrum with measurement.

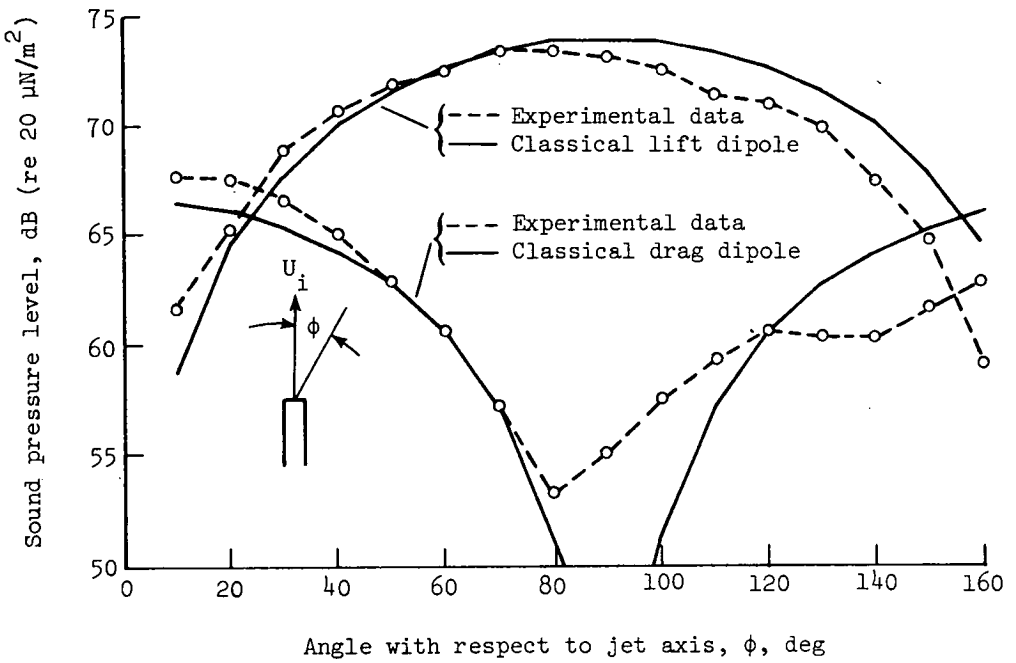

Figure 17.- Comparison of Curle's dipole directivity pattern with experiment. 1250 Hz – 1/3-octave band; $\alpha = 0^{\circ}$; $U_i = 82$ m/sec; data matched to theory at $\phi = 70^{\circ}$.

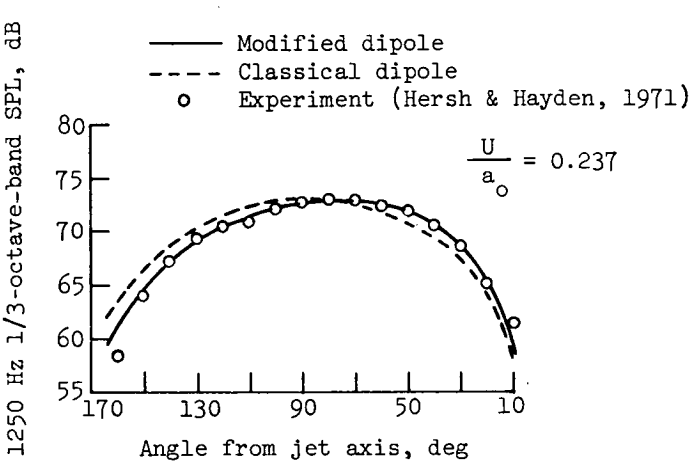

Figure 18.- Comparison of directivity theory and experiment.

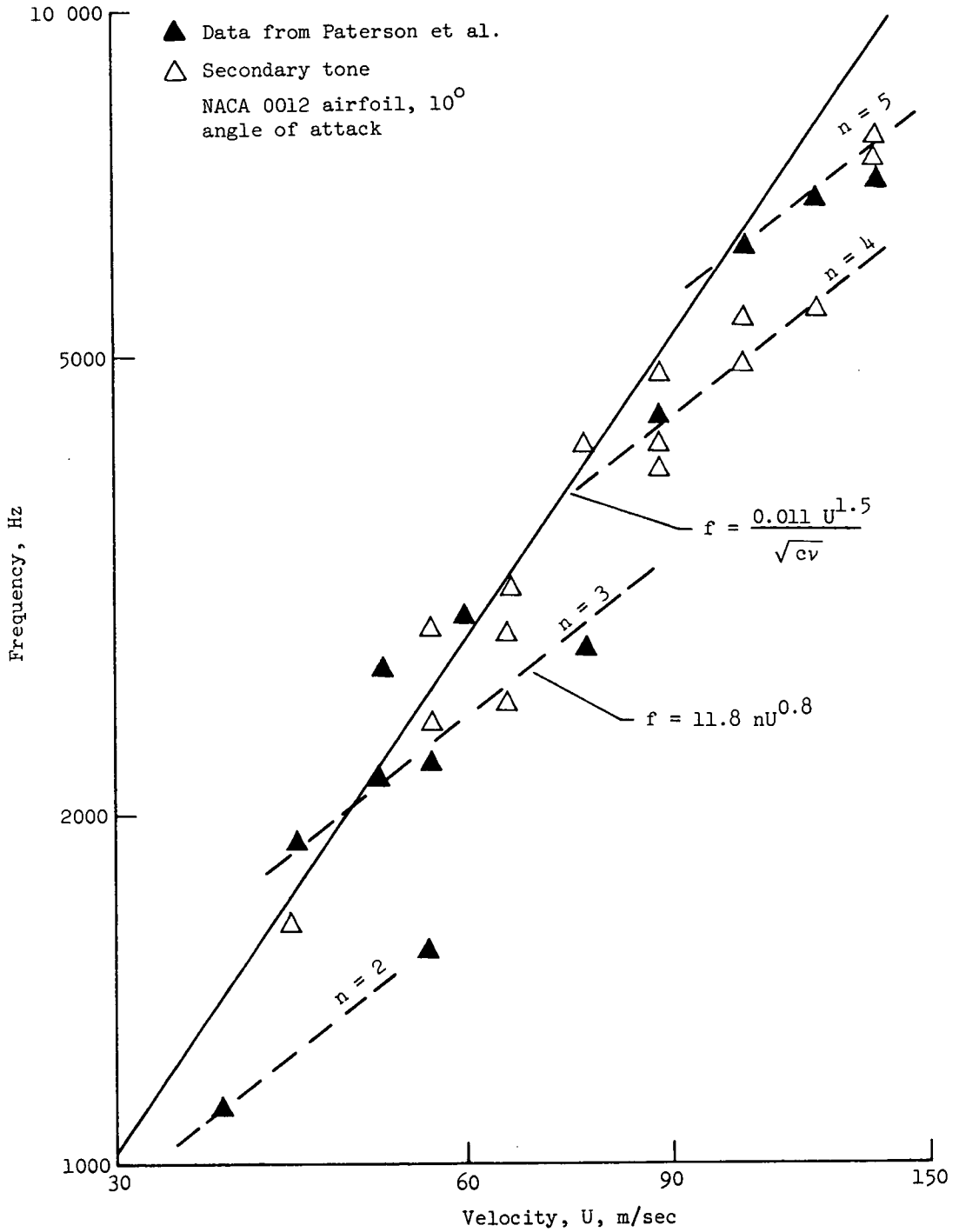

Figure 19.- Effect of velocity on tone frequencies at an angle of attack of 10°.

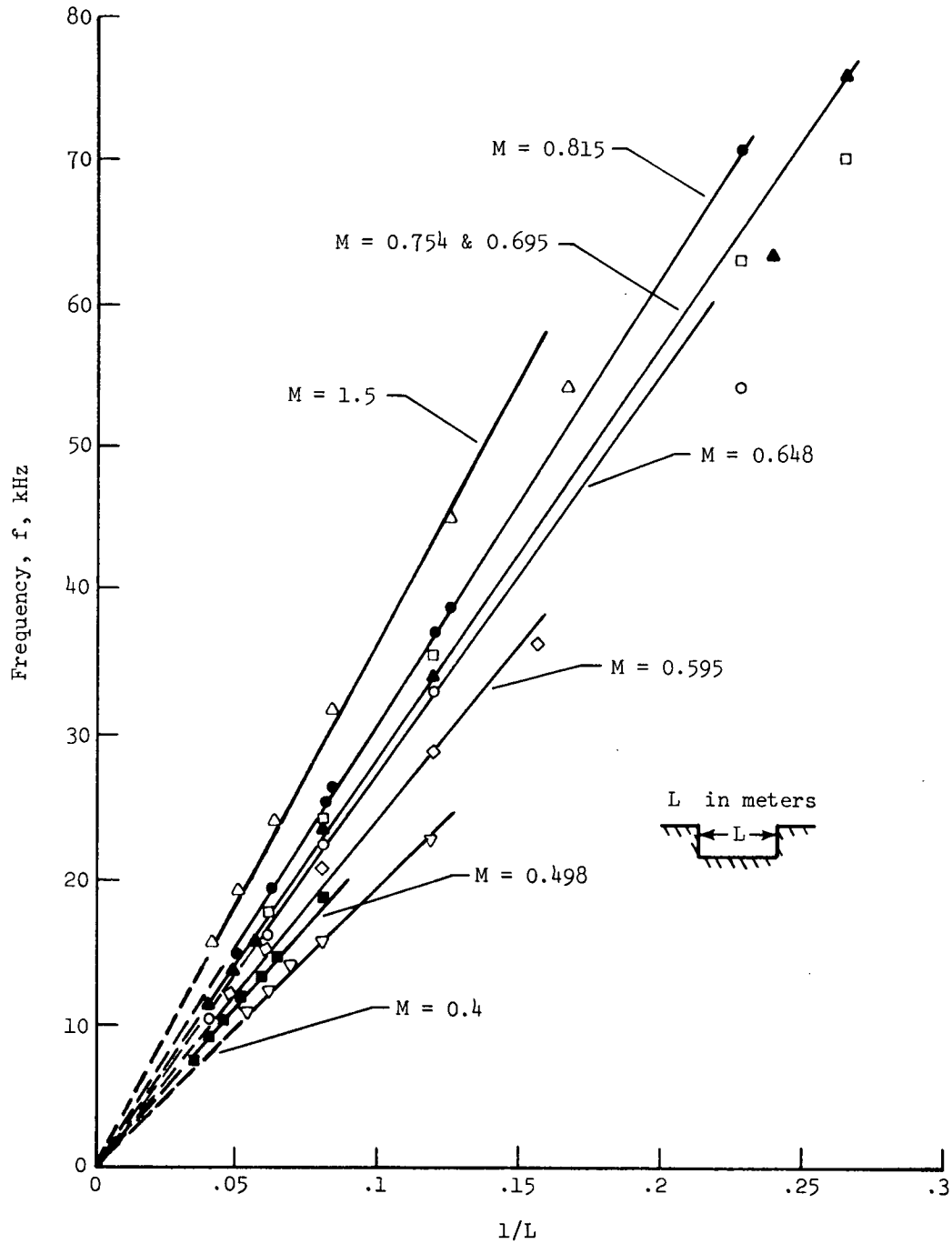

Figure 20.- Results of frequency measurements for laminar flow at different Mach numbers.

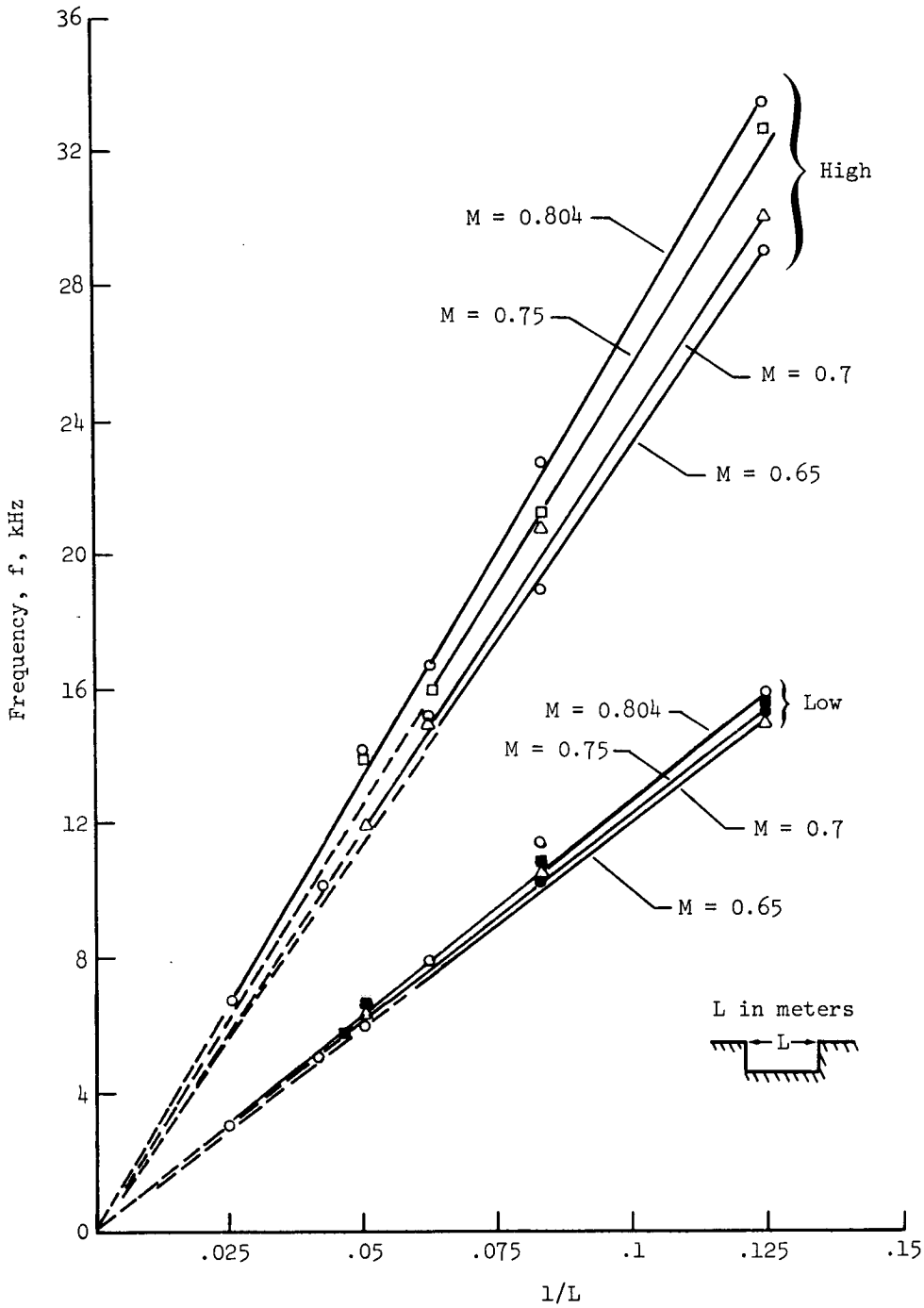

Figure 21.- Results of frequency measurements for turbulent flow at different Mach numbers.

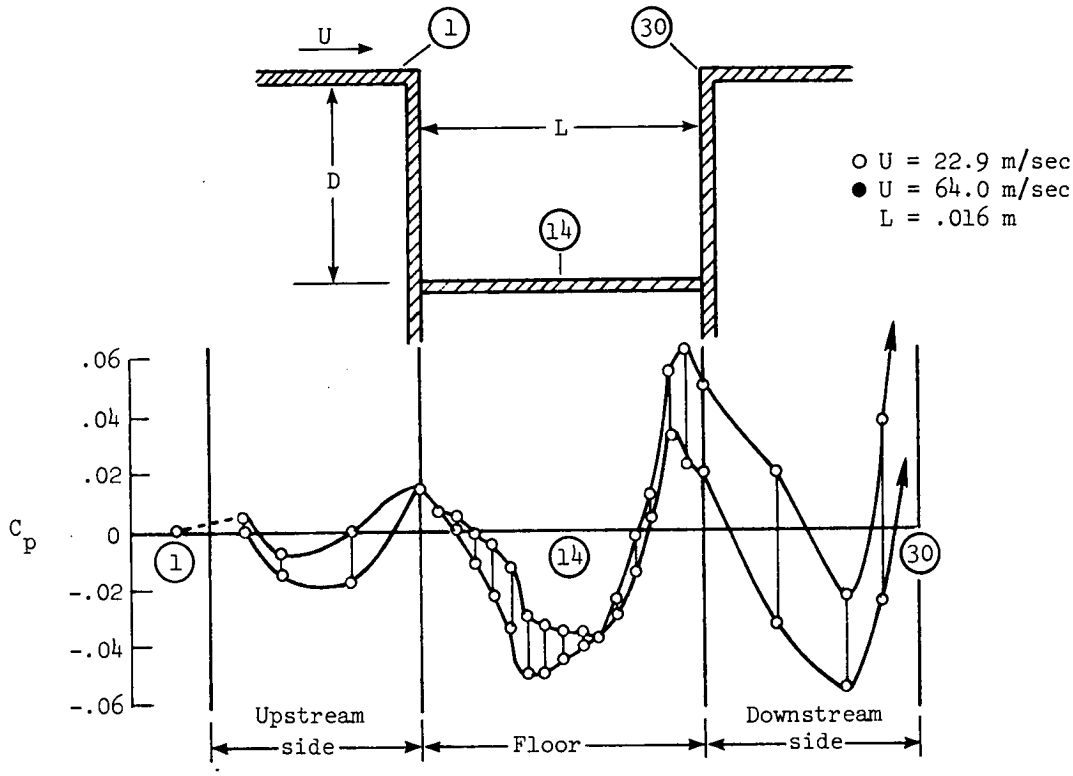

(a) L/D = 0.75.

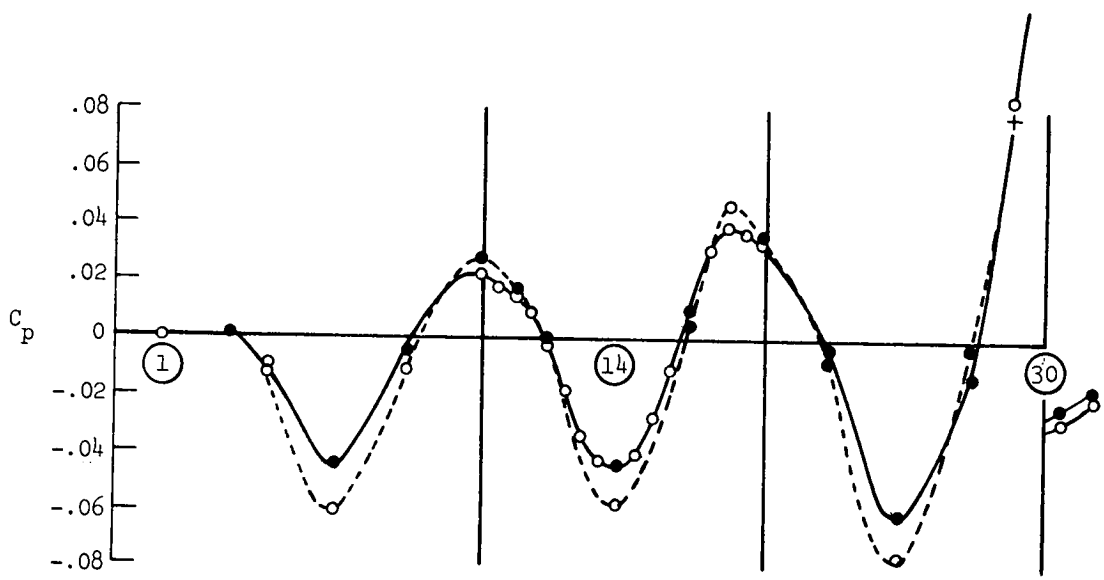

(b) L/D = 1.00.

Figure 22.- Pressure coefficients obtained during cavity traverse.

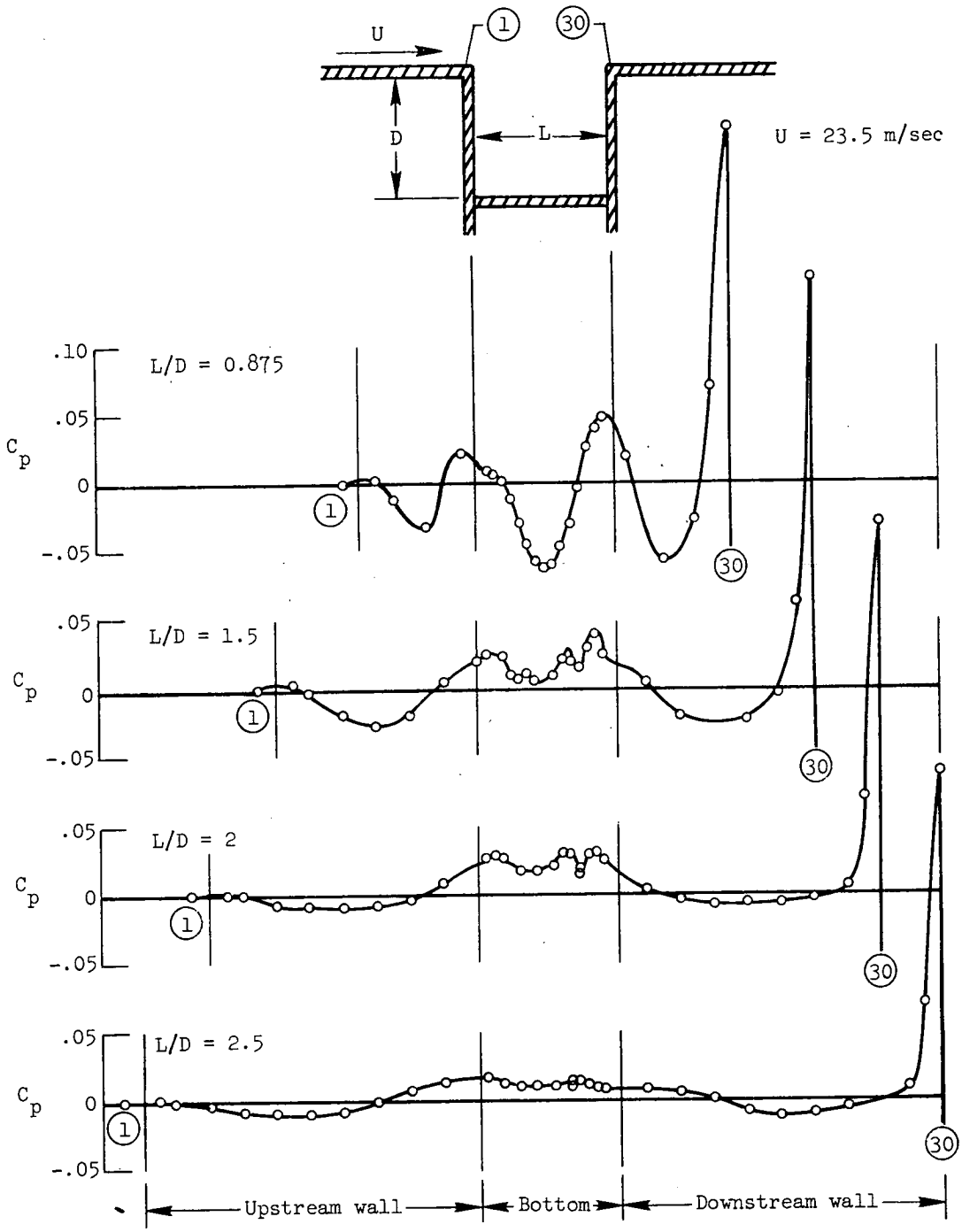

Figure 23.- Pressure traverses for various length-depth ratios.

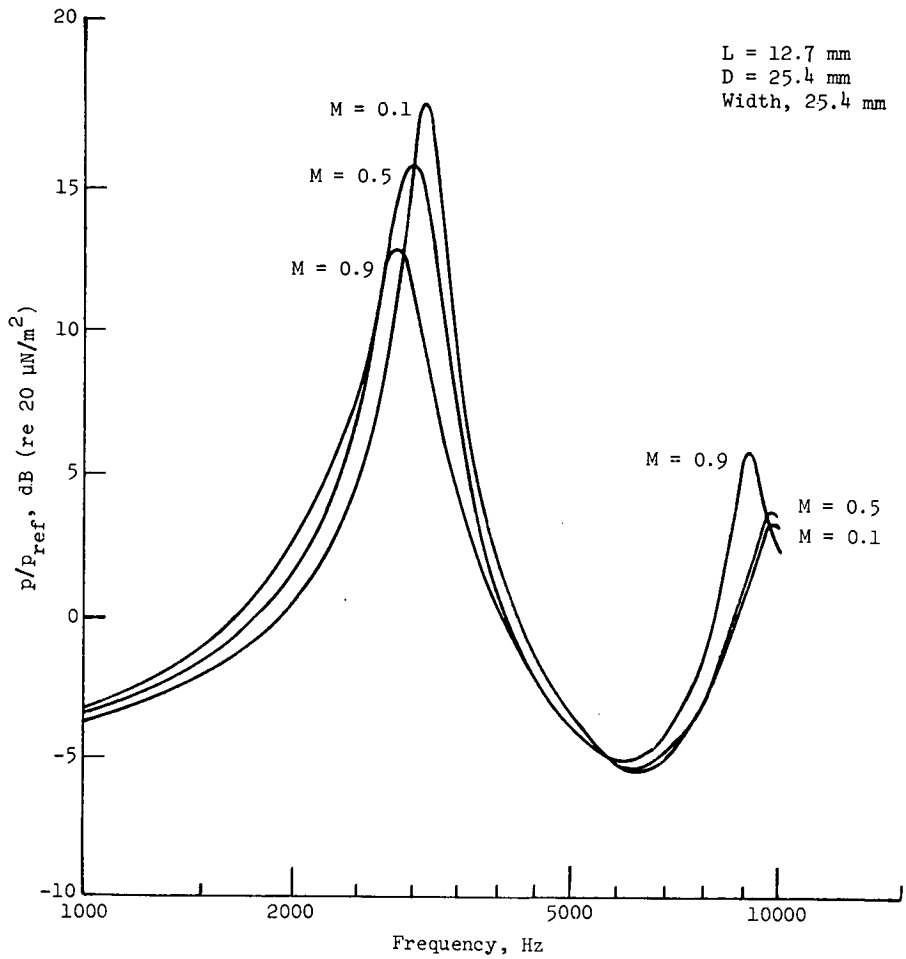

(a) Theoretical amplification of short cavity.

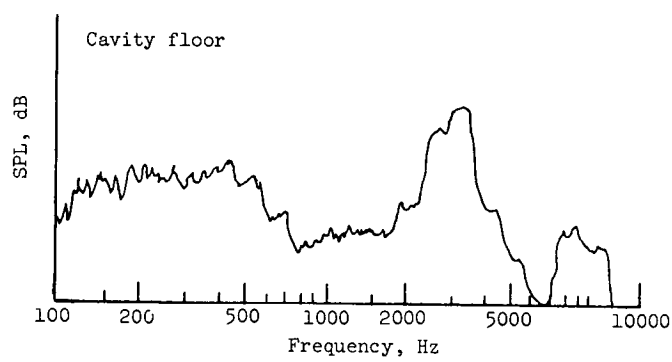

(b) Experimental response spectra.

Figure 24.- Comparison of theoretical and experimental cavity responses.

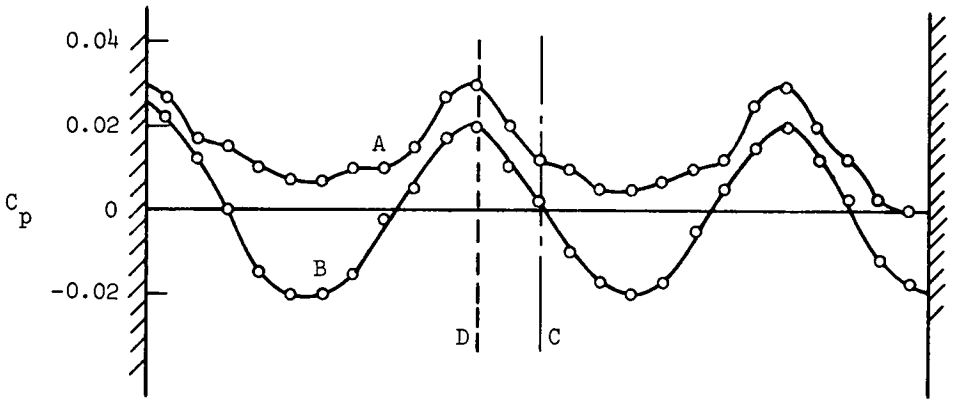

(a) Pressure distribution along span.

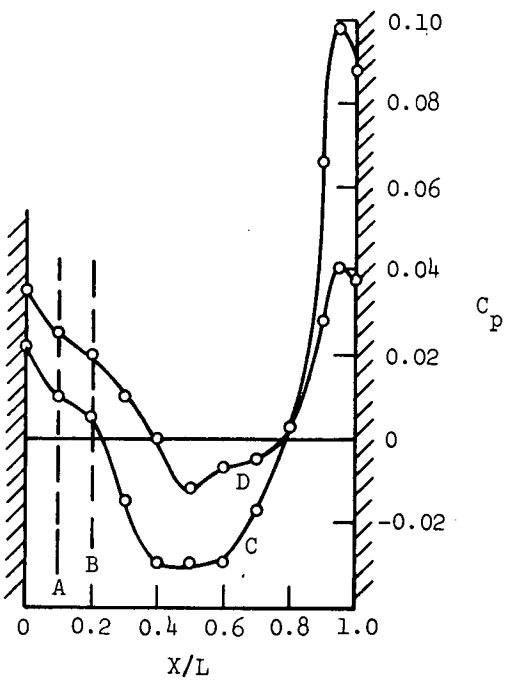

(b) Pressure distribution along chord.

Figure 25.- Typical spanwise and chordwise pressure distributions.

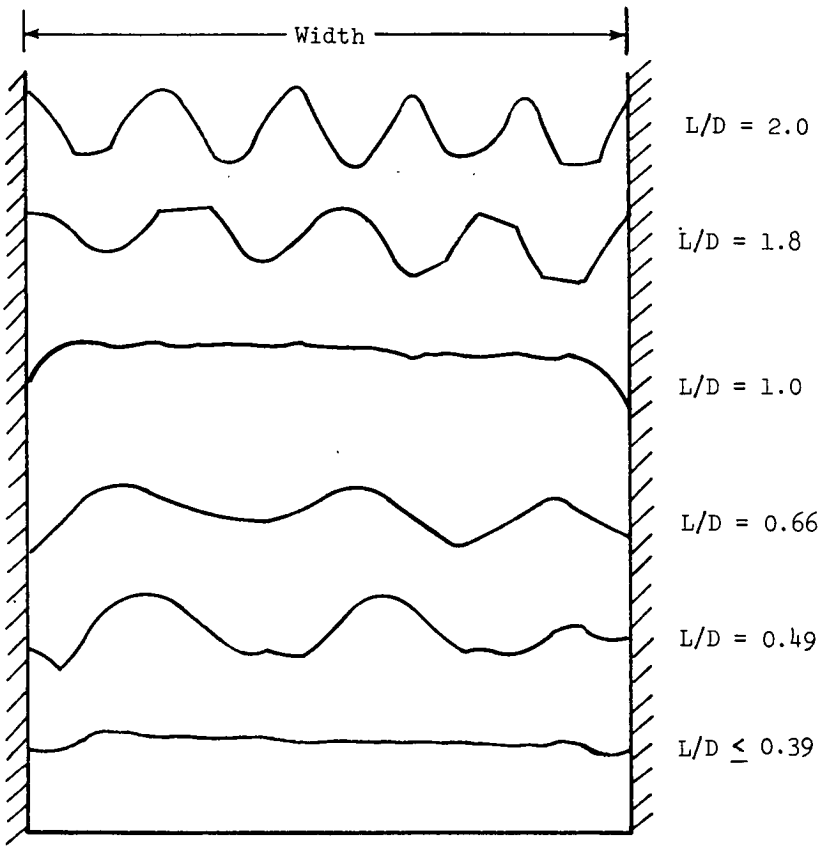

Figure 26.- Spanwise pressure distribution for varying L/D. Width/L = 9.0; C_p = 0.02.

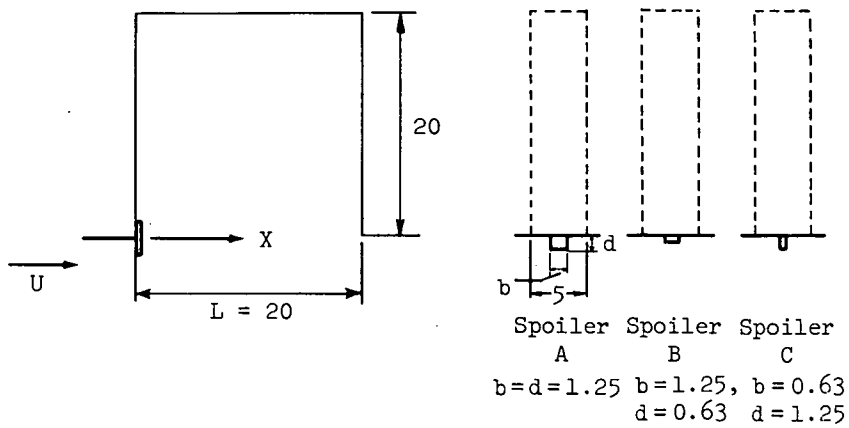

(a) Sketch of spoilers used with cavity with L/D = 1.0. All units are in cm.

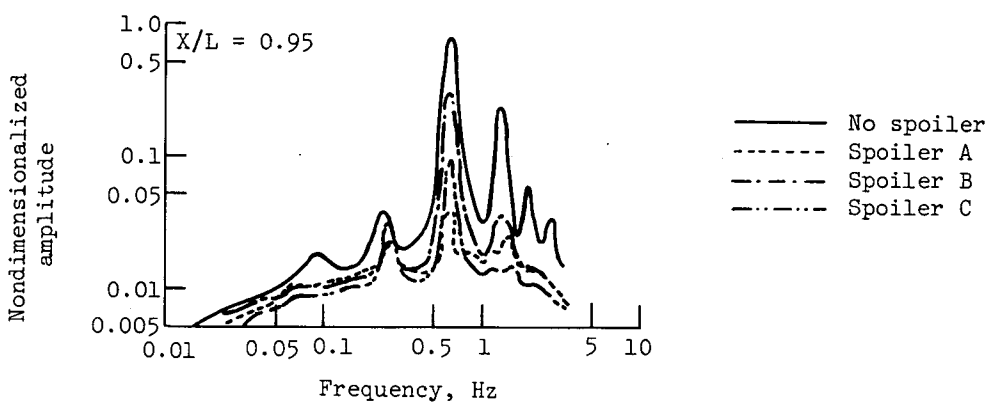

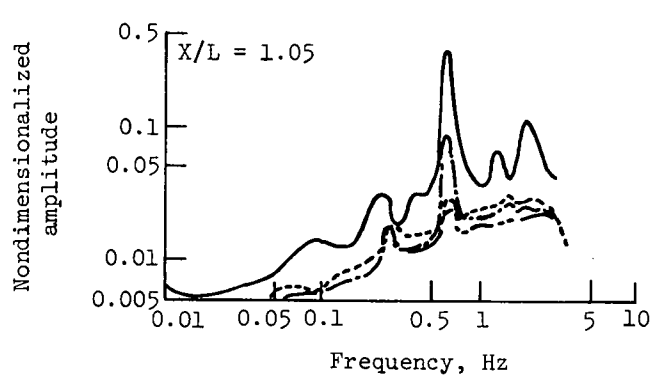

(b) Effect of spoilers on unsteady pressures. L/D = 1.0; M = 0.9.

Figure 27.- Effect of spoilers on cavity response.

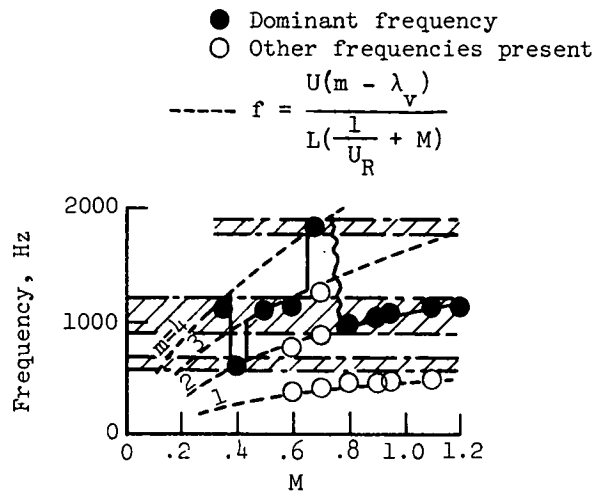

(a) L/D = 2.

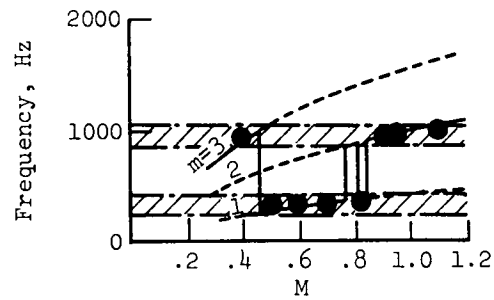

(b) L/D = 1.

Figure 28.- Periodic frequencies in deep cavities.

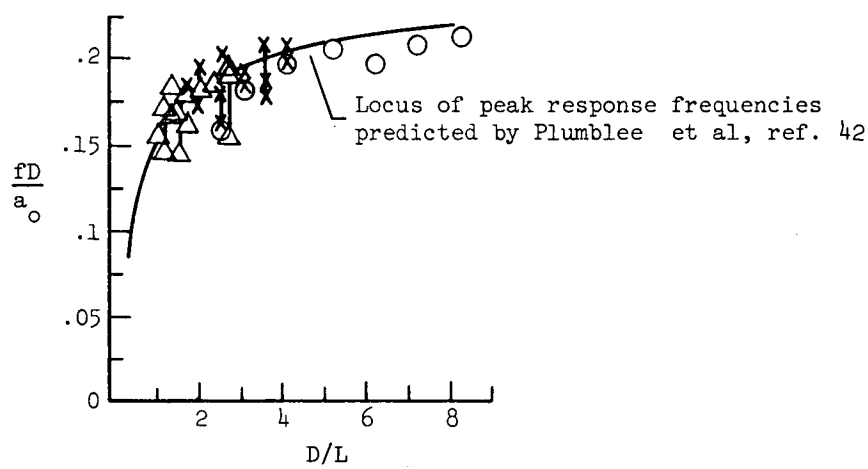

Figure 29.- Plot of resonant conditions. Comparison between theory and experiment.

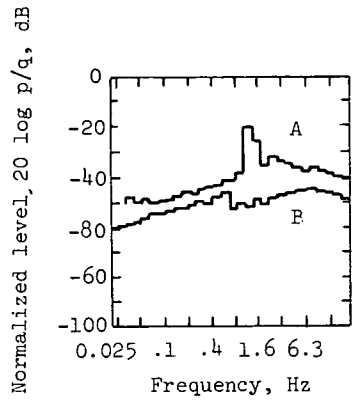

Figure 30.- Comparison of normalized fluctuating pressure spectra at Mach 3 for laminar and turbulent boundary layers. Curve A, laminar boundary layer; Curve B, turbulent boundary layer.

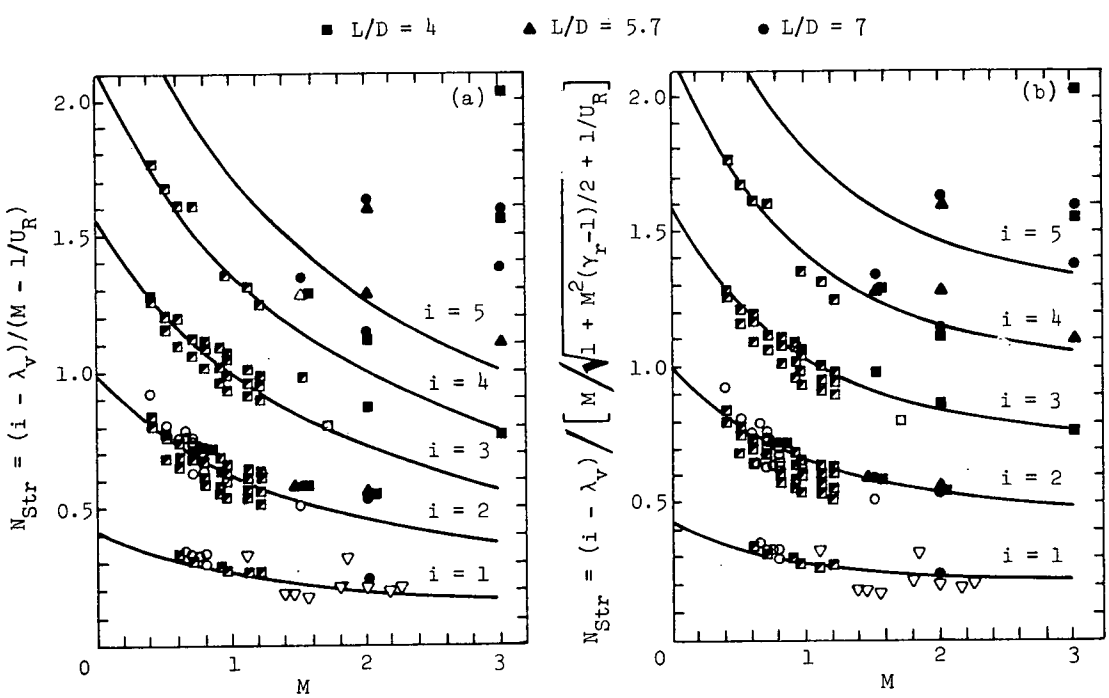

(a) Rossiter's formula. (b) Modification of Rossiter's formula.

Figure 31.- Nondimensional resonant frequencies as functions of Mach number.

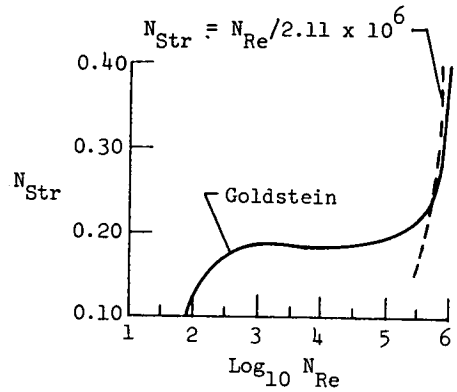

Figure 32.- Variation of N_{Str} with $\log_{10} N_{Re}$ for a circular cylinder.

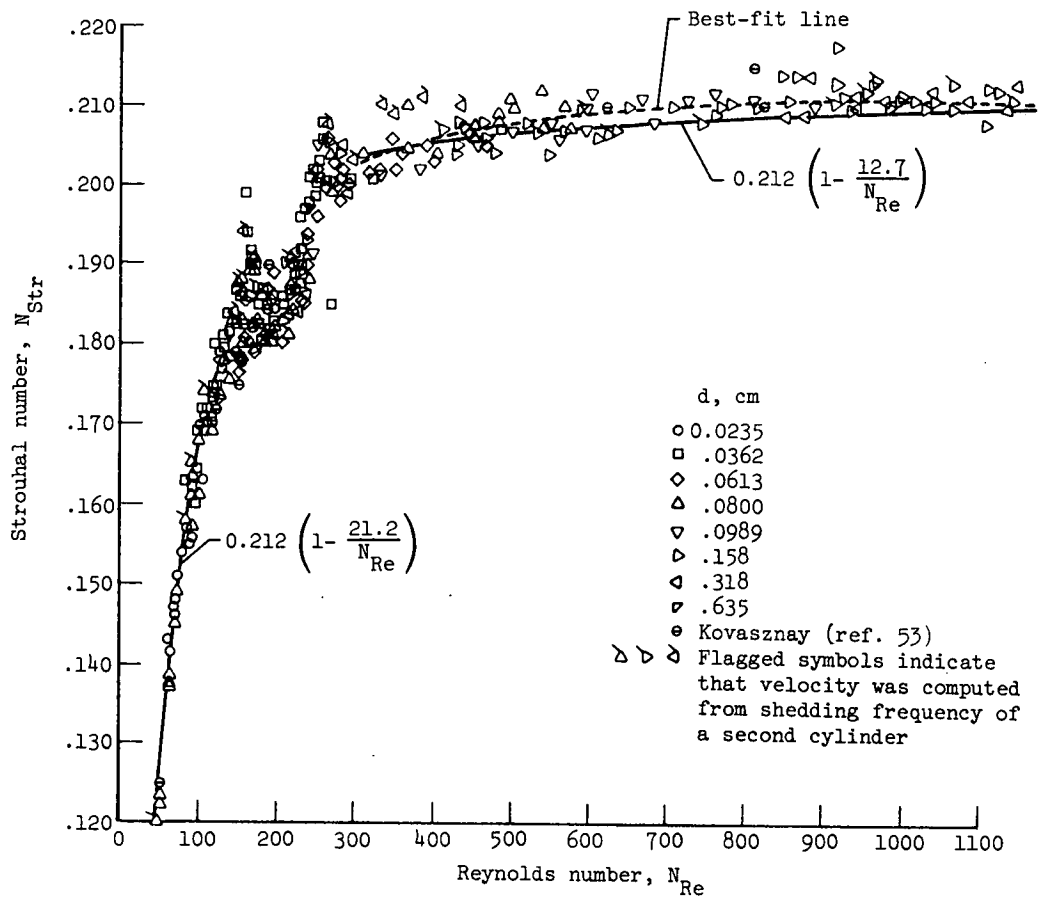

Figure 33.- Variation of N_{Str} with N_{Re} for a circular cylinder.

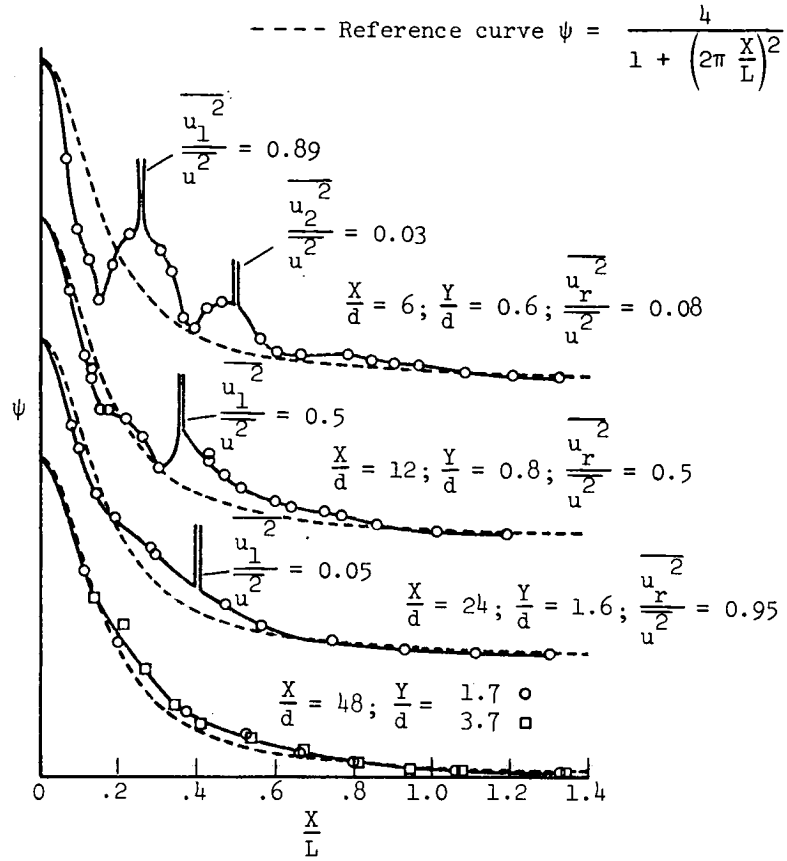

Figure 34.- Downstream development of spectrum. d = 0.190 cm; N_{Re} = 500.

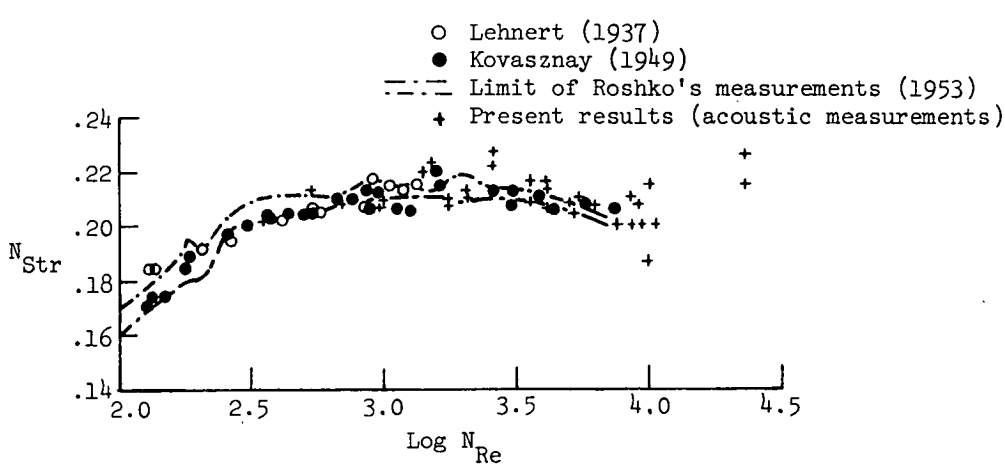

Figure 35.- Nondimensional sound frequency compared with wake frequency.

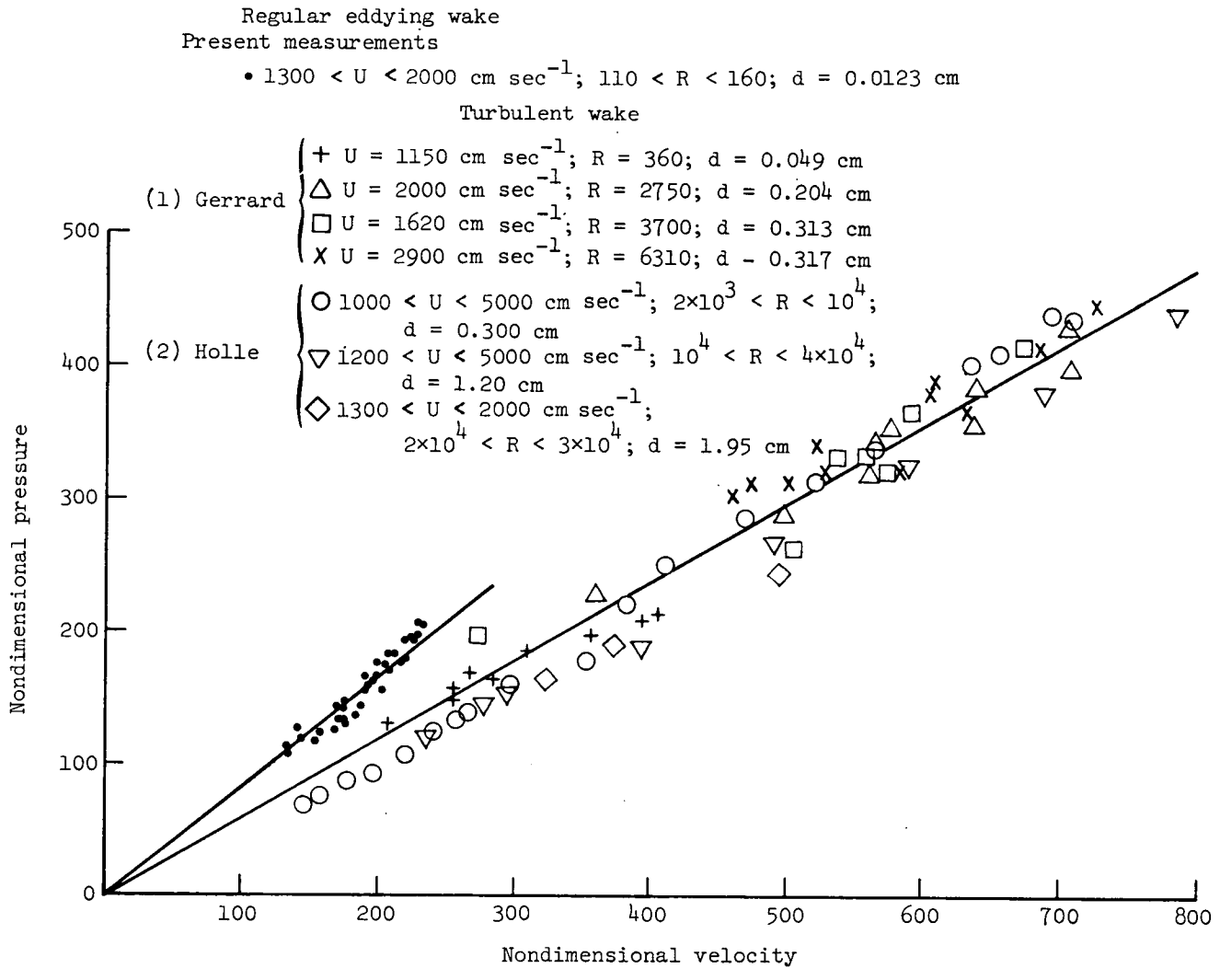

Figure 36.- Mean-square pressure versus velocity.

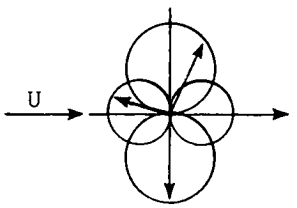

Sound field due to lift,

$$\text{Frequency} = \frac{N_{Str}}{d}$$

Sound field due to drag,

$$\text{Frequency} = \frac{2N_{Str}U}{d}$$

Figure 37.- Sound fields due to oscillating lift and drag in plane x_1,x_2.

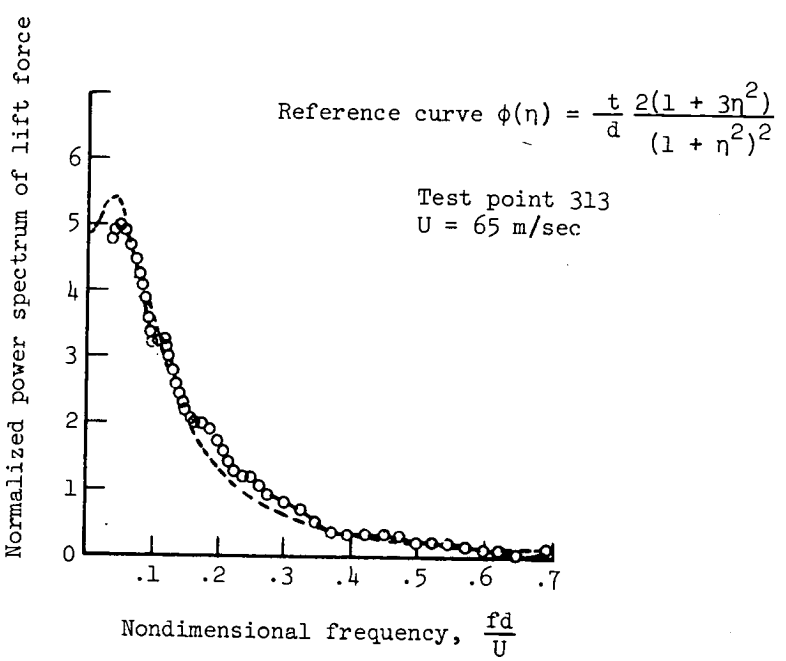

Figure 38.- Normalized power spectrum for the lift force $N_{Re} = 1.27 \times 10^6$; $\eta = \frac{fd}{U}$.

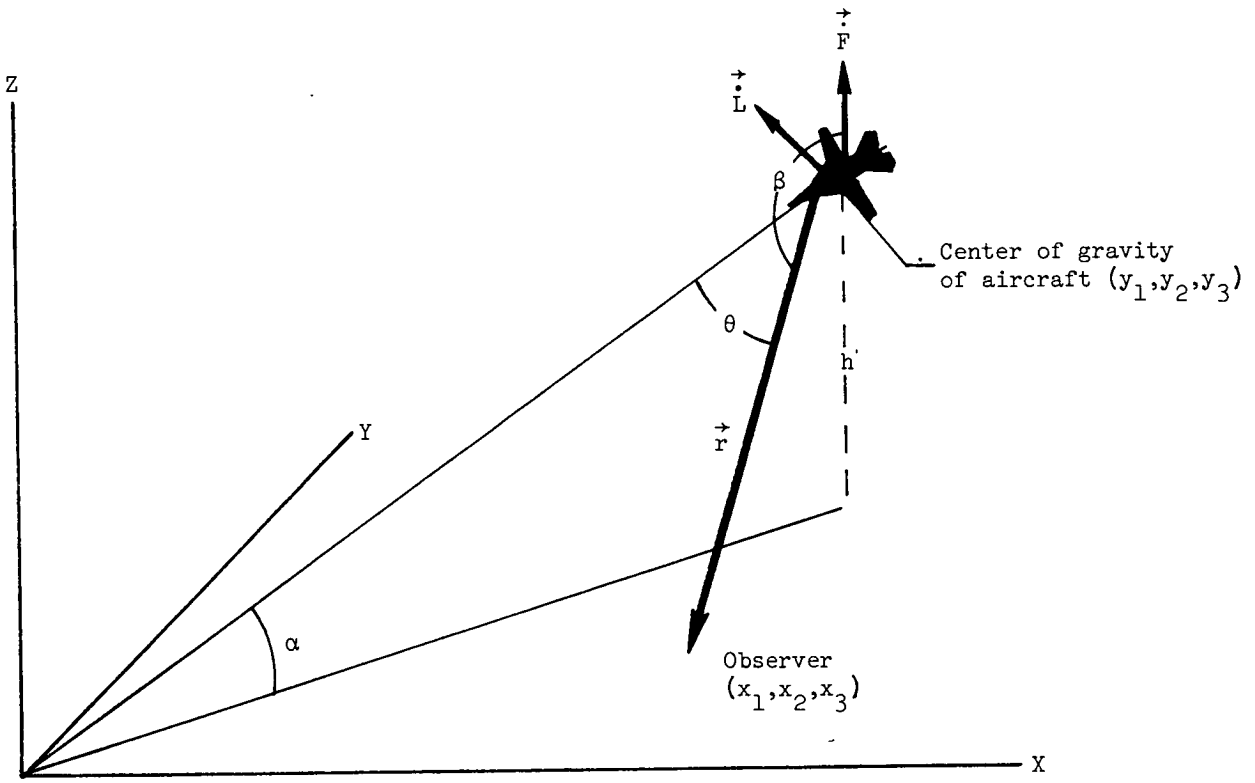

Figure 39.- Geometry for flyover noise analysis.

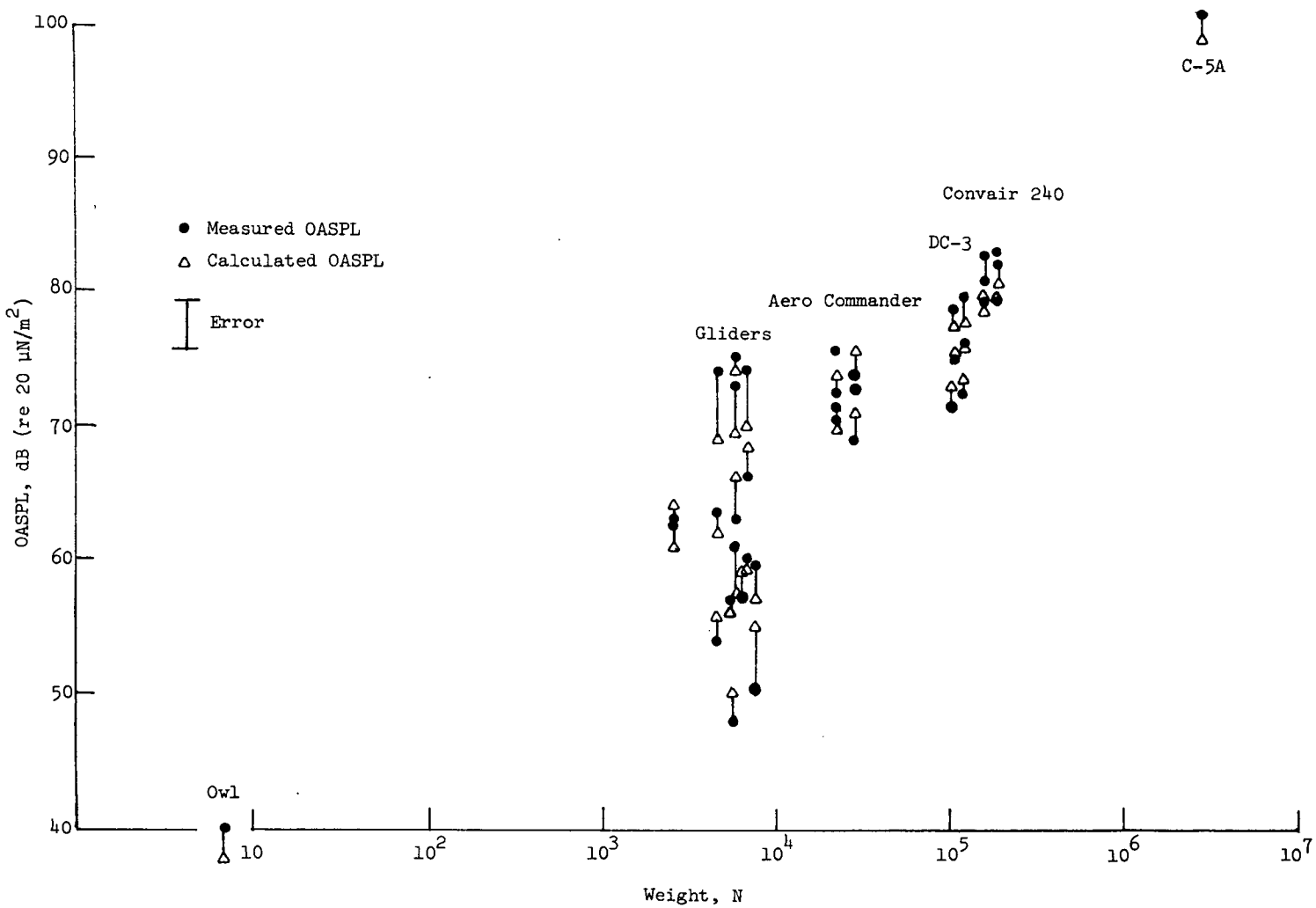

Figure 40.- Comparison of measured and predicted airframe noise levels.

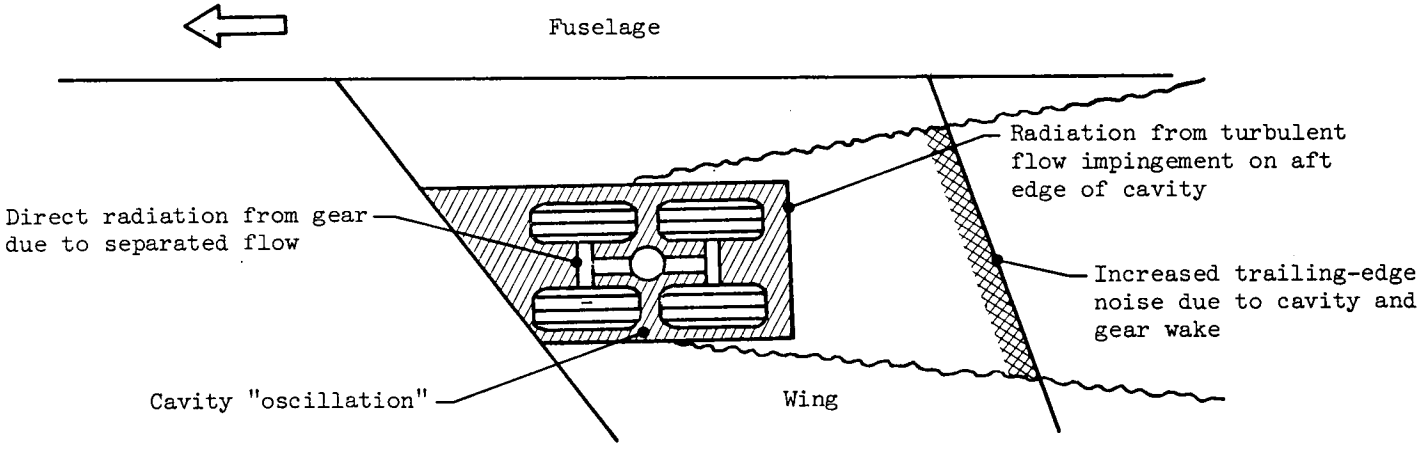

Figure 41.- Schematic of cavity and gear noise sources.

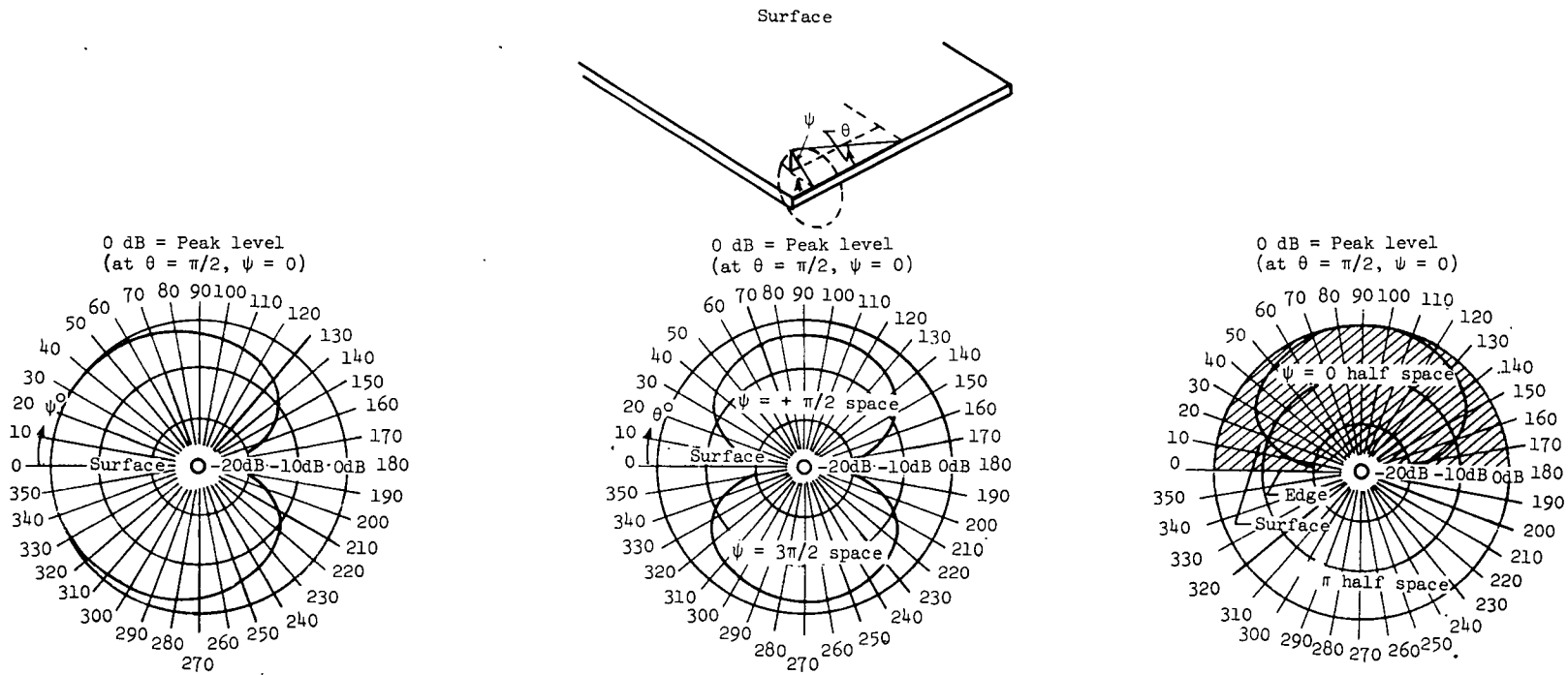

(a) In plane normal to surface and to span.

(b) In plane normal to surface and parallel.

(c) In plane of the surface.

Figure 42.- Directivity of edge sources.

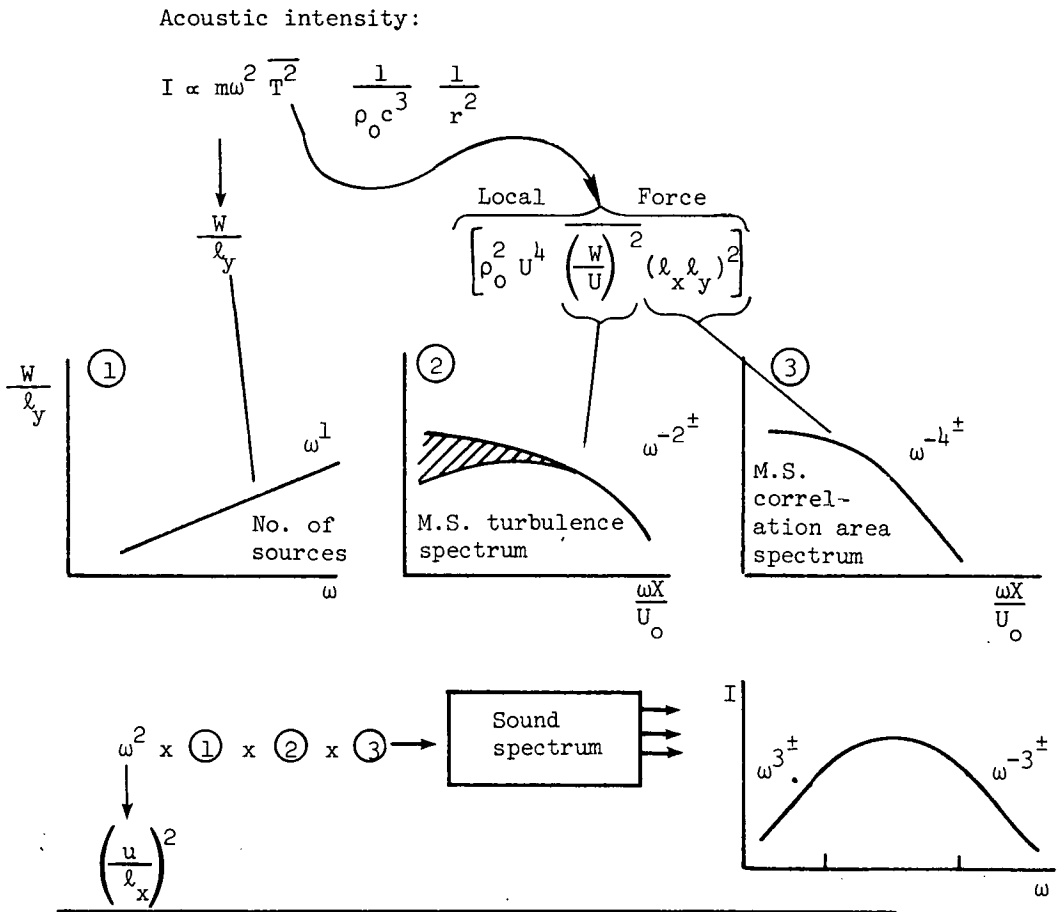

Intensity at constant Strouhal number (or RMS)

$$I \propto \frac{m\omega^2 T^2}{\rho_o c^3} = \left(\frac{W}{\ell_y}\right)\left(\frac{U}{\ell_x}\right)^2 \rho_o^2 U^4 \overline{\left(\frac{W}{U}\right)^2} (\ell_x \ell_y)^2$$

$$I \propto \rho_o \frac{U^6}{c^3} \overline{\left(\frac{W}{U}\right)^2} W \ell_y$$

Figure 43.- Steps in predicting trailing-edge noise.

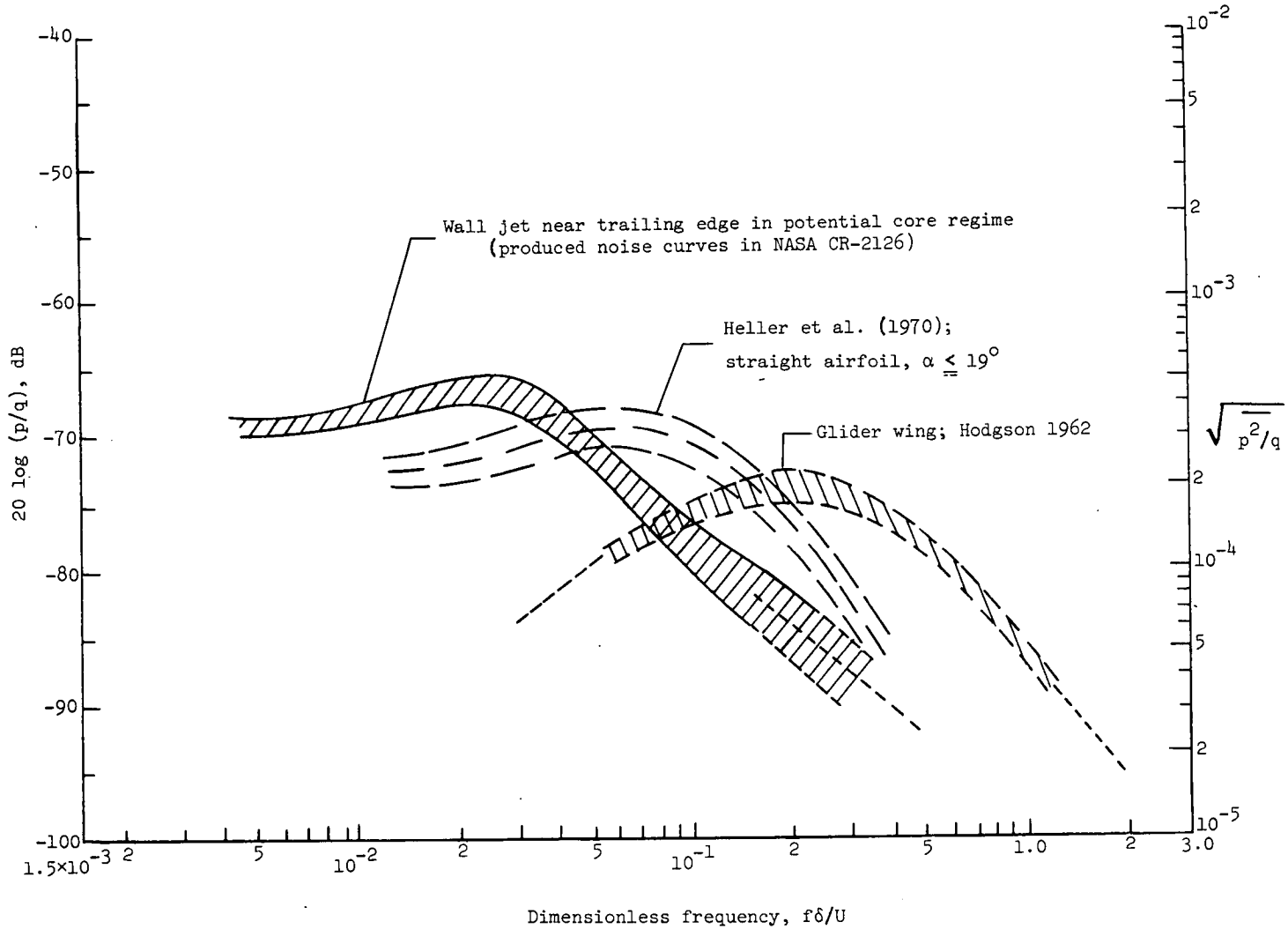

Figure 44.- Comparison of surface pressure spectra for three flow fields for purpose of modifying Hayden's edge noise curve for application to airfoils in smooth flow.

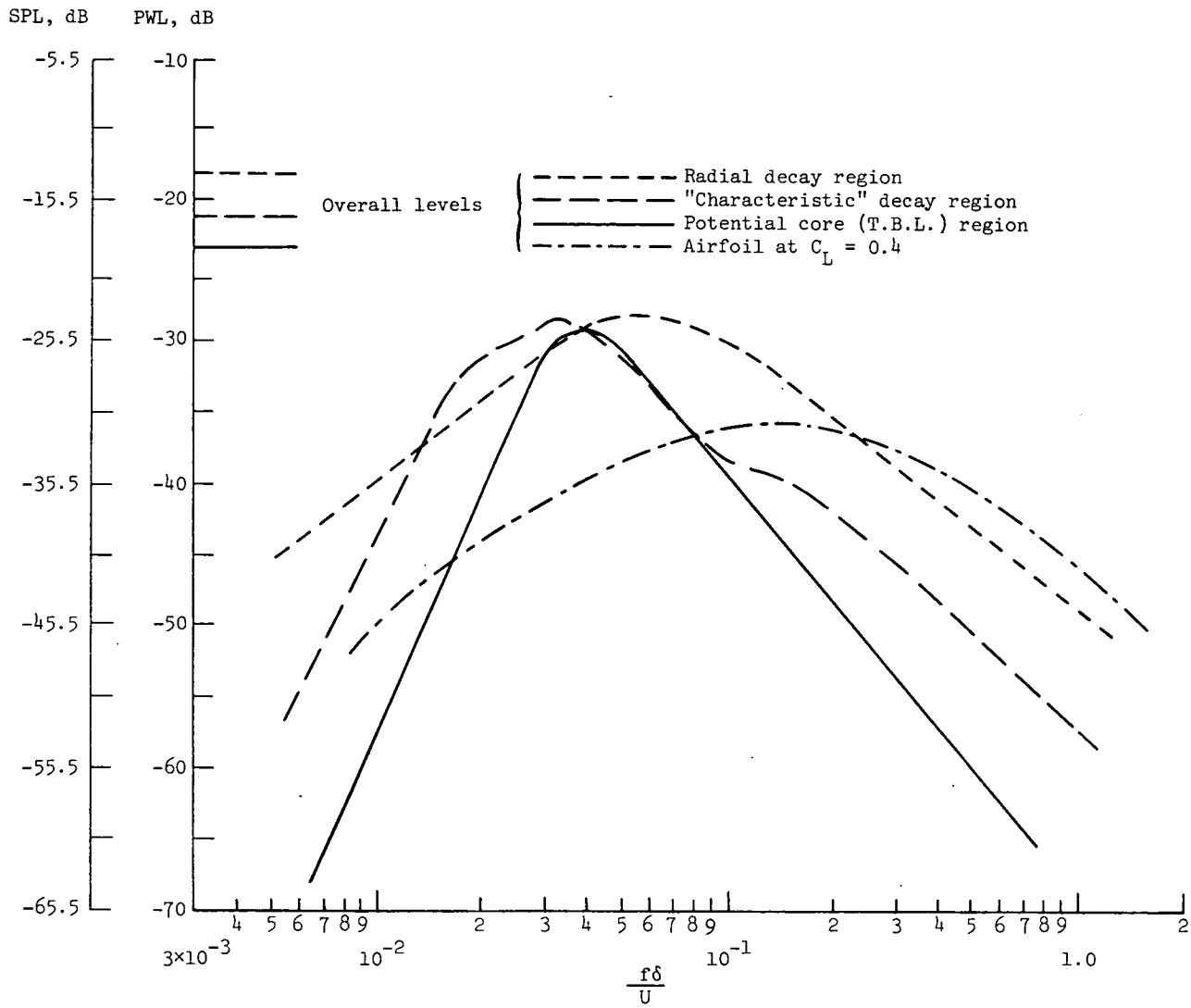

Figure 45.- Normalized one-third-octave-band spectra of trailing-edge noise.

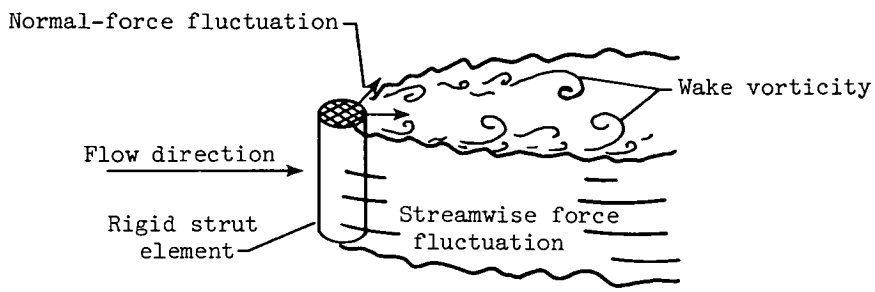

Figure 46.- Schematic of fluid forces associated with strut element.

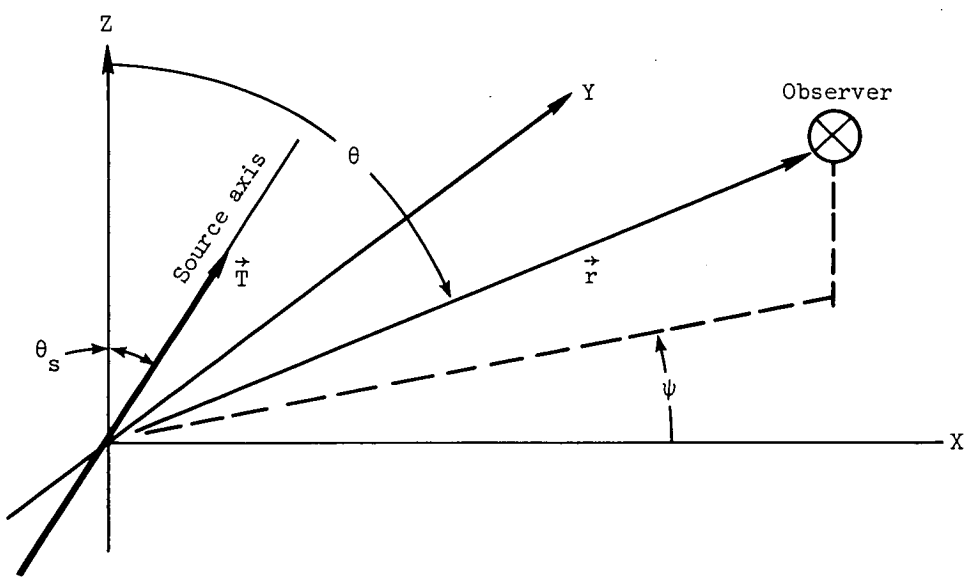

Figure 47.- Coordinate system for computing point dipole sound field.

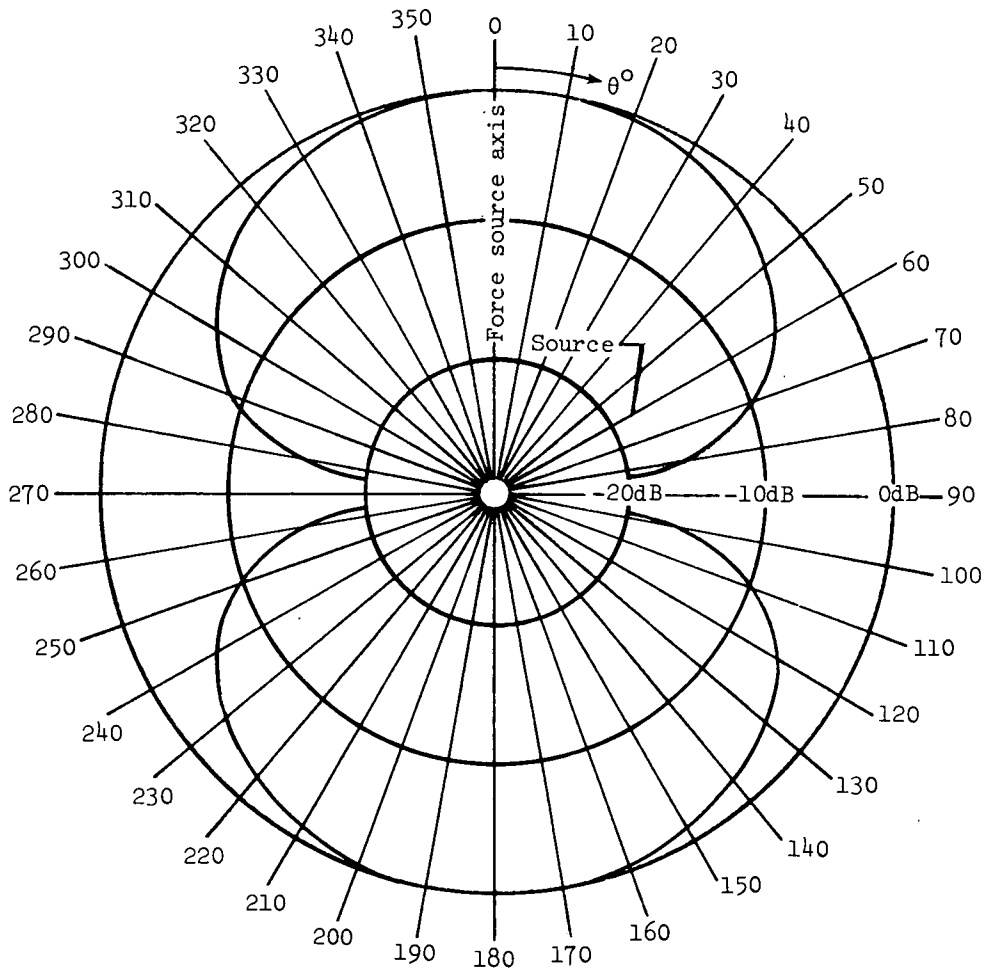

Figure 48.- Sound pressure level directivity for free-field point dipole.

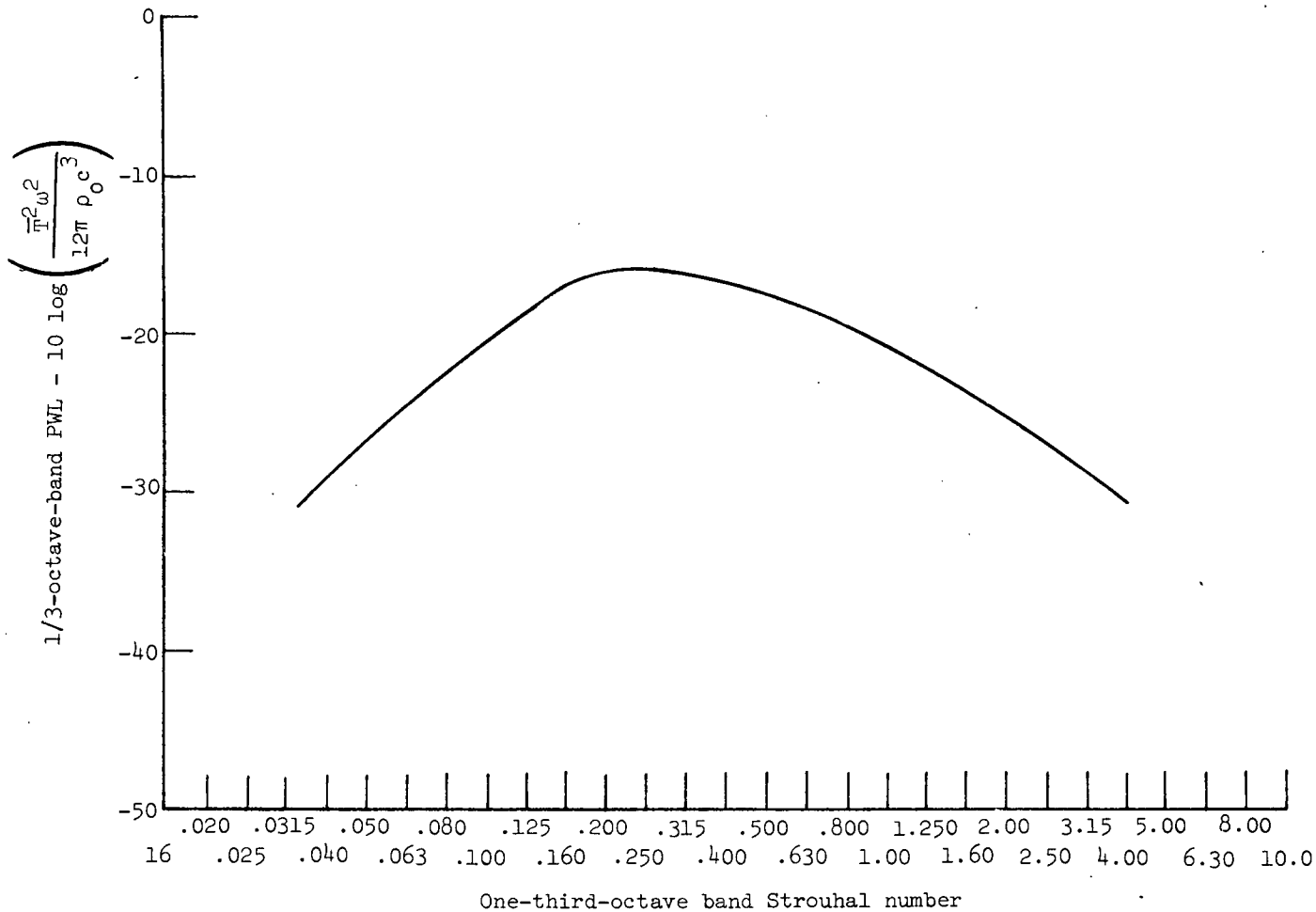

Figure 49.- Spectrum relative to overall level for noise from bluff bodies.

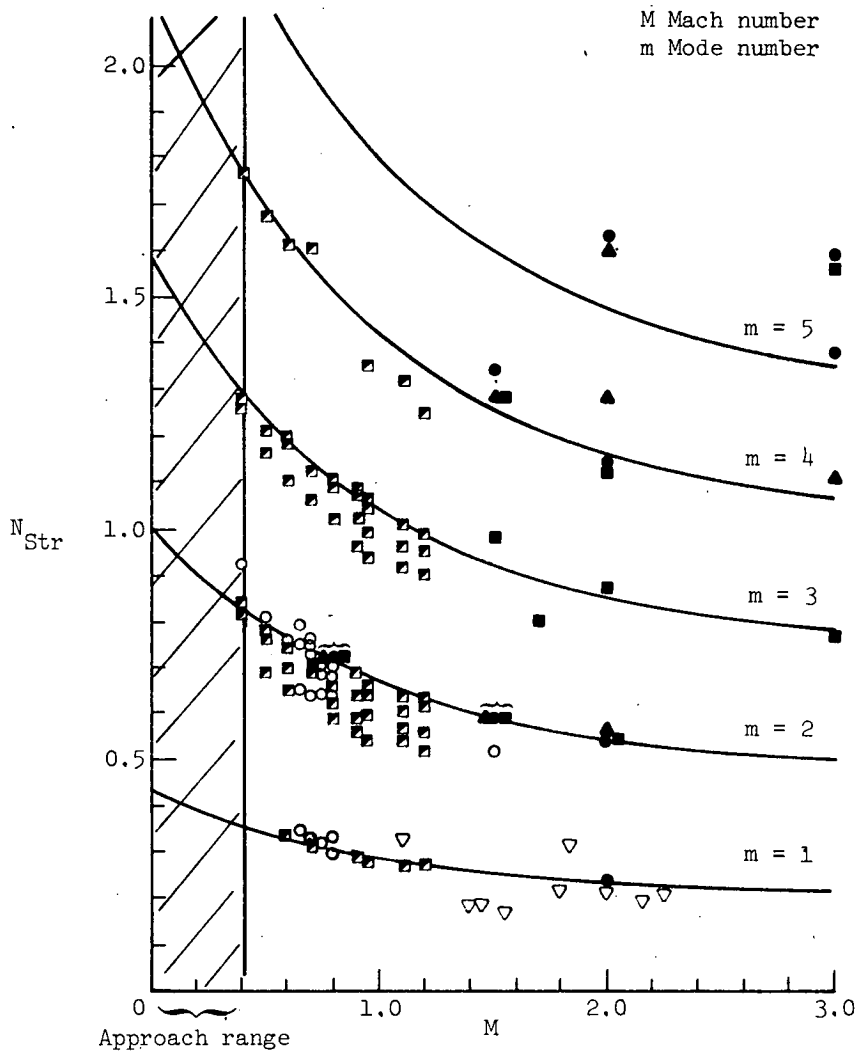

Figure 50.- Nondimensional resonant frequencies of cavities as a function of Mach number.

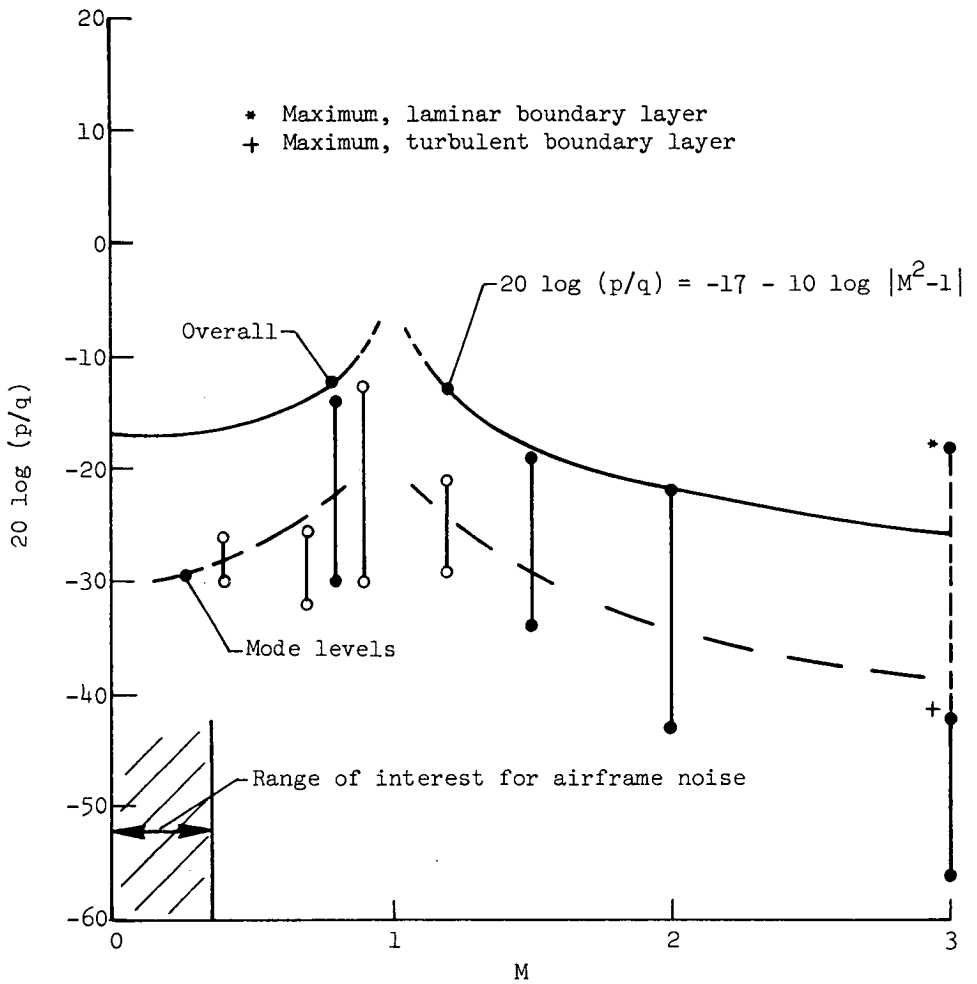

Figure 51.- Peak fluctuating pressure levels inside cavity as a function of Mach number.

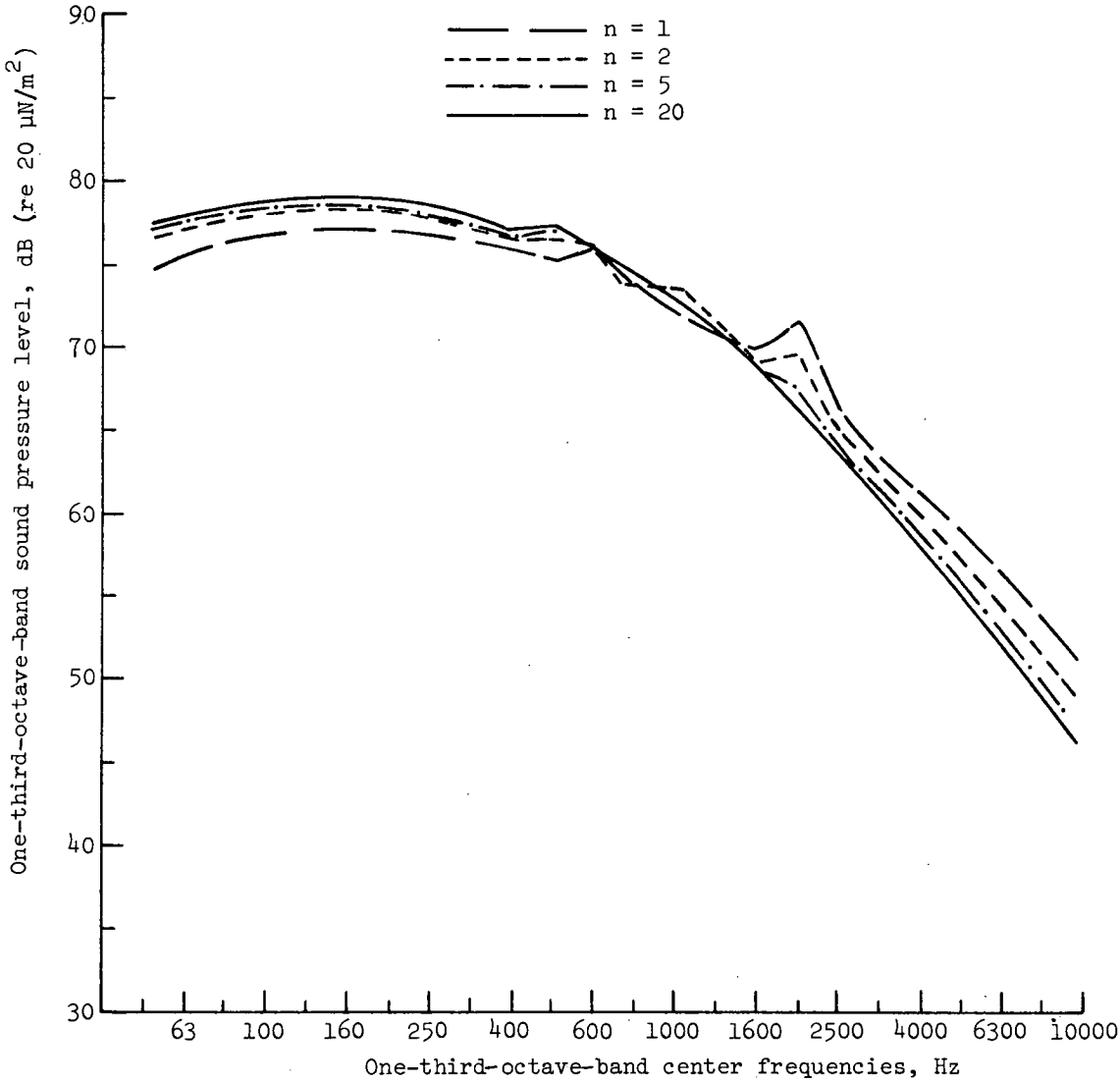

Figure 52.- Sound pressure level spectrum for different n. Noise prediction, Boeing 747; elevation angle, 90°; airspeed, 76 m/sec; flaps at 0°.

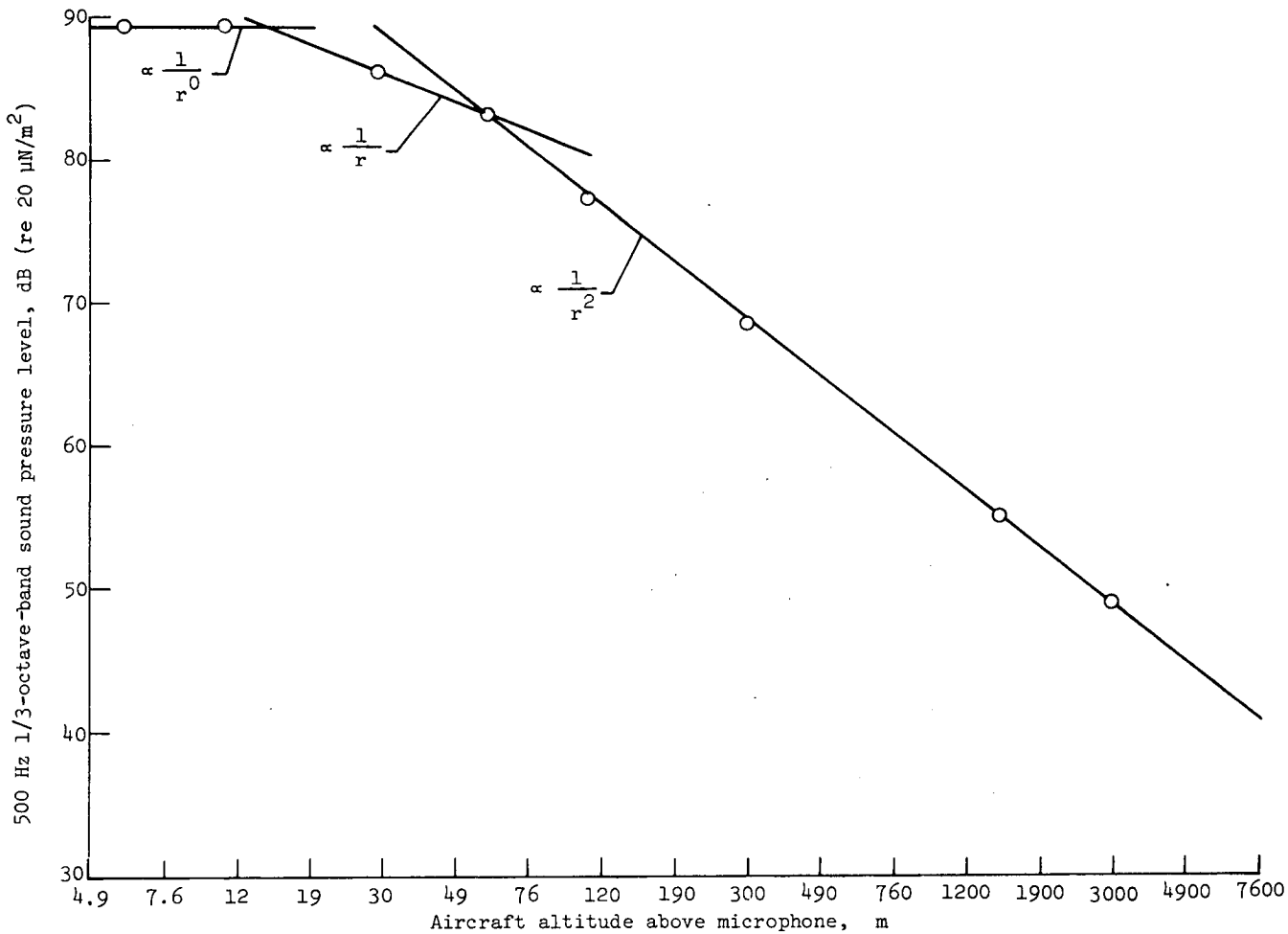

Figure 53.- Sound pressure level in band compared with flight altitude (direct flyover). Boeing 747; airspeed, 75 m/sec; no flap; gear up.

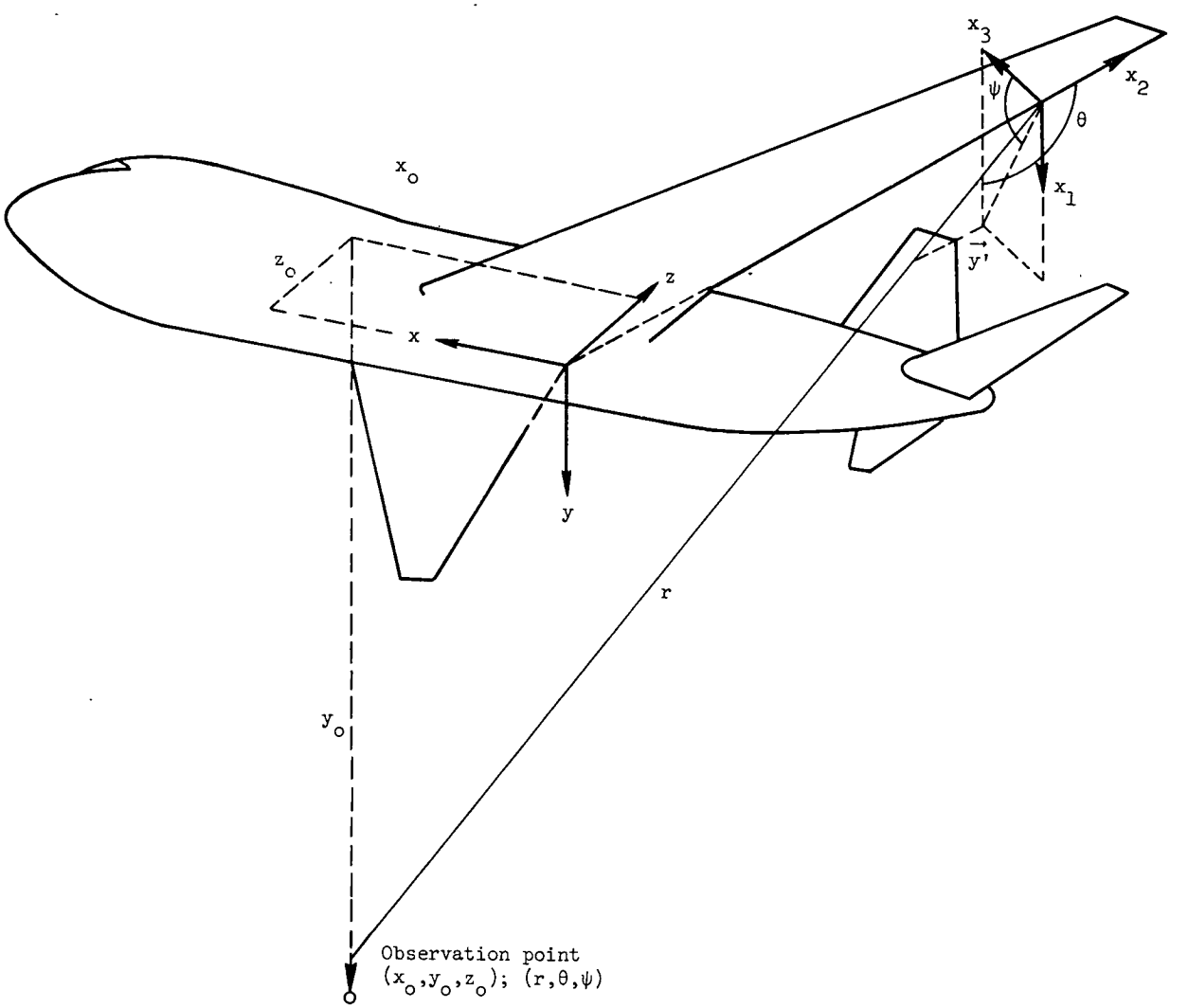

Figure 54.- Geometry for airframe noise calculation.

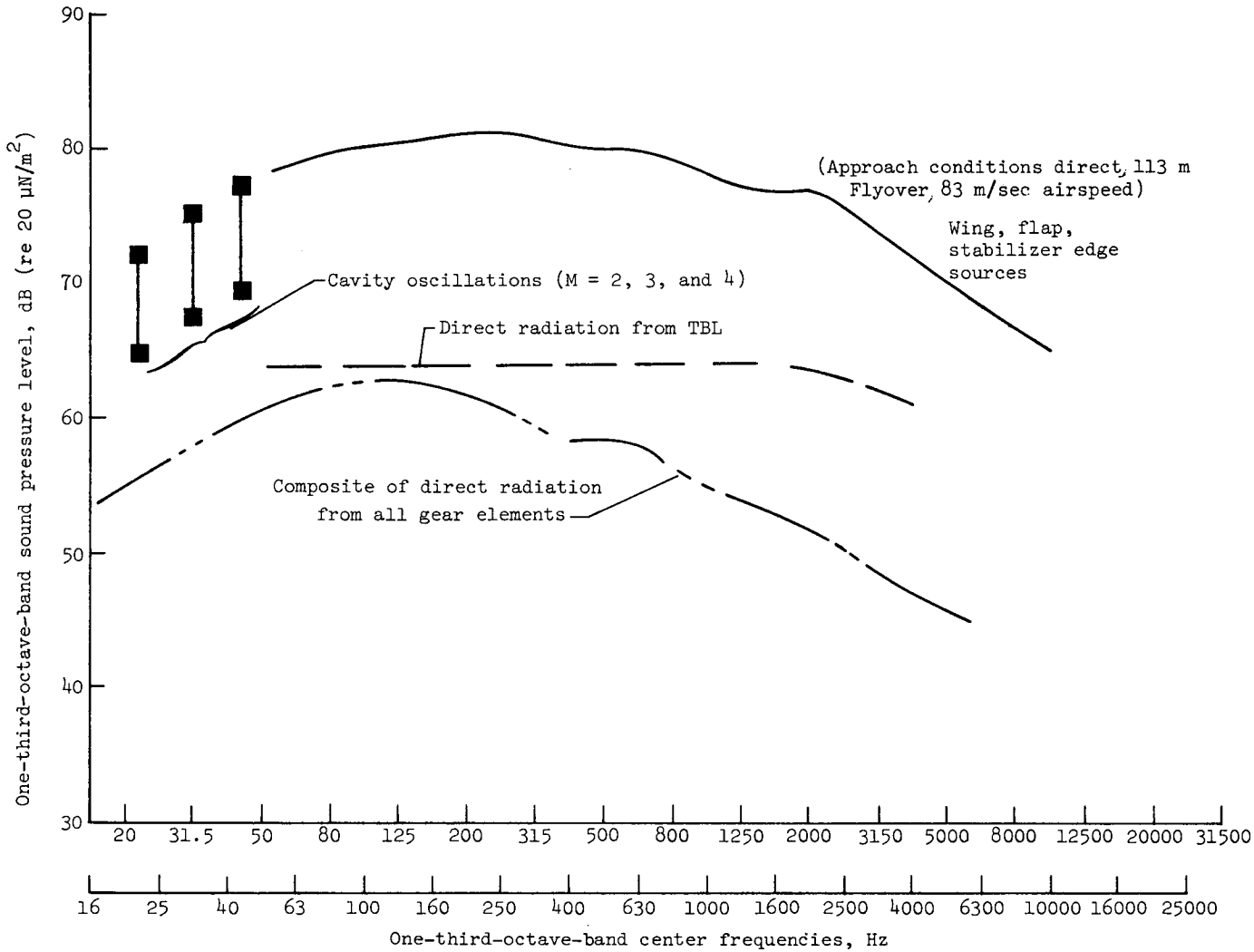

Figure 55.- Comparison of noise source contributions for a 747-type aircraft.

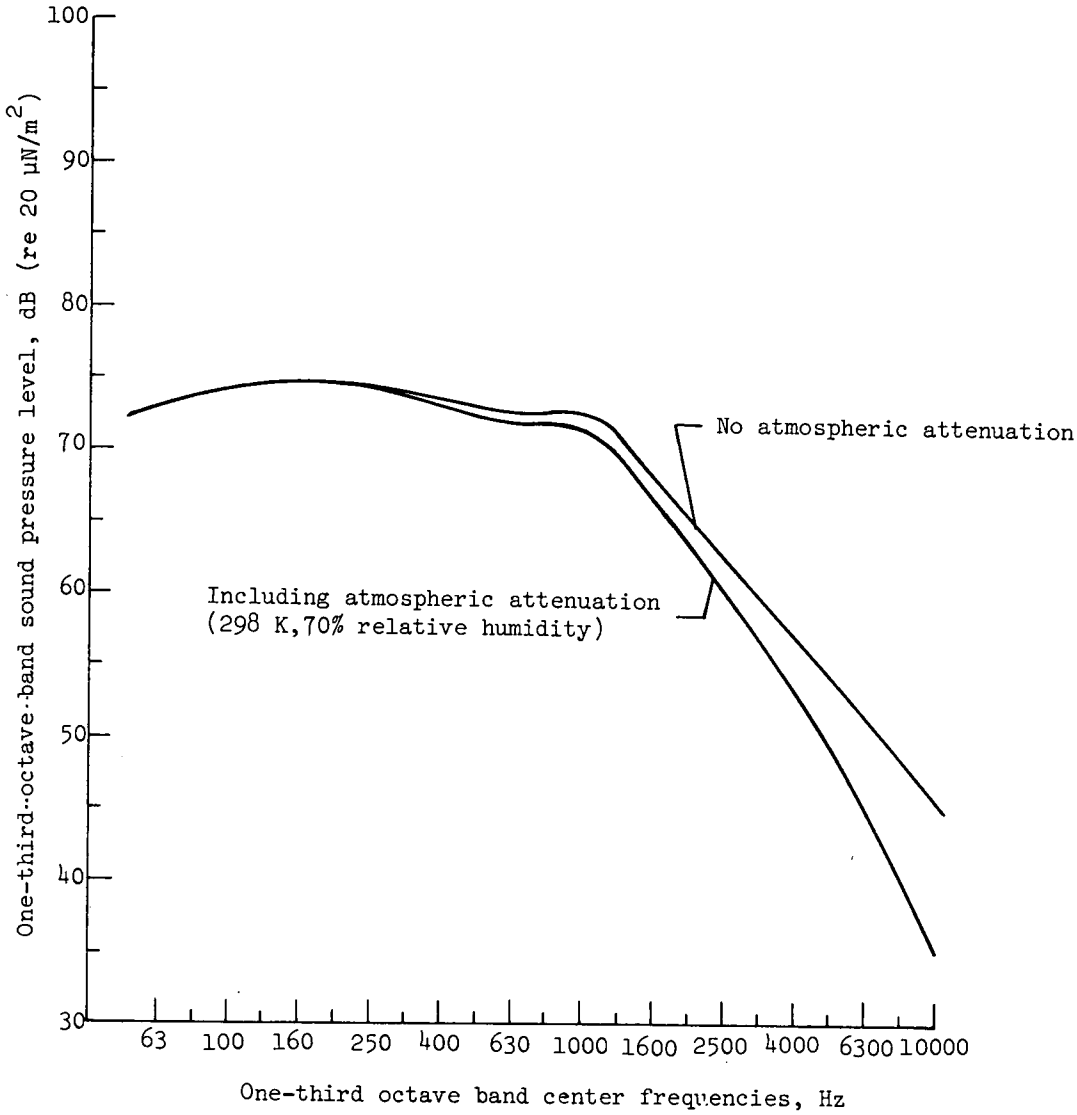

(a) Results of sample noise calculation. Airspeed, 91 m/sec; flaps, 0°; gear up; observer position: 0 m ahead; 61 m below; and 150 m abeam.

Figure 56.- Sample noise calculation.

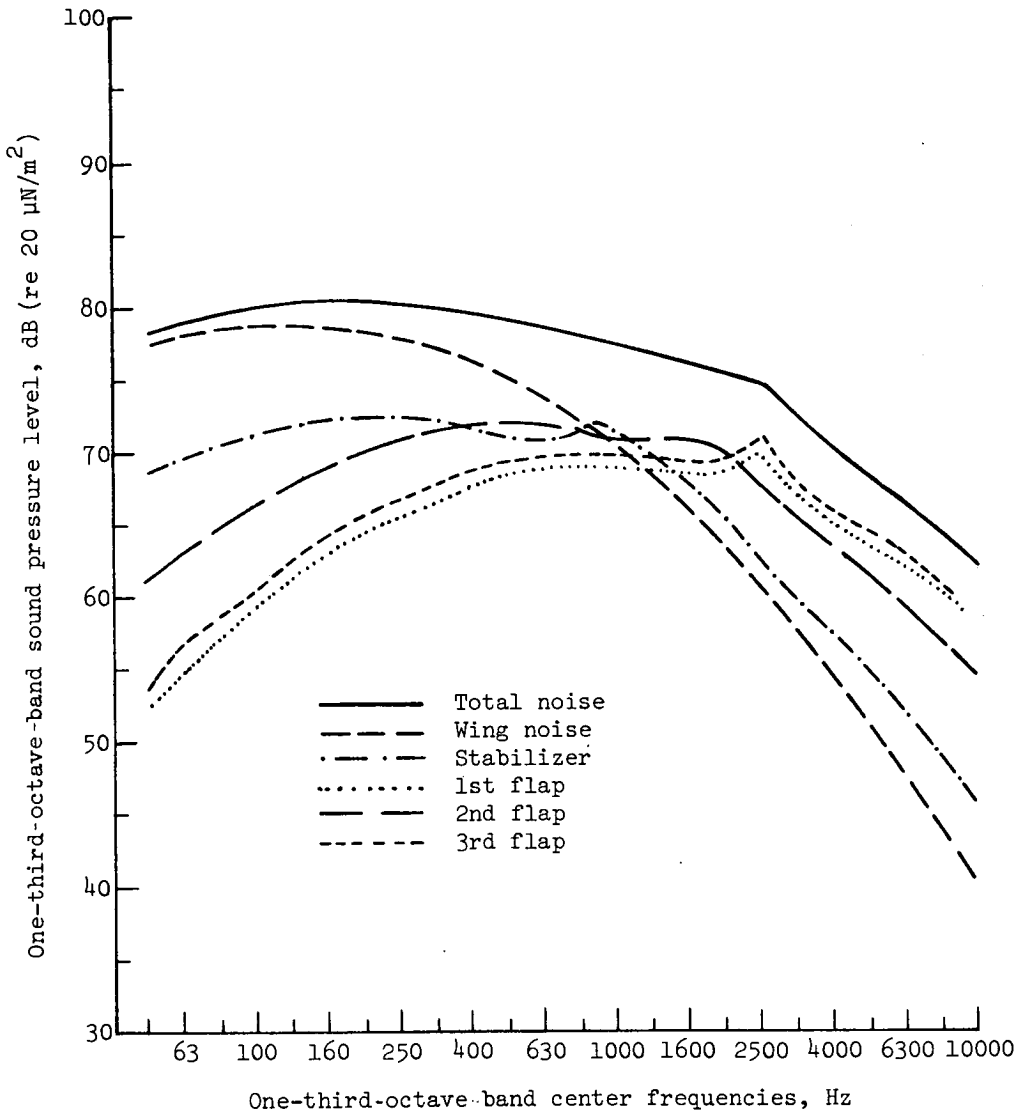

(b) Breakdown of component contribution to airframe noise (edge noise mechanisms). Airspeed, 81 m/sec; flaps, 30°; gear up; observer position: 21 m ahead; 113 m below; and 0 m abeam.

Figure 56.- Concluded.

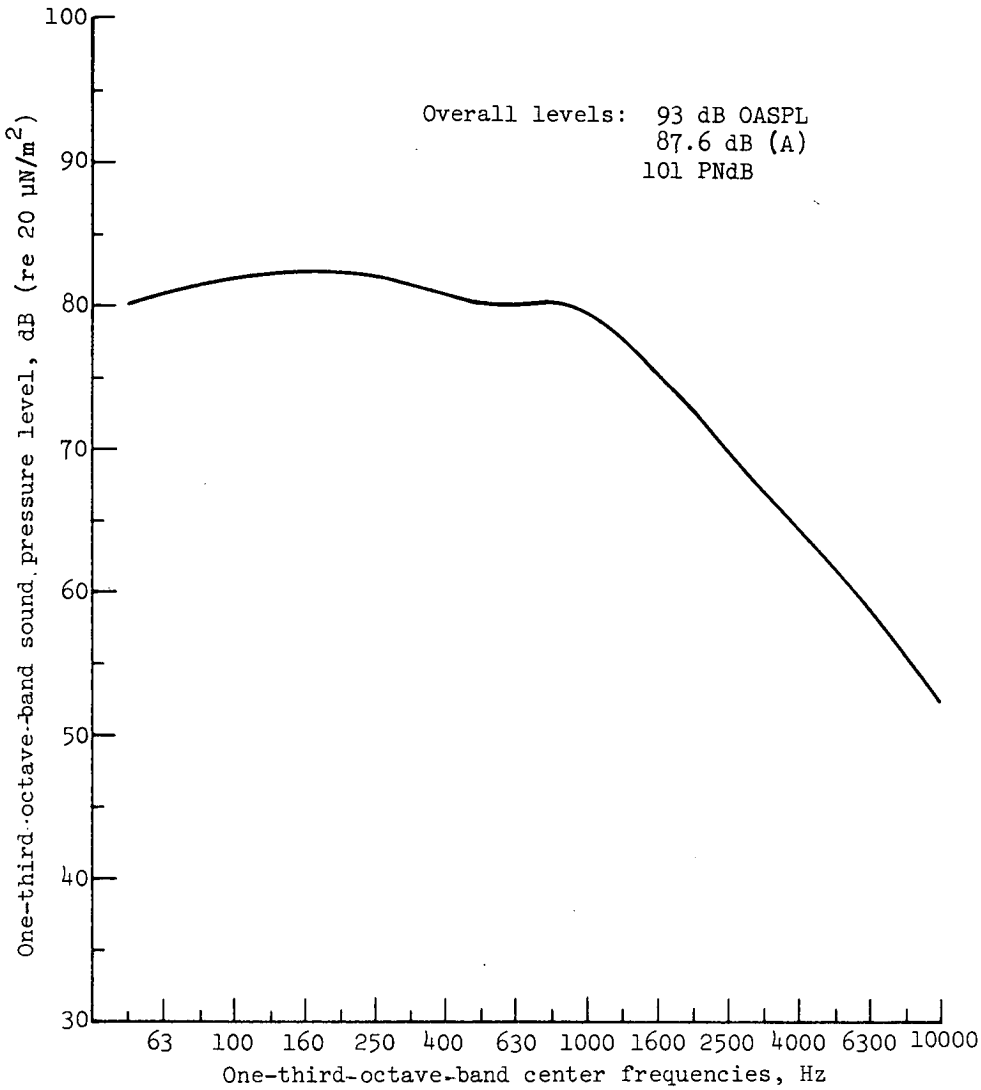

(a) Flaps up. Airspeed, 91 m/sec; flaps, 0°; gear up; observer position: 0 m ahead; 113 m below; and 0 m abeam.

Figure 57.- Flyover noise.

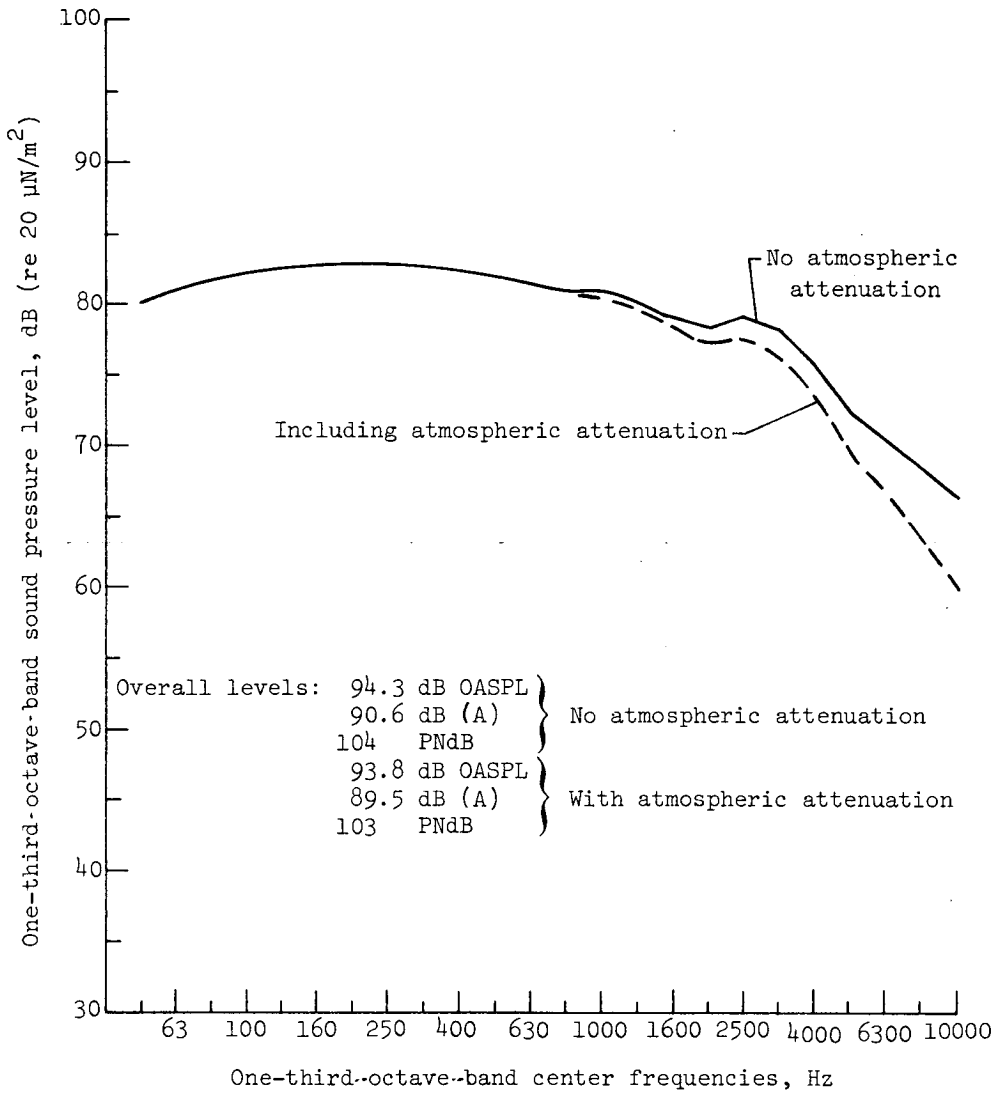

(b) Flaps down. Airspeed, 91 m/sec; flaps, 25°; gear up; observer position: 0 m ahead; 113 m below; and 0 m abeam.

Figure 57.- Concluded.

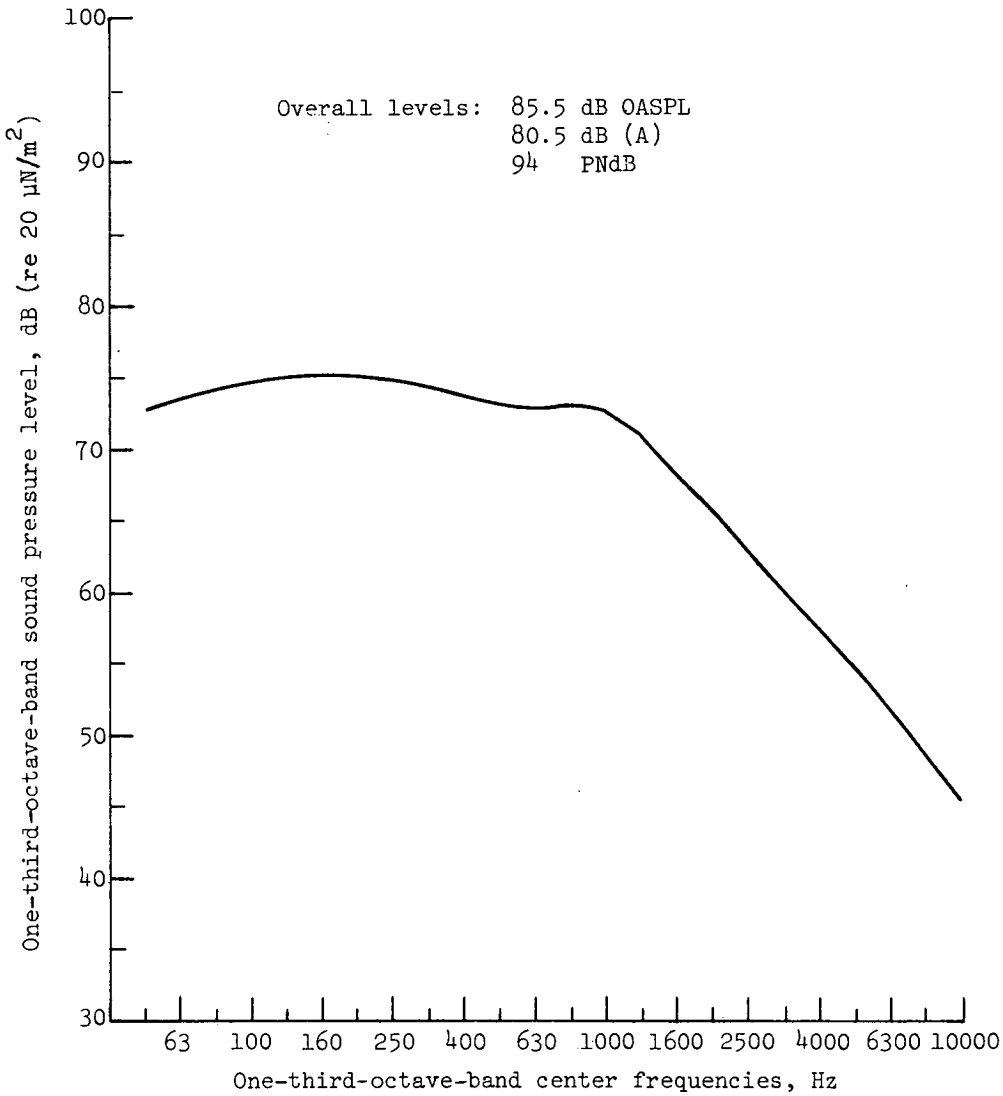

(a) No flaps (no atmospheric attenuation). Airspeed, 91 m/sec; flaps, 0°; gear up; observer position: 0 m ahead; 113 m below; and 150 m abeam.

Figure 58.- Sideline noise.

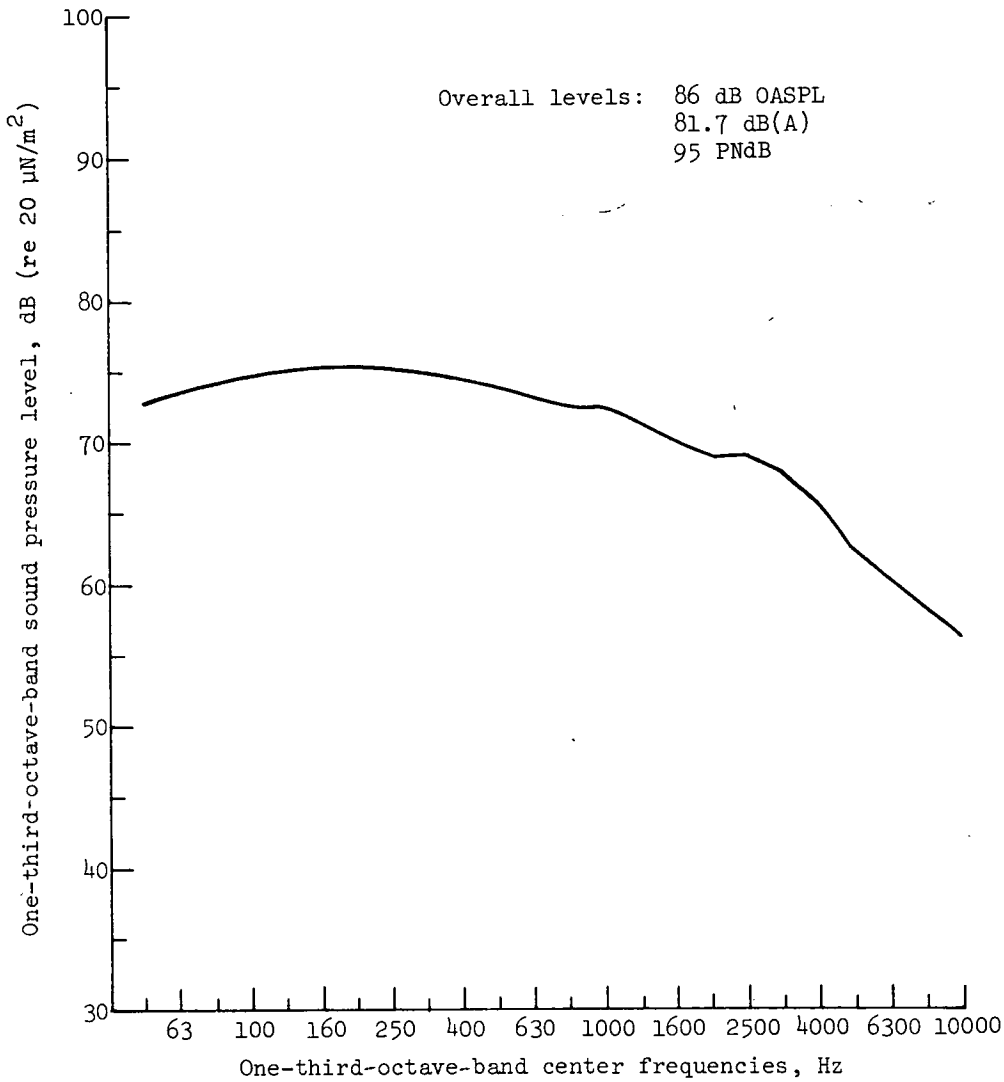

(b) Flaps down (no atmospheric attenuation). Airspeed, 91 m/sec; flaps, 25°; gear up; observer position: 0 m ahead; 113 m below; and 150 m abeam.

Figure 58.- Concluded.

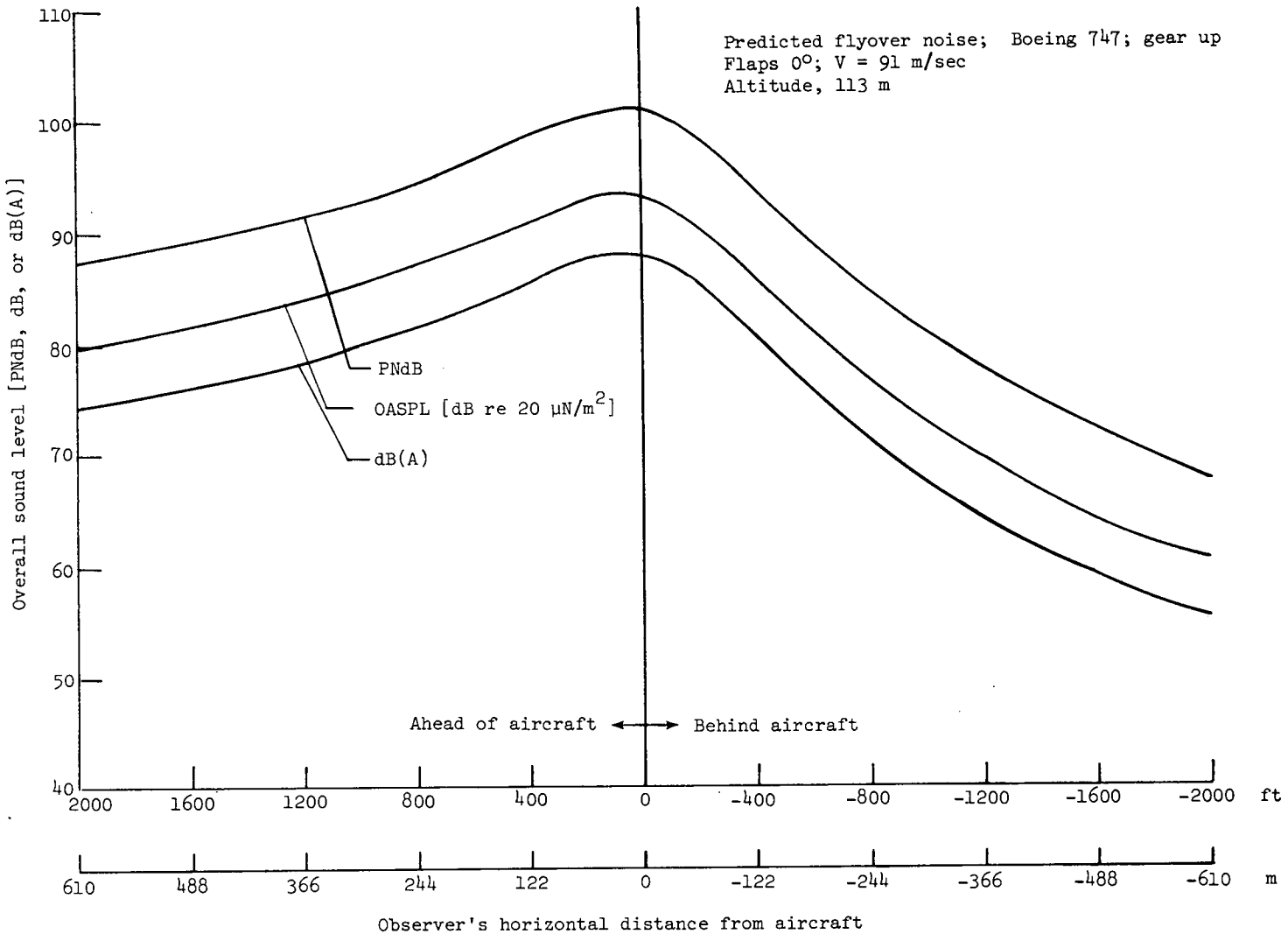

Figure 59.- Relative airframe noise along aircraft path.

NATIONAL AERONAUTICS AND SPACE ADMINISTRATION
WASHINGTON, D.C. 20546

OFFICIAL BUSINESS
PENALTY FOR PRIVATE USE $300

SPECIAL FOURTH-CLASS RATE
BOOK

POSTAGE AND FEES PAID
NATIONAL AERONAUTICS AND
SPACE ADMINISTRATION
451

U.S.MAIL

POSTMASTER: If Undeliverable (Section 158
Postal Manual) Do Not Retu

"The aeronautical and space activities of the United States shall be conducted so as to contribute . . . to the expansion of human knowledge of phenomena in the atmosphere and space. The Administration shall provide for the widest practicable and appropriate dissemination of information concerning its activities and the results thereof."

—NATIONAL AERONAUTICS AND SPACE ACT OF 1958

NASA SCIENTIFIC AND TECHNICAL PUBLICATIONS

TECHNICAL REPORTS: Scientific and technical information considered important, complete, and a lasting contribution to existing knowledge.

TECHNICAL NOTES: Information less broad in scope but nevertheless of importance as a contribution to existing knowledge.

TECHNICAL MEMORANDUMS: Information receiving limited distribution because of preliminary data, security classification, or other reasons. Also includes conference proceedings with either limited or unlimited distribution.

CONTRACTOR REPORTS: Scientific and technical information generated under a NASA contract or grant and considered an important contribution to existing knowledge.

TECHNICAL TRANSLATIONS: Information published in a foreign language considered to merit NASA distribution in English.

SPECIAL PUBLICATIONS: Information derived from or of value to NASA activities. Publications include final reports of major projects, monographs, data compilations, handbooks, sourcebooks, and special bibliographies.

TECHNOLOGY UTILIZATION PUBLICATIONS: Information on technology used by NASA that may be of particular interest in commercial and other non-aerospace applications. Publications include Tech Briefs, Technology Utilization Reports and Technology Surveys.

Details on the availability of these publications may be obtained from:

SCIENTIFIC AND TECHNICAL INFORMATION OFFICE

NATIONAL AERONAUTICS AND SPACE ADMINISTRATION

Washington, D.C. 20546